UNIVERSITY OF CRETE
DEPARTMENT OF CHEMISTRY

GENERAL POSTGRADUATE STUDIES PROGRAMME IN CHEMISTRY

Master Thesis

Development and application of desorption sonic-spray ionization mass spectrometry for the direct analysis of membrane lipids in microorganism cells

LEONIDAS MAVROUDAKIS

Master Thesis Supervisor: Spiros A. Pergantis

HERAKLION 2018

ΠΑΝΕΠΙΣΤΗΜΙΟ ΚΡΗΤΗΣ
ΤΜΗΜΑ ΧΗΜΕΙΑΣ

ΓΕΝΙΚΟ ΜΕΤΑΠΤΥΧΙΑΚΟ ΠΡΟΓΡΑΜΜΑ ΧΗΜΕΙΑΣ

ΜΕΤΑΠΤΥΧΙΑΚΟ ΔΙΠΛΩΜΑ ΕΙΔΙΚΕΥΣΗΣ

Ανάπτυξη και εφαρμογή φασματομετρίας μάζας εκρόφησης με ιοντισμό υπερηχητικής εκνέφωσης για την απ' ευθείας ανάλυση μεμβρανικών λιπιδίων σε κύτταρα μικροοργανισμών

ΛΕΩΝΙΔΑΣ ΜΑΥΡΟΥΔΑΚΗΣ

Υπεύθυνος Καθηγητής(τρια): Σπυρίδων Α. Περγαντής

ΗΡΑΚΛΕΙΟ 2018

This page intentionally left blank.

Στον παππού Λεωνίδα

Examination Committee

Spiros A. Pergantis

Professor of Analytical Chemistry, Dept. of Chemistry, University of Crete

Demetrios F. Ghanotakis

Professor of Biochemistry, Dept. of Chemistry, University of Crete

Nikolaos Lydakis-Simantiris

Professor of Chemistry and Biochemistry, Dept. of Environmental and Natural Resources Engineering, Technological Education Institute of Crete

ACKNOWLEDGEMENTS

First of all, I would like to gratefully acknowledge my supervisor Prof. Spiros Pergantis for the trust and support that he showed me from my very early steps in his lab. His scientific guidance has been invaluable for the completion of this project. Besides project-oriented guidance, I am also very thankful towards him for his advice regarding the initiation of my scientific career. Many thanks go also to my fellow lab members for the pleasant environment created in the lab and especially to PhD candidate Manos Christofakis for his support during the first stages of the analytical technique development.

This work would not be possible without the aid of our collaborator Prof. Nikos Lydakis-Simantiris from Technological Education Institute of Crete as he quite generously provided cell cultures samples and constructive advice regarding cell treatment. Also, PhD candidates Theocharis Nazos and Eleftheria-Angeliki Valsami from the Biochemistry Lab of Prof. Demetrios Ghanotakis are gratefully acknowledged for the cell samples that they provided for my research and their solid advice regarding cell behavior.

Additionally, I would like to thank Dr. Antonis Koumpenakis for the “Maria Hatzimarinaki” award.

The Dept. of Chemistry at the University of Crete is also acknowledged for providing the required infrastructure to complete this project.

Finally, I am more than thankful for the support that my family has showed me all these years and even though they might not understand a single thing from this dissertation, they are always proud of my accomplishments.

CURRICULUM VITAE

LEONIDAS MAVROUDAKIS

leomavr7@gmail.com

EDUCATION

M.Sc. in Analytical Chemistry Oct. 2016 – Sept. 2018
Department of Chemistry, University of Crete

- Master thesis: Development and application of desorption sonic-spray ionization mass spectrometry for the direct analysis of membrane lipids in microorganism cells (Supervisor: Prof. Spiros A. Pergantis)

B.Sc. in Chemistry Sept. 2012 – Jun. 2016
Department of Chemistry, University of Crete

- Awarded B.Sc. with ''Excellent degree (8.73/10)"
- Bachelor thesis: Development of sonic-spray ionization mass spectrometry for the ultrasensitive detection of inorganic anions in water samples (Supervisor: Prof. Spiros A. Pergantis)

EMPLOYMENT

Analytical Chemist (Internship) Jun. 2015 – Sept. 2015
General Chemical State Laboratory, Rhodes, Greece

- Analysis of water samples (chemical and microbiological analyses) and alcoholic beverages

RESEARCH EXPERIENCE

- Mass spectrometric analysis of samples submitted by research groups of the University of Crete (Service to the Dept. of Chemistry)
- Analysis of samples provided by external industrial companies (Service to the Dept. of Chemistry)
- Training of undergraduate students on the use of mass spectrometers for their bachelor projects

PUBLICATIONS

L. Mavroudakis, E. Mavrakis, A. Kouvarakis, S. A. Pergantis, Determination of chlorate, perchlorate and bromate anions in water samples by microbore reversed-phase liquid chromatography coupled to sonic-spray ionization mass spectrometry. *Rapid Comm. Mass Spectrom.* 2017, *31*, 911-918 (Cover page)

CONFERENCES

Presented by L. Mavroudakis:

L. Mavroudakis (poster presentation), Theocharis Nazos, Eleftheria-Angeliki Valsami, Evangelia-Veatriki Sakellaraki, N. Lydakis-Simantiris, Demetrios F. Ghanotakis, S. A. Pergantis, ''Desorption easy ambient sonic-spray ionization mass spectrometry for lipidomic analysis of cyanobacteria and green algae during growth and stress conditions'', 66th Conference on Mass Spectrometry and Allied Topics, American Society for Mass Spectrometry (ASMS), San Diego, CA, USA, 3/6 – 7/6/2018

L. Mavroudakis (poster presentation), G. R. Agnes, E. A. Kapellios, K. Kanaki, S. A. Pergantis, ''Investigating the mechanism for gas-phase ion production in sonic-spray ionization (SSI) mass spectrometry'', 10th International Conference on Instrumental Methods of Analysis: Modern Trends and Applications, Heraklion, Crete, Greece, 17/9 – 21/9/2017

L. Mavroudakis (poster presentation), E. Mavrakis, A. Kouvarakis, S. A. Pergantis, ''Determination of chlorate, perchlorate and bromate anions in water samples by sonic-spray ionization mass spectrometry'', 19th Postgraduates' Conference in Chemistry, University of Crete, Heraklion, Crete, Greece, 2/5 – 4/5/2017

L. Mavroudakis (oral presentation), E. Mavrakis, S. Pergantis, ''Development of sonic-spray ionization mass spectrometry for the ultrasensitive (ppt) detection of inorganic anions in water samples'', 22th Panhellenic Conference in Chemistry, Thessaloniki, Greece, 2/12 – 4/12/2016

Presented by other members of my group:

S. Grafanaki, Leonidas Mavroudakis, Spiros A. Pergantis (poster presentation), ''Coanda effect sonic-spray ionization mass spectrometry (orthogonal-SSI-MS) for coupling conventional and microbore high performance liquid chromatography to mass spectrometry'', 66th Conference on Mass Spectrometry and Allied Topics, American Society for Mass Spectrometry (ASMS), San Diego, CA, USA, 3/6 – 7/6/2018

E. Mavrakis, L. Mavroudakis, S. Pergantis (poster presentation), ''Paired-Ion Sonic-Spray Ionization Mass Spectrometry (PI-SSI-MS) for the analysis of anionic ions: Progress towards even lower limits of detection'' ,64th Conference on Mass Spectrometry and Allied Topics, American Society for Mass Spectrometry (ASMS), San Antonio, Texas, USA, 5/6 – 9/6/2016

E. Mavrakis (oral presentation), L. Mavroudakis, S. Pergantis, ''Development of sonic-spray ionization mass spectrometry (SSI-MS) for peptide analysis and sensitive detection of anions'', 18th Postgraduates' Conference in Chemistry, University of Crete, Heraklion, Crete, Greece, 26/3 – 27/3/2016

LANGUAGES

Greek (Native Language)
English (Certificate of Competency in English, B2, University of Michigan)
German (Goethe – Zertifikat B1)

TEACHING EXPERIENCE

- Teaching assistant at the Undergraduate Laboratory of Analytical Chemistry, Department of Chemistry, University of Crete, Greece (Feb. 2017 – Jun. 2017)

HONORS AND AWARDS

''Maria Hatzimarinaki'' Award Dec. 2017
Award granted by Department of Chemistry, University of Crete, Greece for excellence in postgraduate studies in the field of Analytical Chemistry, awarded 1000 €.

SKILLS

Conference Organization
Chairman of the Organizing Committee of the 20th Postgraduates' Conference in Chemistry which was organized by the Chemistry Postgraduates' Association of University of Crete, Crete, Greece, 25/6 – 27/6/2018

Software
ECDL Expert: Word, Excel, Powerpoint, Access
Xcalibur (Thermo Fisher Scientific)
OriginPro (OriginLab)

ABSTRACT

In this thesis, Desorption Sonic-Spray Ionization Mass Spectrometry (DeSSI-MS) was developed and applied for the rapid analysis of *C. reinhardtii* CC-1690 and *Synechocystis* sp. PCC 6803 cells under different growth conditions. The sample preparation of the cells was minimal and only involved the washing of cells with water to remove media components. No extraction protocols were used prior to mass spectrometric analysis of these cells. Under these conditions, mass spectra in positive and negative ion mode were obtained and membrane lipids such as monogalactosyldiacylglycerol (MGDG), digalactosyldiacylglycerol (DGDG), phosphatidylglycerol (PG), sulfoquinovosyldiacylglycerol (SQDG), phosphatidylinositol (PI) and 1,2-diacylglyceryl-3-O-4'-(N,N,N- trimethyl)-homoserine (DGTS) were detected.

The effect of toxic metals (Cd(II), Pb(II)) and metalloids (As(III), As(V)) under various concentration on membrane lipids of *C. reinhardtii* cells was studied and the obtained results indicate possible membrane lipid reorganization and reduction induced by these metals.

Also, the effect of nitrogen deprivation on *Synechocystis* sp. PCC 6803 cells was investigated and it was found that physiological conversion of membrane lipids from more unsaturated to less unsaturated was disrupted, however, upon resuspension in N-containing medium the cells culture was able to return to its normal state.

To the best of our knowledge this is the first time that DeSSI-MS was applied for membrane lipid analysis of cells grown under different stress conditions.

Keywords: *desorption sonic-spray ionization; mass spectrometry; membrane lipids; green algae; cyanobacteria;*

ΠΕΡΙΛΗΨΗ

Στην παρούσα εργασία η τεχνική της φασματομετρίας μάζας με ιοντισμό εκρόφησης υπερηχητικής εκνέφωσης (Desorption Sonic-Spray Ionization Mass Spectrometry, DeSSI-MS) αναπτύχθηκε και εφαρμόστηκε για πρώτη φορά με σκοπό την γρήγορη ανάλυση κυττάρων *C. reinhardtii* CC-1690 και *Synechocystis* sp PCC 6803 τα οποία είχαν αναπτυχθεί υπό διάφορες συνθήκες στρες. Η προετοιμασία των δειγμάτων ήταν ελάχιστη και περιελάμβανε την πλύση των κυττάρων με απιονισμένο νερό με σκοπό την απομάκρυνση των συστατικών των θρεπτικών διαλυμάτων. Δεν εφαρμόστηκαν πρωτόκολλα εκχύλισης για την εξαγωγή μορίων από τα κύτταρα πριν την ανάλυσή τους με φασματομετρία μάζας. Κατά την ανάλυση των κυττάρων με φασματομετρία μάζας με ιοντισμό εκρόφησης υπερηχητικής εκνέφωσης, λήφθηκαν φάσματα μάζας τόσο στον θετικό όσο και στον αρνητικό ιοντισμό τα οποία παρείχαν πληροφορίες σχετικά με τα μεμβρανικά λιπίδια των κυττάρων. Τα μεμβρανικά λιπίδια τα οποία ανιχνεύτηκαν ήταν: μονογαλακτοζυλο-διακυλογλυκερόλη (MGDG), διγαλακτοζυλο-διακυλογλυκερόλη (DGDG), φωσφατιδυλο-γλυκερόλη (PG), σουλφοκινοβοσυλο-διακυλογλυκερόλη (SQDG), φωσφατιδυλο-ινοσιτόλη (PI) και 1,2-διακυλογλυκερυλο-3-O-4’-(N,N,N-τριμεθυλο)-ομοσερίνη (DGTS).

Η επίδραση των τοξικών μετάλλων (Cd(II), Pb(II)) και μεταλλοειδών (As(III), As(V)), υπό διάφορες συγκεντρώσεις, στα μεμβρανικά λιπίδια των κυττάρων *C. reinhardtii* μελετήθηκε και τα αποτελέσματα υποδεικνύουν πιθανή αναδιοργάνωση των λιπιδίων των μεμβρανών και μείωση της ακορεστότητάς τους η οποία επάγεται από την παρουσία αυτών των μετάλλων και μεταλλοειδών.

Επίσης, μελετήθηκε η επίδραση της στέρησης αζώτου από το θρεπτικό υλικό των κυττάρων *Synechocystis* sp PCC 6803 και βρέθηκε ότι αυτή η αλλαγή επηρεάζει την φυσιολογική μετατροπή συγκεκριμένων μεμβρανικών λιπιδίων, από περισσότερο ακόρεστα σε λιγότερο ακόρεστα. Τα κύτταρα τα οποία αναπτύχθηκαν υπό στέρηση αζώτου όταν επαναιωρήθηκαν σε φυσιολογικό θρεπτικό υλικό με άζωτο, κατάφεραν να επανέλθουν στην αρχική τους κατάσταση και η μετατροπή συγκεκριμένων μεμβρανικών λιπιδίων από περισσότερο ακόρεστα σε λιγότερο ακόρεστα ήταν ξανά ορατή.

Λέξεις-κλειδιά: εκρόφηση με ιοντισμό υπερηχητικής εκνέφωσης, φασματομετρία μάζας, μεμβρανικά λιπίδια, πράσινα άλγη, κυανοβακτήρια

This page intentionally left blank.

CONTENTS

ABBREVATIONS

DeSSI	Desorption sonic-spray ionization
PEEK	Polyether ether ketone
DeSSI-MS	Desorption sonic-spray ionization mass spectrometry
EI	Electron ionization
APCI	Atmospheric pressure chemical chemical ionization
MALDI	Matrix-assisted laser desorption ionization
DESI	Desorption electrospray ionization
ESI	Electrospray ionization
SSI	Sonic-spray ionization
EASI	Easy ambient sonic-spray ionization
UV	Ultraviolet
RF	Radiofrequency
SRM	Selected reaction monitoring
ID	Internal diameter
OD	Outer diameter
ACN	Acetonitrile
DMF	N,N-dimethylformamide
TAP	Tris acetate phosphate
DGTS	1,2-diacylglyceryl-3-O-4'-(N,N,N-trimethyl)-homoserine
DGDG	Digalactosyldiacylglycerol
PG	Phosphatidylglycerol
SQDG	Sulfoquinovosyldiacylglycerol
PI	Phosphatidylinositol
MGDG	Monogalactosyldiacylglycerol
SD	Standard deviation

LIST OF FIGURES

LIST OF TABLES

Objective of the thesis

Ambient mass spectrometry is an emerging field of mass spectrometry which aims to increase the throughput of analytical methods by enabling the analysis of samples in their native state with little or no sample preparation. It was introduced in 2004 and finds a plethora of applications in many fields of mass spectrometry. Desorption sonic-spray ionization mass spectrometry (DeSSI-MS) is such an ambient ionization mass spectrometric technique that enables the analysis of samples with minimal sample preparation in open-air environment. The objective of this thesis was to develop a home-built DeSSI source and apply it for the rapid analysis of intact cells of microorganisms. More specifically, this work was focused on the effect of stress conditions such as nutrient deprivation and toxic metal incubation on the membrane lipids of green algae and cyanobacteria. Studying the effect of various stress parameters is of interest because it can provide insights into possible mechanisms of toxicity.

1. INTRODUCTION

1.1 Mass Spectrometry

Mass spectrometry is a versatile analytical technique that can be used for the analysis of a wide range of samples in the fields of chemistry, biochemistry, health and forensic sciences, pharmaceutical and research industry, environmental science and space research. It is a very sensitive analytical technique that requires minute amounts of sample and can provide both qualitative and quantitative information. Advances in ionization sources, ion optics efficiency and mass analyzers have established mass spectrometry as the essential analytical technique for the investigation of samples in which the analytes of interest are present in very low amounts.

A typical mass spectrometric analysis workflow is relatively simple and involves the ionization of the sample in the ionization source and the transmission of ions via a series of ion optics inside the mass spectrometer which operates under vacuum

conditions in order to avoid collisions of ions with air molecules. Subsequently, the gas-phase ions are analyzed by the mass analyzer and separated based on their mass to charge ratio (m/z). Finally, the separated ions are directed towards the detector which converts the ions into electrons that generate electric current proportional to the abundance of the ions and the recorded electric current (y-axis) for each m/z value (x-axis) of detected ions is used for the recording of a mass spectrum.

1.2 Ambient mass spectrometry

In 1989 the mass spectrometry community experienced a revolution with the introduction of electrospray ionization (ESI).[1] This new ionization source allowed the production of ions outside the mass spectrometer, without the need for vacuum conditions, from molecules that pre-existed as ions in the solution. For this work, John B. Fehn was awarded part of the 2002 Nobel prize in Chemistry as he contributed significantly to the broadening of mass spectrometry applications. Fifteen years later, in 2004, a second revolution occurred with the introduction of desorption electrospray ionization (DESI)[2] and direct analysis in real time (DART)[3] that established the field of ambient mass spectrometry. These ionization techniques enabled the analysis of samples in their native state with little or no sample preparation and without the need for pre-separation techniques, thus, increasing the high-throughput of the analytical methods. The ions are created outside of the mass spectrometer, under ambient conditions, by using high-energy charged particles and laser beams that desorb and ionize the analyte molecules from the sample surface. Since then, the field of ambient mass spectrometry has experienced a tremendous growth[4–7] and many new ionization sources have been introduced. It is said that more than 80 ambient ionization techniques have been reported[8] indicating the strong interest on the further development and application of ambient mass spectrometry. Some of these ambient ionization techniques include desorption sonic-spray ionization (DeSSI), paper spray ionization (PSI), matrix-assisted laser desorption electrospray ionization (MALDESI), atmospheric solids analysis probe (ASAP) and rapid evaporative ionization mass spectrometry (REIMS).

The applications of ambient mass spectrometry are spread over a wide range of fields including biological applications [9], cancer research [10], forensics [11], food analysis [12], metabolomics [13] to name just a few.

1.3 Ionization methods – Sonic spray ionization

There are several ionization methods used in mass spectrometry depending on the physical state of the sample (solid, gas or liquid). The most widely used ionization methods include electron ionization (EI)[14], electrospray ionization (ESI)[1], atmospheric pressure chemical ionization (APCI)[14], matrix assisted laser desorption ionization (MALDI)[15], desorption electrospray ionization (DESI)[2] and desorption sonic spray ionization (DeSSI)[16]. For the most recent advances in ionization methods in mass spectrometry the reader is encouraged to consult the review article by Peacock *et al.*[17] In the following paragraph, the theoretical background regarding the ionization method of sonic-spray ionization (SSI) will be established. Sonic-spray ionization is the basis of desorption sonic-spray ionization technique, which is used in this thesis.

Sonic-spray ionization was mentioned in the literature for the very first time in 1994 by Atsumu Hirabayashi as an interface for atmospheric pressure ionization mass spectrometry.[18] Interestingly, this phenomenon was discovered by chance. In this ionization technique it is not necessary to apply an external electric field as it is the case in ESI for the production of gas-phase ions from a solution. Similar to ESI, SSI operates under atmospheric pressure and creates gas-phase ions from pre-existing ions in solution. The sample solution that flows through a capillary is sprayed by the co-axial flow of nebulizing gas, which is usually nitrogen. For the production of a fine aerosol, high flow rates of nebulizing gas are required and the technique was named “sonic-spray ionization” because the maximum ion intensity obtained was at nebulizing gas velocities near sonic velocity. The first setup for SSI is shown in **Figure 1.3-1** and includes a fused silica capillary for the sample solution delivery, a stainless-steel capillary that holds the fused silica capillary in place. The sample solution is sprayed

under atmospheric pressure with gas flow co-axial to the fused silica capillary and then the produced ions and droplets are inserted into the mass spectrometer.

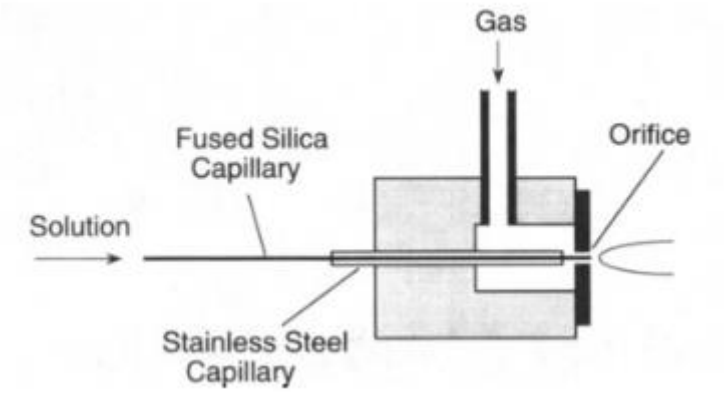

Figure 1.3-1. Schematic representation of sonic-spray ionization source developed by A. Hirabayashi (ref. 18).

The mechanism governing the production of charged droplets and subsequently ions, is not yet fully understood and it is believed that it follows the charge residue model[19]. According to this model, during the droplet formation the majority of them will be neutral since the charge distribution is even. However, in some droplets small variations in charge distribution can lead to statistically imbalanced charged droplets giving rise to droplets with net charge. The mechanism underlying the process of the conversion of a large droplet into smaller ones was investigated by Zilch *et al.*[20] and the model of bag-annulus was proposed. The authors found that in SSI, initial droplets with 10-100 μm radii were downsized to 2-3 μm radii and at that point no further breakup occurs. Using the proposed bag-annulus model for aerodynamic breakup of droplets and the electrical bilayer at the surface of water, the charge separation could be explained. In **Figure 1.3-2**, a cartoon representation of the bag-annulus mechanisms is shown for the aerodynamic breakup of a droplet. As the gas flow velocity is faster than the droplet velocity, an aerodynamic force on the droplet is causing it to accelerate and then break. Initially, the droplet flattens (**Figure 1.3-2a**), a cavity is formed due to the high velocity of the nebulizing gas (**Figure 1.3-2b**) and as the formed bag which is supported by the annulus is blown out from the droplet, it finally breaks into smaller droplets (**Figure 1.3-2d-f)**. The abovementioned model was used to explain the aerodynamic breakup of droplets.

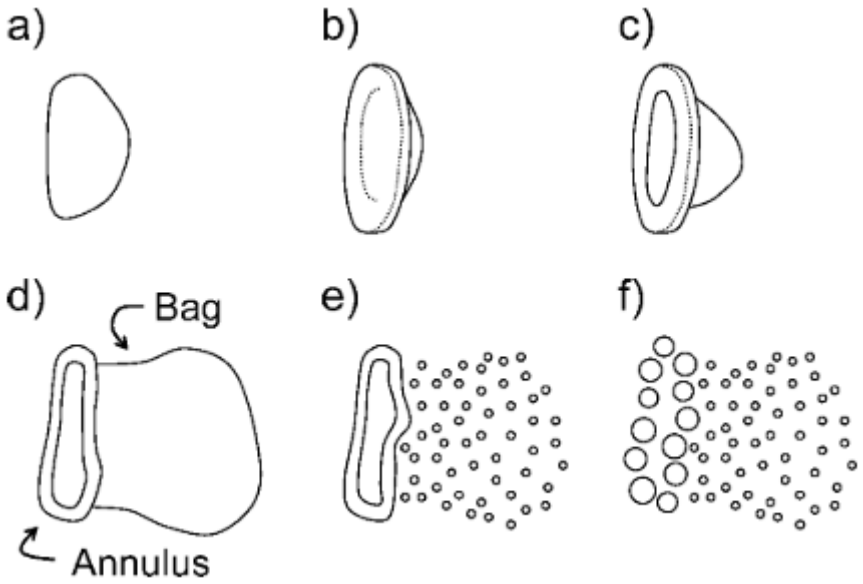

Figure 1.3-2. Cartoon representation of bag-annulus model proposed by Zilch *et al.* for the aerodynamic breakup of a droplet (ref. 20).

The same model was also taken into account to explain the charge separation occurring in droplets produced by a sonic-spray source. More specifically, in **Figure 1.3-3**, a cartoon representation of how the charge separation could occur according to the bag-annulus mechanism.

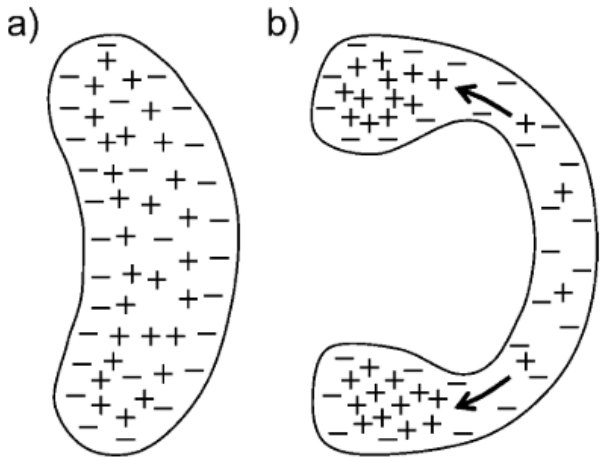

Figure 1.3-3. Cartoon representation of charge separation in droplets during aerodynamic breakup by the bag-annulus mechanism (ref. 20).

Sonic-spray has been characterized as a soft ionization technique, causing little to no fragmentation on the analyte molecules[21] and some of its applications include the

analysis of labile coordination complexes, redox active compounds and proteins [22], metal-assembled cage structures [23] and environmental samples [24].

1.4 Desorption Sonic-Spray Ionization Mass Spectrometry

Desorption sonic-spray ionization mass spectrometry (DeSSI-MS) is an ambient ionization technique that was developed in 2006[16] and is the simpler version of desorption electrospray ionization mass spectrometry (DESI-MS)[2]. In fact, the main difference between these two techniques is the absence of external electric field applied in the solvent. DESI-MS is based on the desorption of ions from the sample surface by directing a stream of charged solvent droplet produced by electrospray ionization while the basis of DeSSI-MS is the sonic-spray effect. Two years after the introduction of DeSSI as an ambient ionization technique it was renamed to Easy Ambient Sonic-Spray Ionization (EASI) to emphasize its easiness. Since then, it has been widely applied in many fields such as food safety, pharmaceuticals and drugs of abuse analysis, explosives detection, metabolomics and proteomics, molecular imaging of biological tissues and monitoring of reactions[25]. The first report on EASI employed a nebulizer design which was similar to the one that Takats *et al*.[21] used for SSI and it can be seen schematically in **Figure 1.4-1**.

The solvent (typically used solvent include mixture of water and methanol) is delivered through the inner fused silica capillary and at the tip of this capillary the high velocity of nitrogen gas results in the solvent nebulization and formation of minute droplets that are directed towards the sample.

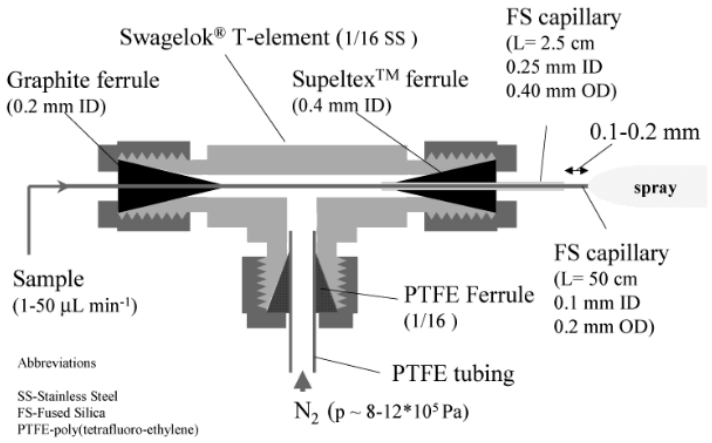

Figure 1.4-1. Schematic view (cross section) of the nebulizer used for SSI (ref. 21) and later employed for DeSSI (ref. 16).

From a mechanistic point of view, DeSSI uses high flow rates of nitrogen gas that mechanically disrupt the solvent droplets that were created upon nebulization and create a statistical imbalance on the droplet charge, just like in SSI. Due to the nature of SSI, DeSSI delivers a bipolar (positively and negatively charged) stream of droplets on the sample surface and then "droplet pick-up" occurs[26] in which the analyte molecules are extracted into the departing droplets. After the extraction, proton (H^+) or cation (usually Na^+ and K^+) transfer reactions are taking place yielding analyte ions that subsequently are transferred. To be more precise, on the sample surface a localized solvent layer is created and upon arrival of more spraying solvent droplets on the droplet, this layer builds up and contributes to the efficient extraction of analyte molecules from the sample into the liquid. Subsequently, progeny droplets are created from the sample surface solvent layer due to the arrival of new spraying solvent droplets and these progeny droplets, that carry the analyte molecules, are transmitted into the inlet capillary of the mass spectrometer due to hydrodynamic forces such as the nebulizing gas and the reduced pressure caused by the inlet of the mass spectrometer[27]. Finally, gas-phase ions are emitted from the progeny droplets and detected by the mass spectrometer. Since, DeSSI does not use heating, high voltages, corona discharges, laser beams and ultraviolet (UV) light it is the simplest and softest ambient ionization technique that produces intact analyte molecule ions[25].

1.5 Mass analyzers – Quadrupole ion traps

Following the ionization of the sample and the transfer of the analyte molecules into the gas-phase, the ions are transmitted inside the mass spectrometer towards the mass analyzer by the assistance of ion optics. The mass analyzer separates the ions based on their mass to charge ratio, m/z, using electric or magnetic fields to efficiently separate the ions and direct them towards the detector. There are many different mass analyzers such as quadrupoles, ion traps, time of flight, ion cyclotron resonance giving rise to mass spectrometers that use either one type of mass analyzer or combine two mass analyzers (hybrid instruments)[28]. In this thesis we will focus on the ion trap mass analyzers that include, linear ion traps, electrostatic ion traps (Orbitrap®) and quadrupole ion traps. More specifically, the basic principles of a quadrupole ion trap

will be introduced as this was the mass analyzer used in the instrument that was employed for work described herein.

A quadrupole ion trap, also known as Paul ion trap or 3D ion trap, is one the most common mass analyzers employed in mass spectrometry. Their small and compact size render them quite affordable in the majority of mass spectrometers. A quadrupole ion trap consists of two hyperbolic electrode plates that face each other and a hyperbolic ring electrode placed in between them[28], as it can be seen in **Figure 1.5-1**.

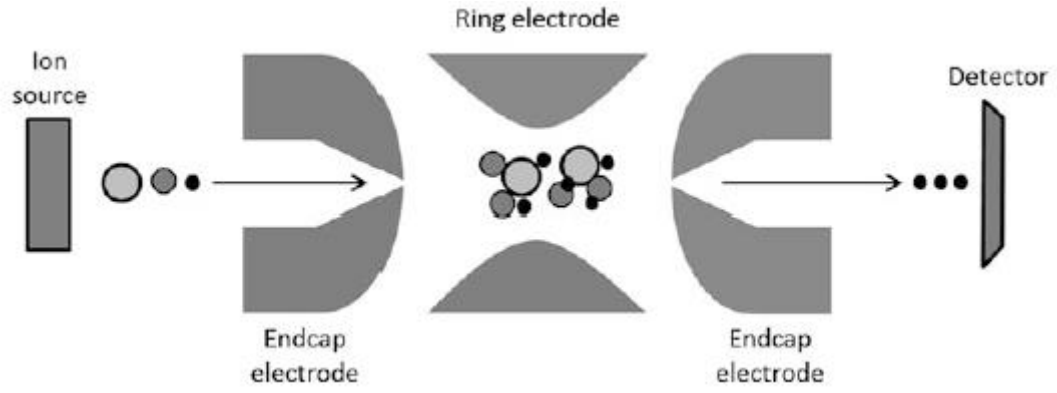

Figure 1.5-1. Schematic cross-section view of a quadrupole ion trap (ref 28.)

The ions are inserted into the trap from the passage of the endcap electrode by applying a proper DC offset voltage to the mass analyzer electrodes. Then, they are trapped by using an oscillating radio frequency (RF) and a superimposed direct current (DC) electromagnetic field. Subsequently, the ions are ejected from the trap by varying the RF potential and directed towards the detector.

Helium gas inside the mass analyzer cavity is used as damping gas and collision activation partner, at a partial pressure of 10^{-3} Torr [29] (p. 2-28). The presence of damping gas is necessary so that the high kinetic energy ions entering the ion trap collide with helium molecules, thus, slowing down and being focused to the center of the cavity. This results in enhanced sensitivity and improved mass spectral resolution. Helium gas also serves as collision activation partner inside the ion trap. This is useful in selected reaction monitoring (SRM) or MS/MS experiments in which a particular ion is isolated in the mass analyzer and fragmented. Subsequently, we can detect either one single fragment of the parent ion (SRM experiment) or monitor all the product ions that were produced due to the fragmentation (full scan MS/MS experiment). In quadrupole ion traps a resonance excitation RF voltage is applied to the endcap electrodes that causes the isolated ions to gain kinetic energy and collide with helium

molecules present in the mass analyzer cavity to produce fragment ions that are ejected from the ion trap and detected.

Quadrupole ion traps have the advantage of providing enhanced sensitivity due to the fact that they accumulate ions over time[28]. Also, they are capable of performing MS^n experiments in which a fragment of the parent ion can be isolated and further fragmented by collision induced dissociation with helium inside the mass analyzer cavity. These experiments are very useful when the structure of an ion is to be determined.

1.6 Ion detection system

Once the ions are ejected from the ion trap, they are directed towards the ion detection system which is located behind the mass analyzer and consists of 15-kV conversion dynode and a channel electron multiplier. The conversion dynode is a concave metal surface positioned at an angle of 90° to the ion beam. As an ion strikes the conversion dynode surface, one or more secondary particles are produced. More specifically, when a positive ion strikes a negatively charged conversion dynode then negative ions and electrons are produced. Positive secondary ions are produced when a negative ion strikes a positively charged conversion dynode. Subsequently, the secondary particles produced are focused by the curved surface of the conversion dynode and accelerated towards the electron multiplier. The electron multiplier includes a cathode and an anode (**Figure 1.6-1**). The secondary particles generated by the ions striking the conversion dynode, impact the inner walls of the electron multiplier cathode and produce electrons which are accelerated further into the cathode. The ejected electrons strike again the inner walls of the cathode producing more electrons and finally a cascade of electrons is created resulting in measurable current in the anode of the electron multiplier.

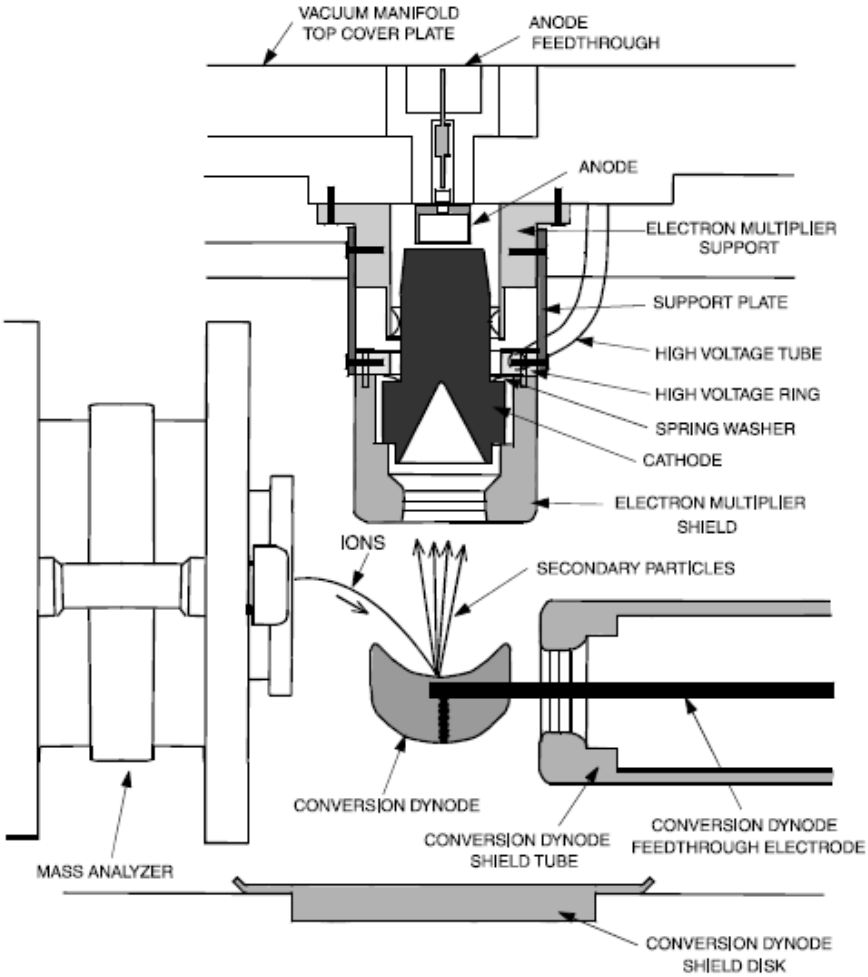

Figure 1.6-1. Schematic cross-sectional view of the ion detection system (ref. 29, p.2-32)

2. MATERIALS AND METHODS

2.1 Desorption Sonic-Spray Ionization Source

DeSSI nebulizer was constructed using common laboratory parts such as T-unions and fused silica capillaries, according to the design of Takats *et al.*[21] More specifically, the DeSSI nebulizer consisted of a plastic T-union, PEEK nuts to secure the fused silica capillaries, PEEK tubing (I.D. 0.762 mm, O.D. 1.58 mm)) to hold the outer fused silica capillary (I.D. 540 μm, O.D. 690 μm). The inner fused silica capillary had I.D. of 50 μm and O.D. of 360 μm.

The dimensions of the fused silica capillaries used are an important parameter of the DeSSI source. In our initial experiments we were using an outer fused silica capillary with I.D. of 321 μm and O.D. of 434 μm and inner fused silica capillary with I.D. of 100 μm and O.D. of 200 μm. However, during the experiments of optimizing the DeSSI source we found that the combination of outer fused silica capillary with I.D. of 540 μm and O.D. of 690 μm and inner fused silica capillary with I.D. of 50 μm and O.D. of 360 μm yielded higher signal intensities in the tested application. Based on this observation, we decided to continue our optimization efforts using the latter combination of fused silica capillaries.

The nebulizing gas used was nitrogen from a compressed cylinder (99.99 % purity) at a backpressure of 8 bar. Again, during our optimization experiments we found that higher backpressure of nitrogen gas resulted in higher signal intensities, so we used the highest nitrogen backpressure provided by the pressure regulator used. This was in accordance with other works that employed EASI-MS and used nebulizing backpressure up to 10 bar[30–32].

The nebulizer was mounted on a custom-made base that allowed adjustment of its angle and also movement in x-y-z directions with a manual stage (increment 0.5 mm). At this point it should be stated that there are several geometrical parameters of the DeSSI source that need to be considered so that the analyte desorption and transfer into the mass spectrometer is efficient. Important geometrical parameters of the DeSSI source include:

α: incident angle

β: collection angle

a: nebulizer to MS distance

b: nebulizer to sample spot distance

c: sample spot to MS distance

d: sample surface to MS distance

All the above parameters are shown in **Figure 2.1-1.** After optimization experiments that tested various different values of the aforementioned parameters, the optimal conditions and those that were further used, are shown in **Table 2.1-1**.

Table 2.1-1. Optimized geometrical parameters of the DeSSI source.

Parameter	Value
α	40°
β	9.5° – 11.3° (calculated)
a	~7.5 – 6.5 mm
b	2 mm
c	5 – 6 mm
d	1 mm

The DeSSI source was placed in front of the mass spectrometer inlet and a custom-made plexiglass cover with a fume hood attached was used to enclose the whole set up so that the operator does not directly come in contact with solvent aerosols.

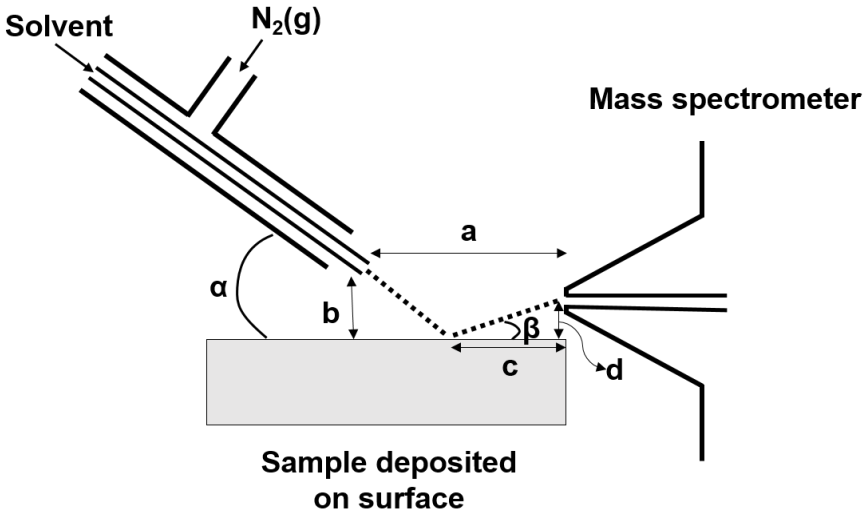

Figure 2.1-1. Schematic view of the nebulizer in front of the mass spectrometer.

The sample surface was either a glass slide or a Teflon-coated glass slide and it was mounted on a x-y stage that allowed for manual positioning of the sample surface with respect to the MS and the nebulizer.

The solvents used for DeSSI-MS experiments included acetonitrile, ACN (CHROMASOLV® grade, >99.9 %, Sigma Aldrich) and N,N-dimethylformamide, DMF (ACS reagent, ≥99.8 %, Honeywell) in a mixture of 1:1 v/v. Several other solvents and solvents mixtures were tested like ACN, DMF, H_2O, Ethanol, Acetone, Methanol, Chloroform, Tetrahydrofuran (THF), DMF:Ethanol 1:1 v/v, DMF:Methanol 1:1 v/v, DMF:$CHCl_3$ 1:1 v/v, DMF:H_2O 1:1 v/v, Methanol:$CHCl_3$ 1:1 v/v, DMF:THF 1:1 v/v, ACN:Ethanol 1:1 v/v, ACN:$CHCl_3$ 1:1 v/v, THF:H_2O 1:1 v/v, ACN:DMF:H_2O 1:1:1 v/v/v. The fused silica capillary of the nebulizer was connected via a union with a PEEK tubing (I.D. 0.254 mm, O.D. 1.58 mm) for the solvent introduction using a syringe pump (Cole Parmer) operated at flow rate of 5 µl min^{-1}.

2.2 Mass Spectrometry

In this work, a quadrupole ion trap mass spectrometer (LCQ Advantage, Thermo Finnigan) was used for the DeSSI-MS experiments. Initially, the electrospray interface was removed and the custom-made DeSSI source platform was mounted in front of the mass spectrometer inlet. When necessary, the instrument was mass calibrated using the ESI source by infusing a solution of sodium trifluoroacetate that is used as a tuning and calibrating solution in mass spectrometry[33]. Because it is not practical and easy to tune the mass spectrometer for each analyte investigated using the DeSSI-MS approach, we were tuning the instrument using the sodium trifluoroacetate m/z ions that were the closest to the m/z of the analyte. The parameters that were tuned were capillary voltage and tube lens offset and their values were -34 V and -20 V, respectively, for negative ion mode and 20 V for both capillary voltage and tube lens offset for positive ion mode. The ion transfer capillary temperature was set to 300 °C to efficiently desolvate the droplets that enter the capillary.

The mass spectrometer was operated in positive and negative ion modes, in full scan mode (500-1000 m/z) and MS^n (n=2-3) experiments were also done to confirm the identity of the analytes.

The ESI source parameters used were spray voltage: 4.5 kV, sheath gas flow rate: 45 arbitrary units, aux. gas flow rate: 5 arbitrary units. Tube lens offset and capillary voltage were the same as in the DeSSI-MS experiments.

For the MS^n experiments both DeSSI and ESI sources, the desired ion was isolated in the trap with an isolation width of 1.5 m/z, activation time of 30 ms, activation Q of 0.2-0.25 and normalized collision energy of up to 50 %. Normalized collision energy is a measure of the amplitude of the resonance excitation RF voltage applied to the endcap electrodes. The activation Q parameters indicates the RF frequency used for fragmentation. Using lower activation Q values, lower energy is deposited on the ions and lower m/z fragment ions are observed. A higher activation Q results in higher energy deposition, in the favor of "losing" lower m/z fragment ions as they are not stable in the trap and thus are ejected without being detected. Activation time is the time in milliseconds that the RF used for fragmentation is applied. In general, shorter activation times result in less fragmentation and longer activation time in more fragmentation.

The mass spectra were recorded and processed using the software Xcalibur 2.0.7 (Thermo Fisher Scientific).

2.3 Pharmaceutical samples

In our initial efforts to test and optimize the developed DeSSI source, a series of pharmaceutical samples including ointments, tablets and solutions were analyzed.

A full list of all samples that were analyzed is given in the Appendix along with the corresponding mass spectra obtained and experimental parameters such as spraying solvent used, flow rate and nebulizing gas backpressure.

A thin film of the ointment sample was placed on Teflon-coated glass slide using a cotton swab and left to dry under ambient conditions. Subsequently, the sample was analyzed by DeSSI-MS using acetonitrile as the spraying solvent at a flow rate of 30 μl min^{-1} and nitrogen backpressure of 6 bar.

For the analysis of pharmaceutical tablets, the sample was fixed with double sided adhesive tape on the sample holder in front of the mass spectrometer and sprayed with methanol at a flow rate of 20 μl min^{-1} at nitrogen backpressure of 6 bar.

Also, a pharmaceutical solution was analyzed by DeSSI-MS. One μl of the sample was placed on Teflon-coated glass slide, left to dry under ambient conditions and analyzed by DeSSI-MS using acetonitrile at a flow rate of 30 μl min^{-1} as the spraying solvent and 6 bar nitrogen backpressure.

2.4 Cell cultures

The cells that were used for DeSSI-MS analysis were the green algae *C. reinhardtii* CC-1690 (wild type) and the cyanobacteria *Synechocystis* sp PCC 6803 (wild type). The cyanobacteria samples were provided by Prof. Demetrios F. Ghanotakis research group (Biochemistry division, Dept. of Chemistry, University of Crete) and the green algae samples were provided by Prof. Nikolaos Lydakis-Simantiris (Laboratory of Environmental Chemistry and of Biochemical Processes, Dept. of Environmental and Natural Resources Engineering, Technological Education Institute of Crete).

C. reinhardtii CC-1690 cell colonies were transferred from agar plates in 3 liters of cultivation medium (tris-acetate-phosphate, TAP, supplied by acetic acid as organic carbon source, pH 7-7.2) under continuous illumination at 25 ºC and stirring. The cells were grown in that medium for 5 days and subsequently the cells were centrifuged and transferred in a new liquid culture in which the TAP medium was spiked with appropriate amounts of cadmium, lead and arsenic compounds. The added salts included $Pb(NO_3)_2$, $Cd(NO_3)_2$, $AsHNa_2O_4 \cdot 7H_2O$ and $NaAsO_2$. The final concentrations of metals in the cultures were 0.63, 6.26 and 12.5 mg L^{-1} (ppm) for Pb(II), 0.36, 3.6 and 7.29 mg L^{-1} for Cd(II), 7.5, 15, 22.5 and 30 ppm for As(III) and 15, 22.5 and 30 ppm for As(V). For the control experiments, the cells were transferred in fresh TAP medium in which no toxic metal was added. The cells were harvested at the end of log phase, that was after 5 days of cultivation, washed with a washing buffer (150 Mm NaCl, 4 mM $MgCl_2 \cdot 6H_2O$, 20 Mm Trizma base, pH 7.0) and kept in a high density sucrose solution (0.8 M sucrose, 50 mM Trizma base, pH 7.0) at -80 ºC until use.

Liquid cultures of *Synechocystis* sp. PCC 6803 (wild type strain) were grown in 25 mM phosphate buffered BG-11 medium (pH 7.5) at 28 °C, under constant aeration and continuous light at 50 μmol photons m^{-2} s^{-1}. Nitrogen starved cultures were obtained after centrifugation of the cells from the late exponential growth phase at 4500 rpm for 10 min and resuspended into nitrogen deprived BG-11 medium, previously being washed twice with this medium. These cultures remained in that medium for 7 days in the abovementioned experimental conditions and then cells were transferred into fresh nitrogen-containing BG-11 medium for 6 days. One ml of culture sample was collected and stored at -20 ºC until use.

2.5 Sample preparation

A small aliquot of cell culture (150 μl for *C. reinhardtii* and 1 ml for *Synechocystis*) was washed three times by centrifugation at 6000 rpm for 2 min with 1 ml of nanopure water to remove cultivation media components and the high density sucrose solution that the *C. reinhardtii* cells were stored. This step was necessary in order to avoid ionization suppression caused by the salts in the cultivation media. After the washing steps, the cell pellets were resuspended in 10-20 μL of nanopure water and 1 μL of that suspension was placed on glass slide and left to dry at ambient conditions. No further sample preparation procedures were undertaken. Following sample drying the glass slide was placed in front of the mass spectrometer for DeSSI-MS analysis.

Also, to verify that the ions detected using the DeSSI source were indeed membrane lipids extracted from the cells, a quick extraction of a small aliquot of cells with 80 % acetone and also ACN:DMF 1:1 v/v was performed. The choice of these extraction solvents was based on previous knowledge of the extraction ability of 80 % acetone and also, ACN:DMF 1:1 v/v was the spraying solvent used in DeSSI-MS, thus, it was necessary to check its extraction ability. More specifically, 150 μl of *C. reinhardtii* cell suspension grown under normal conditions was washed twice with 1 ml of nanopore water by centrifuging at 6000 rpm for 2 min. Then the cell pellets were resuspended in 40 μl of nanopore water and 10 μl of this resuspension was mixed with 1 ml of the aforementioned extraction solvent, vortexed and centrifuged at 8000 rpm for 4 min.

The supernatant, which was colored green indicating the extraction of chlorophylls, was removed, centrifuged again at 8000 rpm for 4 min and subjected to ESI-MS analysis with direct infusion at a flow rate of 10 μl min^{-1}.

3. RESULTS AND DISCUSSION

3.1 Spraying solvent optimization

The choice of the spraying solvent is a very important parameter for the detection of membrane lipids directly from intact cells. Generally, organic solvents are preferred since they are able to extract lipids from cells, thus, a series of organic solvents and their mixtures were selected as candidates for DeSSI-MS analysis of intact cells. These solvents have been tested before with respect to the effect on the tissue morphology on DESI-MS imaging experiments[34] and it was found that when DMF was present in the solvent, high signal intensity and tissue preservation was achieved. To evaluate the efficiency of each solvent, a cell culture sample grown under normal conditions was used. The cells were prepared as described in **Section 2.5** and 1 μl of cell suspension was placed on glass slide for DeSSI-MS analysis. After testing each solvent, the syringe used for solvent introduction and the PEEK tubing connecting the syringe with the fused silica capillary of the nebulizer, were rinsed thoroughly with the appropriate solvent. After the new solvent had rinsed all the parts of the DeSSI source, it was ready to be tested.

In **Appendix section A.4** the mass spectra in positive and negative ion mode obtained from all solvents tested are shown. The following solvents were not able to extract membrane lipids from cells: ACN, THF, acetone, ethanol, $CHCl_3$, methanol, ACN:Ethanol 1:1 v/v, Methanol:$CHCl_3$ 1:1 v/v and ACN:$CHCl_3$ 1:1 v/v. DMF solvent and all of its mixtures with other solvents allowed for the detection of membrane lipids from intact cells. More specifically, the combination of ACN:DMF 1:1 v/v was found to provide the highest signal intensity in both positive and negative ion mode, with the exception of DMF:THF for which a slightly higher signal intensity was achieved in the negative ion mode but lower signal intensity in the positive ion mode. Thus, ACN:DMF

1:1 v/v was chosen as the best spraying solvent for DeSSI-MS experiments of intact cells, as was also the case in the work of Liu *et al*.[30] where EASI-MS was applied for the analysis of intact cyanobacteria. Whereas methanol:water 1:1 v/v was used as the spraying solvent for DESI-MS analysis of bacteria[35–37] and 10 % water – 90 % methanol was used for nanoDESI-MS, a variant of DESI-MS[38].

3.2 Spraying solvent flow rate

Different flow rates of spraying solvent ACN:DMF 1:1 v/v were tested in the range 3 – 25 μl min^{-1}. This was done in order to find the best compromise between signal intensity and signal stability. Low spraying solvent flow rate results in lower signal intensity due to less solvent deposition on the sample and less extraction taking place but the signal is more stable. Higher spraying solvent flow rate deposits more solvent on the sample, thus, more extraction taking place and the signal intensity is higher. However, the signal has less duration as the cells are washed away from the surface faster.

In these experiments, several spots of *C. reinhardtii* cells were prepared and deposited for testing optimum flow rates. The nebulizer started from a spot where no cells were present (blank) and then it was moved over the cell sample spots. The spectrum was recorded until there was substantial decrease in the signal intensity. Each flow rate was evaluated in terms of 1) average signal intensity and number of data points for which the signal was stable and 2) seconds until the signal dropped to approximately 50 % of the maximum intensity. In **Figure 3.2-1** a recorded spectrum for 5 μl min^{-1} can be seen. In the top panel there is the extracted ion chromatogram (XIC) in the m/z range 730-740 (positive ion mode) where the most abundant lipids are present and in the lower panel there is the mass spectrum. On the XIC, the time period where the signal is the most stable can be seen and also the time required for the signal to drop to half maximum. On the mass spectrum the average signal intensity (NL) is denoted.

Table 3.2-1. Effect of spraying solvent flow rate on spectrum quality.

Flow rate (µl min^{-1})	Signal intensity	Data points	Stable signal time (s)	Time until signal reached half maximum (s)
3	2.06E4	15	17	30
5	4.95E4	16	16	23
10	1.09E5	14	10	30
15	1.71E5	10	6	24
20	2.15E5	7	4	12
25	2.15E5	9	5	17

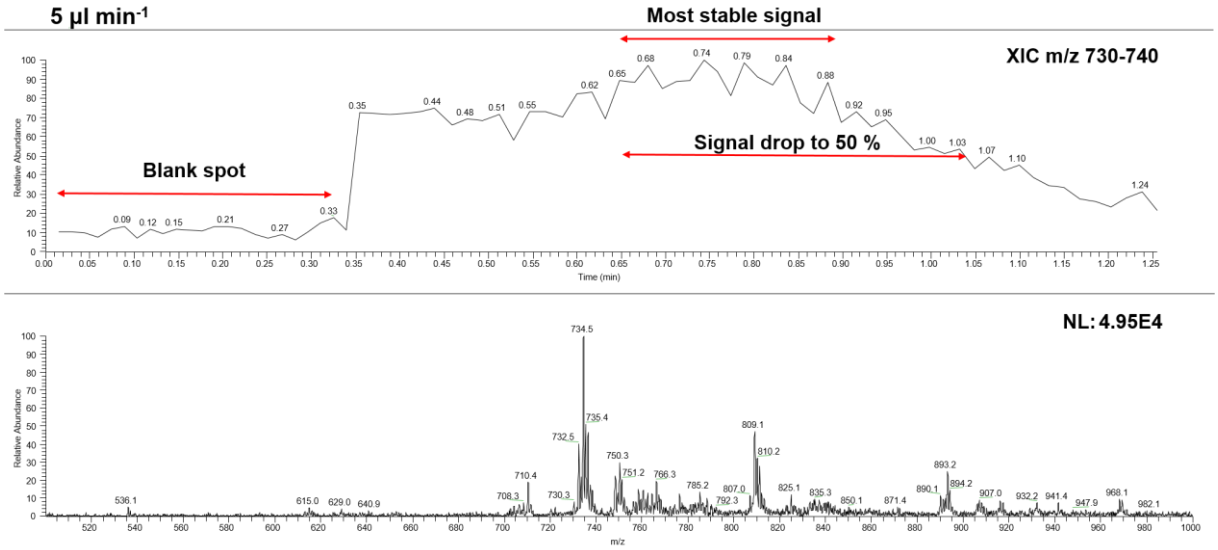

Figure 3.2-1. Spectrum recorded from DeSSI-MS analysis (positive ion mode) of C. reinhardtii cells at spraying solvent flow rate of 5 µl min^{-1}. The mass spectrum is the average of all the spectra acquired in during the "most stable signal" region shown in the XIC trace.

In **Table 3.2-1** the effect of spraying solvent flow rate on spectrum quality parameters such as signal intensity, data points, time period where the signal was stable and time until the signal was halved are shown. As the flow rate increases, the signal intensity increases until it reaches a plateau, however, the stable signal intensity duration and number of data points decreases which gives spectra of lower quality. Also, the time until the signal intensity is halved also decreases with increasing flow rate, thus, resulting in signals with high variance. Based on this a flow rate of 5 µl min^{-1} was a good compromise between signal intensity and spectrum quality.

3.3 Nebulizing gas backpressure

To find the optimum nebulizing gas backpressure that yielded the highest signal intensity, spots of *Synechocystis* sp PCC 6803 cells grown under control conditions were analyzed using ACN:DMF 1:1 v/v as the spraying solvent at a flow rate of 5 µl min^{-1}. In **Figure 3.3-1** the spectra in the negative ion mode obtained at different N_2 backpressures are shown. In every case the detected ions are the same, however, it is evident that at higher nebulizing gas backpressure the signal intensity (NL) is higher.

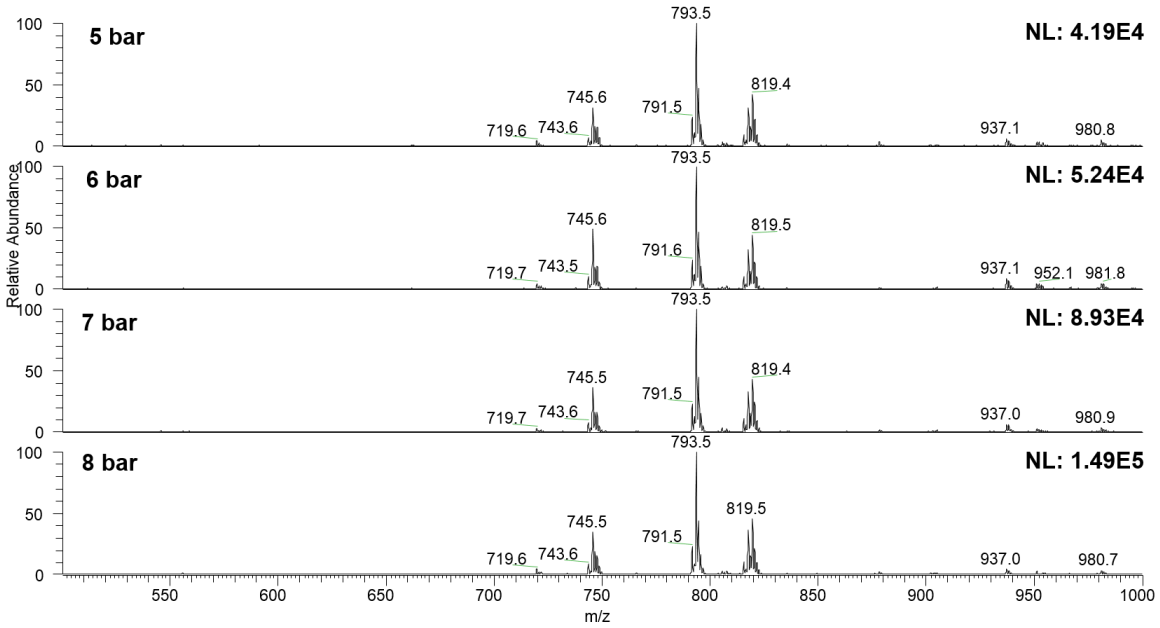

Figure 3.3-1. Lipid profiles (negative ion mode) of *Synechocystis* sp PCC 6803 cells obtained by DeSSI-MS using different nebulizing gas backpressure.

At 5 bar of nitrogen backpressure the signal intensity for the most abundant peak is 4.19E4 while at 8 bar the corresponding signal intensity is 1.49E5. Thus, 8 bar of nebulizing gas backpressure was found to be the optimum for maximum signal intensity.

3.4 Cell integrity

It is known that when changing the medium of the cells from a buffer that contains salts to water, the latter can enter the cell in large amounts causing osmotic shock that might result in cell swelling. The cell subsequently can either burst or undergo apoptosis. Having this in mind, the integrity of the cells after the washing steps was investigated. We observed the *C. reinhardtii* cells under a microscope and cells that were intact could clearly been observed. Thus, the washing step does not cause cells to burst.

Also, we were interested to find out about the integrity of the cells that were placed on the glass slide and left to dry. To investigate that, a typical sample preparation procedure was repeated with *C. reinhardtii* cells, including the washing step. After the cells had completely dried on the glass slide, a small aliquot of water was placed on the dried spot and an attempt to resuspend the dried cells was made. Subsequently, the resuspension from the dried cells was observed under an electron microscope (Electron Microscopy Unit “Vasilis Galanopoulos”, Dept. of Biology, University of Crete). In **Figure 3.4-1**, electron microscopy (left) and fluorescence microscopy (right) images of the resuspended cells that had been dried on glass slide are shown. It is evident that the cells are intact and no cell breakage has occurred during the whole sample preparation procedure. Thus, the spraying solvent that impacts the intact cells should cause cell lysis and extraction of membrane lipids that were detected with the DeSSI-MS.

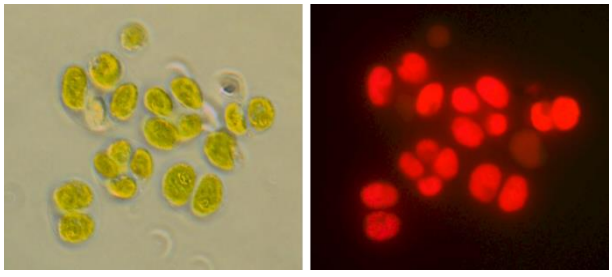

Figure 3.4-1. Electron microscopy (left) and fluorescence microscopy (right) image of *C. reinhardtii* cells that were dried on a glass slide and resuspended in water.

Another interesting question that needed to be addressed was about the intactness of cells that were analyzed by DeSSI-MS. A cell sample spot grown under control conditions, was placed on a glass slide following the sample preparation procedure

described in **Section 2.5** and sprayed with ACN:DMF 1:1 v/v at a flow rate of 5 μl min^{-1} and nitrogen backpressure of 8 bar. The aerosol that was created after the impact of solvent plume on the sample was collected on a second glass slide and then a small amount of water was added to resuspend the cells that had impacted on the second the glass slide. This resulting suspension was observed under an electron microscope and in **Figure 3.4-2** an optical (left) and fluorescence (right) image of a cell that probably has been lysed can be seen. Thus, the initially intact cells upon spraying with the DeSSI source were probably lysed and membrane lipids were extracted from them.

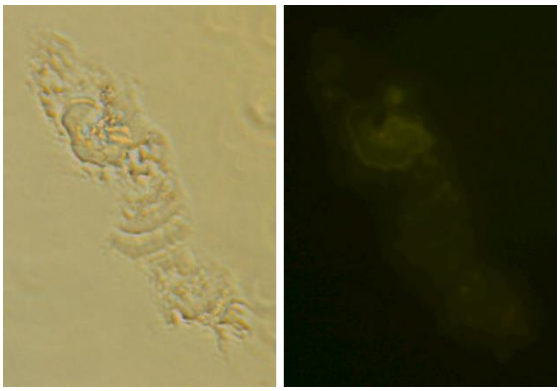

Figure 3.4-2. Optical (left) and fluorescence (right) microscopy images of *C. reinhardtii* CC-1690 cells that were sprayed. The aerosol was collected and resuspended in water.

3.5 DeSSI-MS lipid profiles of *C. reinhardtii* cells

Mass spectra that are very rich in chemical information can be obtained immediately after the DeSSI sprayer is directed towards the cell sample spot. Spectra were recorded in the m/z range 500-1000 in both positive and negative ion mode.

3.5.1 Lipid profiles

In **Figure 3.5.1-2** and **Figure 3.5.1-1** the mass spectra obtained in positive and negative ion mode, respectively, by DeSSI-MS analysis of *C. reinhardtii* cells grown under normal conditions can be seen. In positive ion mode intense peaks were observed in the m/z range 700–950. Following their identification (see following section for details) the main species present were found to be 1,2-diacylglyceryl-3-O-4'-(N,N,N- trimethyl)-homoserine (DGTS) lipids, digalactosyldiacylglycerol (DGDG) lipids

and chlorophylls a and b. In negative ion mode, a very intense peak with m/z 793.6 was observed along with other peaks at m/z range 700 – 900. These ions were identified as phosphatidylglycerol (PG), sulfoquinovosyldiacylglycerol (SQDG) and phosphatidylinositol (PI). DGDG, PG, SQDG and PI are constituents of thylakoid membranes where photosynthesis takes place [39,40]. DGTS lipids in *C. reinhardtii* are substituting for phosphatidylcholine in extraplastidial membranes[41].

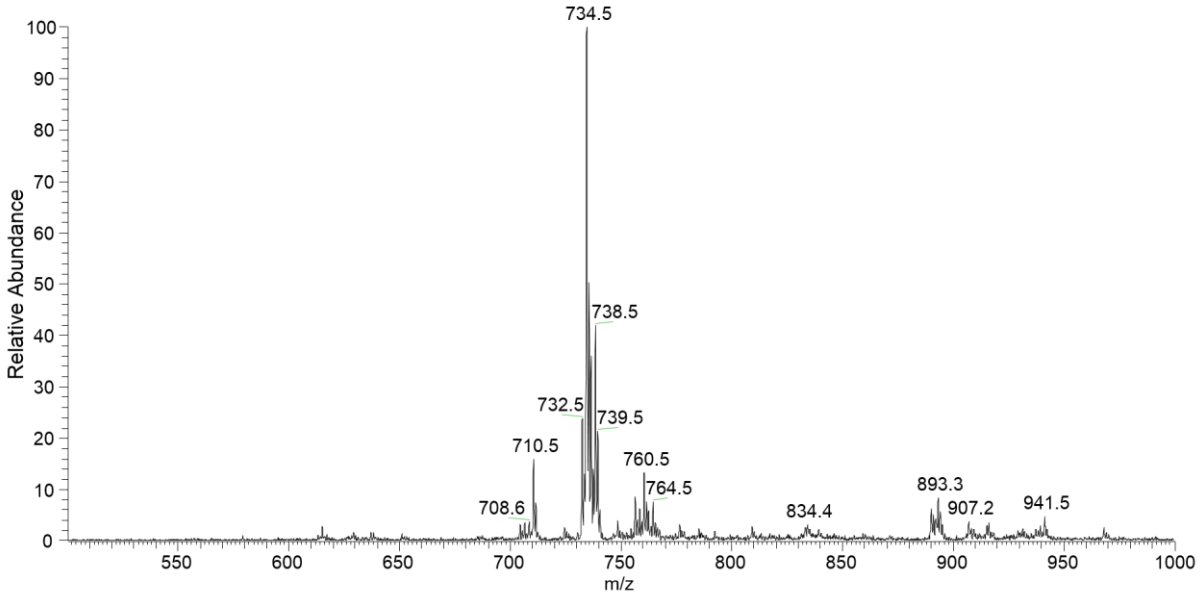

Figure 3.5.1-2. Positive ion mode mass spectrum obtained by DeSSI-MS analysis of *C. reinhardtii* cells grown under normal conditions.

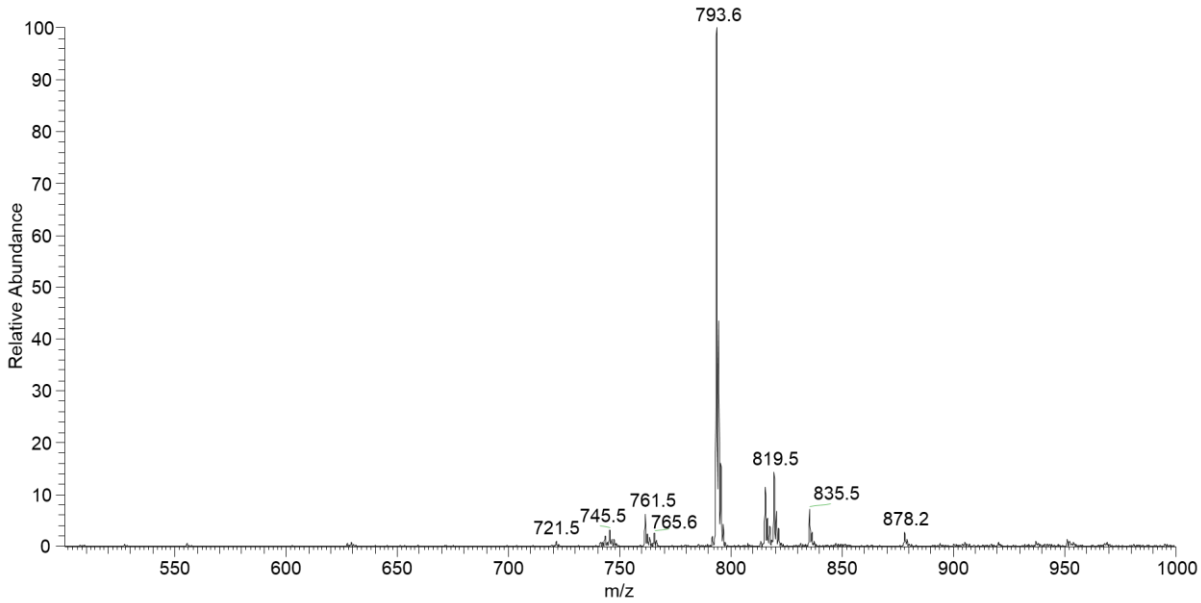

Figure 3.5.1-1. Negative ion mode mass spectrum obtained by DeSSI-MS analysis of *C. reinhardtii* cells grown under control conditions.

3.5.2 Lipids identification

Identification of the detected ions was based on literature results[30,40–42] and manual interpretation of the MS/MS spectra acquired. Also, the NIST MS Search 2.0 with mass spectra libraries[43] was used to compare the experimental MS/MS spectra with spectra from these libraries.

For instance, the ion with m/z 734.5 in positive ion mode was putatively identified as the $[M+H]^+$ adduct of zwitterionic lipid DGTS (16:0/18:3)[41]. The MS/MS spectrum of this ion is shown in **Figure 3.5.2-1**.

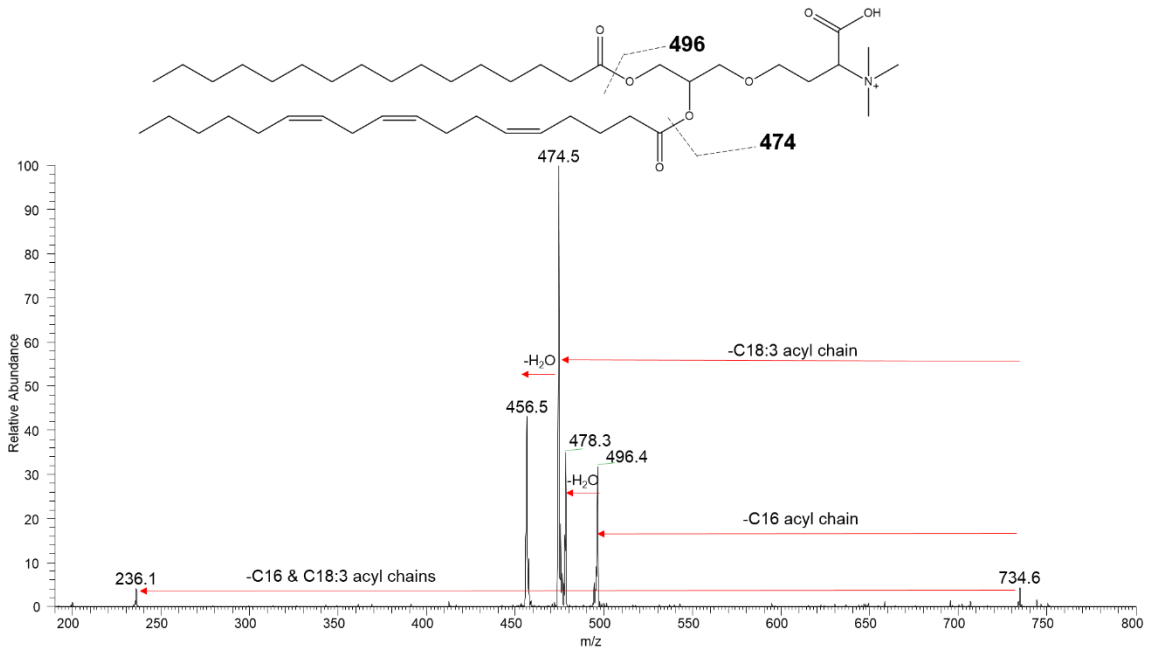

Figure 3.5.2-1. MS/MS of m/z 734.5 putatively identified as DGTS(16:0/18:3). Inset is shown the structure of this lipid and fragmentations that yield the ions 474 and 496.

The major product ions detected in the MS/MS spectrum of m/z 734.5 are 496.4, 478.3, 474.5, 456.5 and 236.1. Neutral loss of C16 acyl chain from the intact precursor ion could yield the ion with m/z 496.4 which upon neutral loss of water could yield the ion with m/z 478.3. Neutral loss of C18:3 acyl chain could yield the ion 474.5 which upon neutral loss of water could yields the ion with m/z 456.5. The ion with m/z 236.1 was identified as the product of both acyl chain losses and was found to be present in all MS/MS spectra of DGTS lipids. Thus, the detection of this ion indicated the presence of DGTS lipid.

In another example, the ion with m/z 732.5 was putatively identified as the $[M+H]^+$ adduct of DGTS(16:0/18:4). Mass difference of 2 amu is a possible indication of the

presence or absence of an additional double bond. For the ion with m/z 732.5, based on the putative identification, a similar fragmentation pattern would be expected as in the case of ion 734.5, however, the difference would be in the neutral loss of C16 acyl chain that would yield the ion with m/z 494.4 due to the presence of an extra double bond.

In **Figure 3.5.2-2**, the MS/MS spectrum of m/z 732.5 can be seen and it is evident that the fragmentation pattern is similar to that of m/z 734.5.

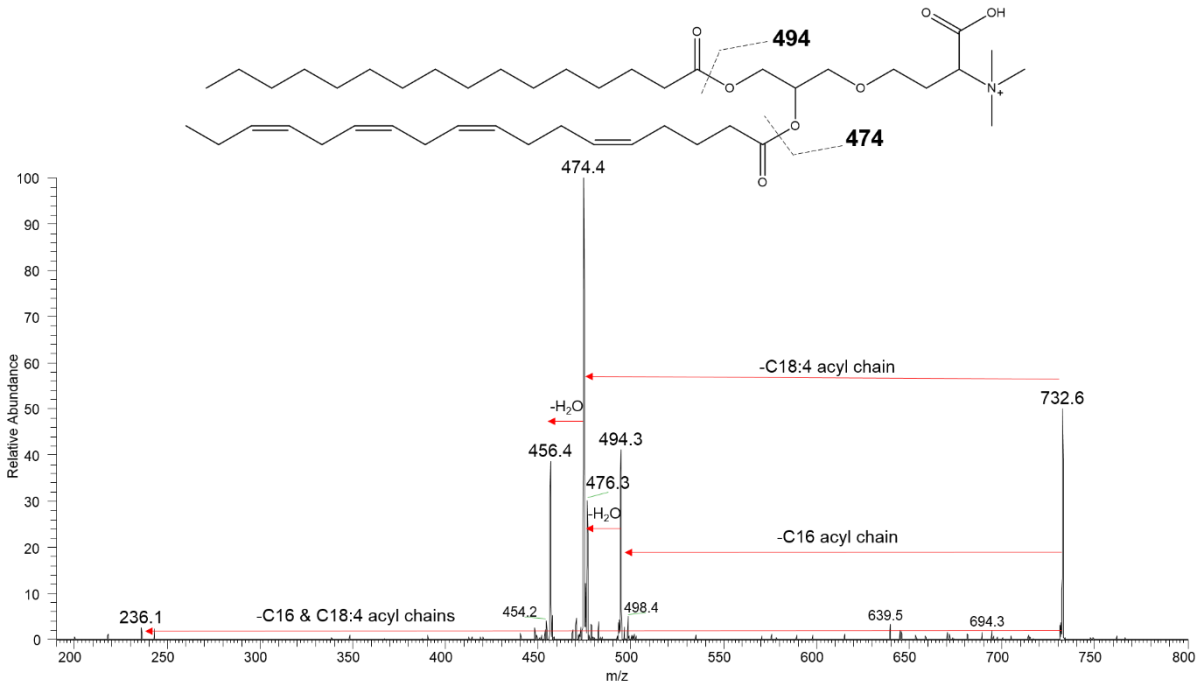

Figure 3.5.2-2. MS/MS of m/z 732.5 putatively identified as DGTS(16:0/18:4). Inset is shown the structure of this lipid and fragmentations that yield the ions 474 and 494.

In the positive ion mode mass spectrum, a peak with m/z 893.3 was also detected (**Figure 3.5.1-2**) which was putatively identified as the $[M+H]^+$ adduct of Chlorophyll a. The MS/MS spectrum of m/z 893.3 gave rise to the ion with m/z 615.2 which was the major fragment. In **Figure 3.5.2-3**, the MS/MS spectrum of m/z 893.3 is shown which confirms the identification of Chlorophyll a based on the fragmentation pattern. The major fragment could possibly be produced as shown in **Figure 3.5.2-3** while the fragments 583.3 and 555.1 could be produced by further neutral loss of CH_3OH and $C_2H_4O_2$, respectively.

Chlorophyll b was also identified in a similar fragmentation pattern as Chlorophyll a. Chlorophyll b was detected as $[M+H]^+$ adduct with m/z 907.5 in the positive ion mode and upon fragmentation yielded the ion with m/z 629.2.

The ion with m/z 941.5 in the positive ion mode mass spectrum was putatively identified as the $[M+Na]^+$ adduct of DGDG(18:1/16:0) and in **Figure 3.5.2-4** the MS/MS spectrum confirmed the presence of this lipid since the major fragments detected corresponded to losses of the fatty acids chains.

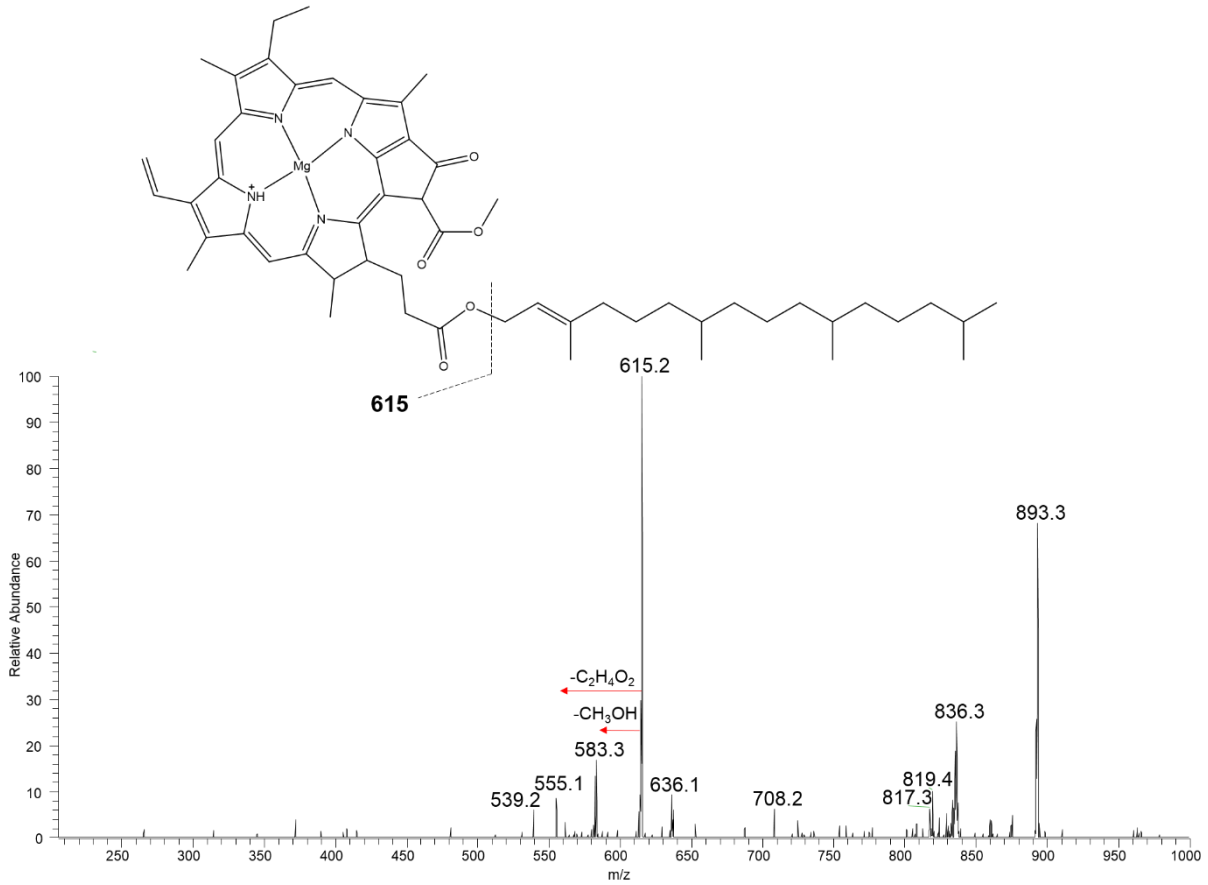

Figure 3.5.2-4. MS/MS spectrum of m/z 893.5 putatively identified as Chlorophyll a. Inset is shown the structure of Chlorophyll a and the fragmentation that could produce the major fragment ion 615.2.

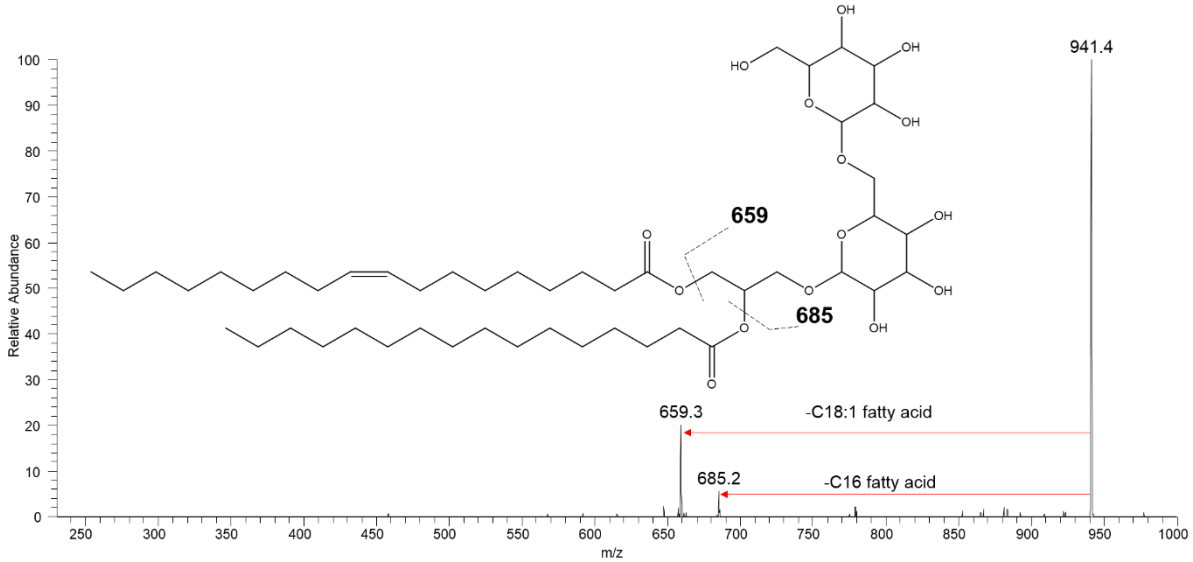

Figure 3.5.2-3. MS/MS spectrum of m/z 941.5 putatively identified as DGDG(18:1/16:0). Inset is shown the structure of DGDG(18:1/16:0). This ion was detected as Na^+ adduct.

In the negative ion mode mass spectrum the ion with m/z 793.5 is the most intense and it was putatively identified as the $[M-H]^-$ adduct of SQDG(16:0/16:0) lipid. In **Figure 3.5.2-5**, the MS/MS spectrum of m/z 793.5 is shown and it can be seen that the main fragment corresponds to the loss of C16 fatty acid that yields the ion with m/z 537.4 and the loss of the sugar unit that yields the ion with m/z 225.3. This latter ion is also characteristic of SQDG lipids, thus, its detection indicates the presence of SQDG lipids.

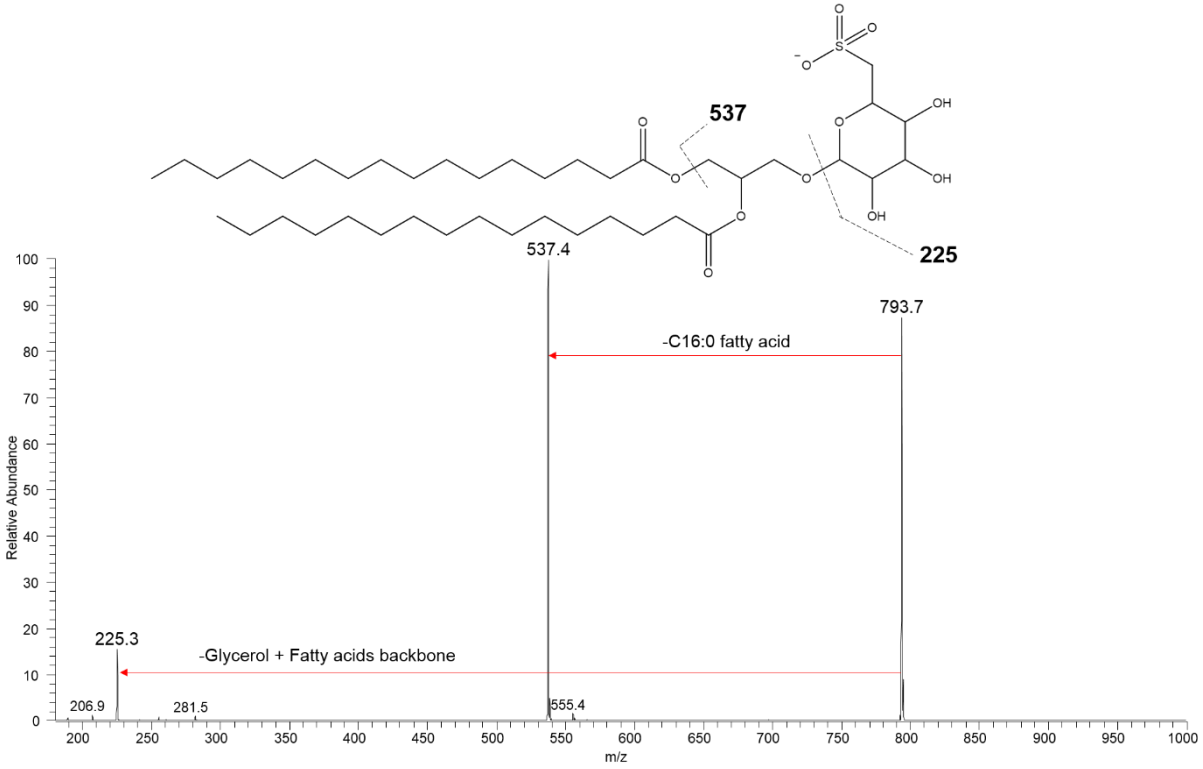

Figure 3.5.2-5. MS/MS spectrum of m/z 793.5 putatively identified as SQDG(16:0/16:0). Inset is shown the structure of this lipid and fragmentations that yield the ions 537 and 225.

The ion with m/z 745.5 in the negative ion mode was putatively identified as PG(18:2/16:0). The MS/MS spectrum of this ion can be seen in **Figure 3.5.2-6**. The neutral loss of C18:2 acyl chain yielded the ion with m/z 483.5 and upon dehydration, the ion with m/z 465.3 was produced. Also, the neutral loss of C16 acyl chain yielded the ion with m/z 507.3 and subsequent dehydration yielded the ion 489.1. Finally, the ion with m/z 279.0 was detected which corresponds to the C18:2 fatty acid. The C16 fatty acid fragment was not detected as ion with m/z 255 since the trapping of ions started from m/z 250, thus this ion was not trapped efficiently inside the ion trap.

Figure 3.5.2-6. MS/MS spectrum of m/z 745.5 putatively identified as PG(18:2/16:0). Inset is shown the structure of PG(18:2/16:0) and fragmentations that yield the ions 483 and 507.

Another class of lipids that were identified in the negative ion mode was the phosphatidylinositols (PI). The ion with m/z 835.5 in the negative ion mode was putatively identified as PI(18:1/16:0). The MS/MS spectrum of this ion is shown in **Figure 3.5.2-7**. The neutral loss of C16 acyl chain yields the ion with m/z 597.5 and upon loss of H_2O the fragment with m/z 579 is produced. The fragment ion with m/z 553 could have been produced by the loss of water and the C18:1 acyl chain. The ion with m/z 435.1 could have been produced from the fragment 597.5 upon cleavage of O-sugar bond. The ion with m/z 416.7 could have been the product of C16 fatty acid loss and subsequent cleavage of O-sugar bond. Neutral loss of C18:1 fatty acid chain and subsequent cleavage of O-sugar bond are possibly the fragmentation reactions that took place to produce the ion with m/z 390.7.

All the species that are reported as identified in this work, have been confirmed by literature results, manual interpretation of MS/MS spectra and searches in mass spectra libraries.

In **Table 3.5.2-1** all the species that were identified in *C. reinhardtii* cells are presented along with their characteristic fragment ions. The majority of the identified species consist of membrane lipids, however, chlorophylls and their breakdown products were also identified.

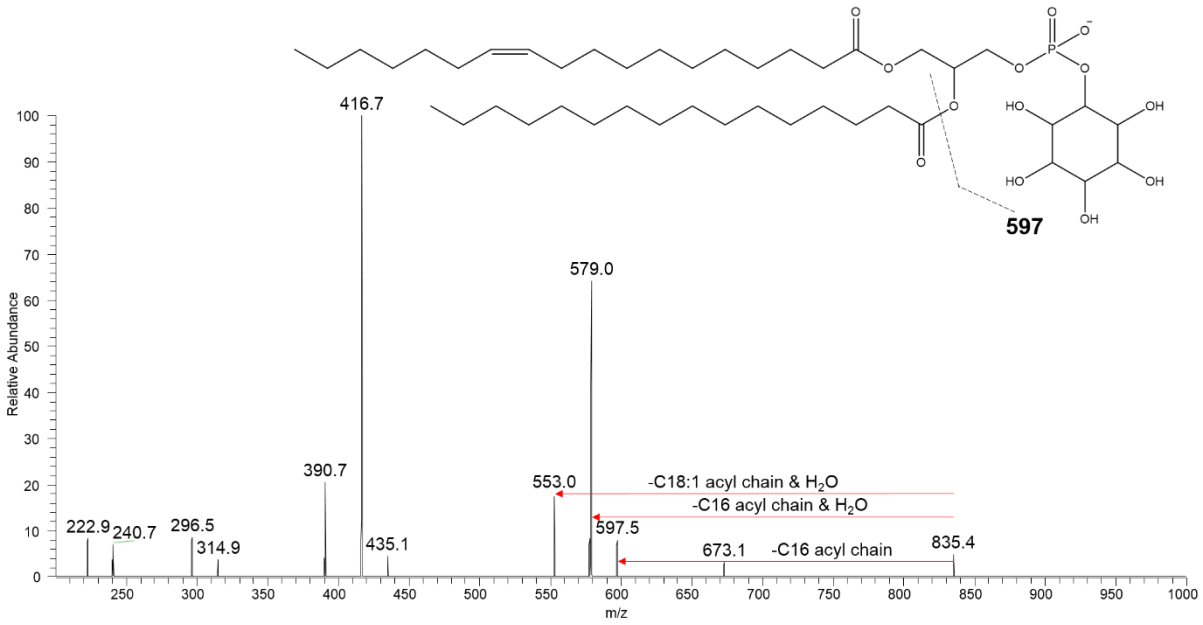

Figure 3.5.2-7. MS/MS spectrum of m/z 835.5 putatively identified as PI(18:1/16:0). Inset is shown the structure of PI(18:1/16:0) and fragmentations that yield the ion 597.

Table 3.5.2-1. Annotations of species identified in *C. reinhardtii* cells

Experimental m/z	Theoretical m/z	Adduct	Identified Species
613.3	613.23	$[M-H]^-$	Chlorophyllide a
627.3	627.21	$[M-H]^-$	Chlorophyllide b and/or Primary fluorescent chlorophyll catabolite
629.3	629.23	$[M-H]^-$	7-hydroxychlorophyllide a
643.3	643.20	$[M-H]^-$	OH-Chlorophyll b
741.5	741.47	$[M-H]^-$	PG(18:3/16:1)
743.5	743.49	$[M-H]^-$	PG(18:3/16:0)
745.5	745.50	$[M-H]^-$	PG(18:2/16:0)
747.5	747.52	$[M-H]^-$	PG(18:1/16:0)
761.5	761.45	$[M-H]^-$	SQDG(14:2/16:0)
791.5	791.50	$[M-H]^-$	SQDG(16:0/16:1)
793.5	793.51	$[M-H]^-$	SQDG(16:0/16:0)
815.5	815.50	$[M-H]^-$	SQDG(18:3/16:0)
817.5	817.51	$[M-H]^-$	SQDG(18:2/16:0)
819.5	819.53	$[M-H]^-$	SQDG(18:1/16:0)
821.5	821.55	$[M-H]^-$	SQDG(18:0/16:0)
831.5	831.53	$[M-H]^-$	SQDG(19:2/16:0)
835.5	835.53	$[M-H]^-$	PI(18:1/16:0)
847.4	847.56	$[M-H]^-$	SQDG(20:1/16:0)
849.4	849.58	$[M-H]^-$	SQDG(20:0/16:0)
474.5	474.38	$[M+H]^+$	LysoDGTS(16:0)
496.4	496.36	$[M+H]^+$	LysoDGTS(18:3)
593.3	593.28	$[M+H]^+$	Pheophorbide a

704.5	704.55	$[M+H]^+$	DGTS(32:4)[a]
706.5	706.56	$[M+H]^+$	DGTS(32:3)[a]
708.5	708.58	$[M+H]^+$	DGTS(32:2)[a]
710.5	710.59	$[M+H]^+$	DGTS(16:0/16:1)
732.5	732.58	$[M+H]^+$	DGTS(16:0/18:4)
734.5	734.59	$[M+H]^+$	DGTS(16:0/18:3)
736.5	736.61	$[M+H]^+$	DGTS(16:0/18:2)
738.5	738.62	$[M+H]^+$	DGTS(16:0/18:1)
748.5	748.61	$[M+H]^+$	DGTS(16:0/19:3)
750.5	750.62	$[M+H]^+$	DGTS(16:0/19:2)
754.5	754.56	$[M+H]^+$	DGTS(18:3/18:4)
756.5	756.58	$[M+H]^+$	DGTS(36:6)[a]
758.5	758.59	$[M+H]^+$	DGTS(36:5)[a]
760.6	760.61	$[M+H]^+$	DGTS(36:4)[a]
762.5	762.62	$[M+H]^+$	DGTS(36:3)[a]
764.5	764.60	$[M+H_2O]^+$	DGTS(16:0/19:4)
766.5	766.62	$[M+H_2O]^+$	DGTS(16:0/19:3)
768.5	768.63	$[M+H_2O]^+$	DGTS(16:0/19:2)
871.3	871.57	$[M+H]^+$	Pheophytin a
893.3	893.54	$[M+H]^+$	Chlorophyll a
907.2	907.51	$[M+H]^+$	Chlorophyll b
915.5	915.53	$[M+Na]^+$	Chlorophyll a
941.5	941.62	$[M+Na]^+$	DGDG(18:1/16:0)

[a]Mixture of isomers

3.5.3 ESI-MS analysis of *C. reinhardtii* cells

To verify the identity of lipids detected by DeSSI-MS, an ESI-MS analysis was also undertaken. The procedure of extracting the lipids from cells grown under control conditions was described in **Section 2.5**. In **Figure 3.5.3-1** the positive ion mode spectra obtained by DeSSI-MS (A), ESI-MS with 80 % acetone as the extraction solvent (B) and ESI-MS with ACN/DMF 1:1 as the extraction solvent (C) can be seen. In all cases it is clear that the lipid profiles obtained are the same. The same lipid profiles were also obtained in the negative ion mode (**Figure A.5-1**). Also, the MS/MS spectra obtained by DeSSI-MS were the same as those obtained by ESI-MS. Thus, the chemical information acquired by these two techniques was the same, however, DeSSI-MS allowed a more rapid lipid profile characterization.

In **Figure 3.5.3-1** the presence of ions with m/z 809 obtained using DeSSI-MS and ESI-MS with ACN/DMF 1:1 as the extraction solvent are observed. These ions correspond to adducts of the detected lipids with mass difference of 75 amu. The exact origin of these adducts has not been elucidated, however, it seems to be solvent-

dependent since when 80 % acetone was used as the extraction solvent then these clusters did not appear. Interestingly, these clusters were not observed in positive ion

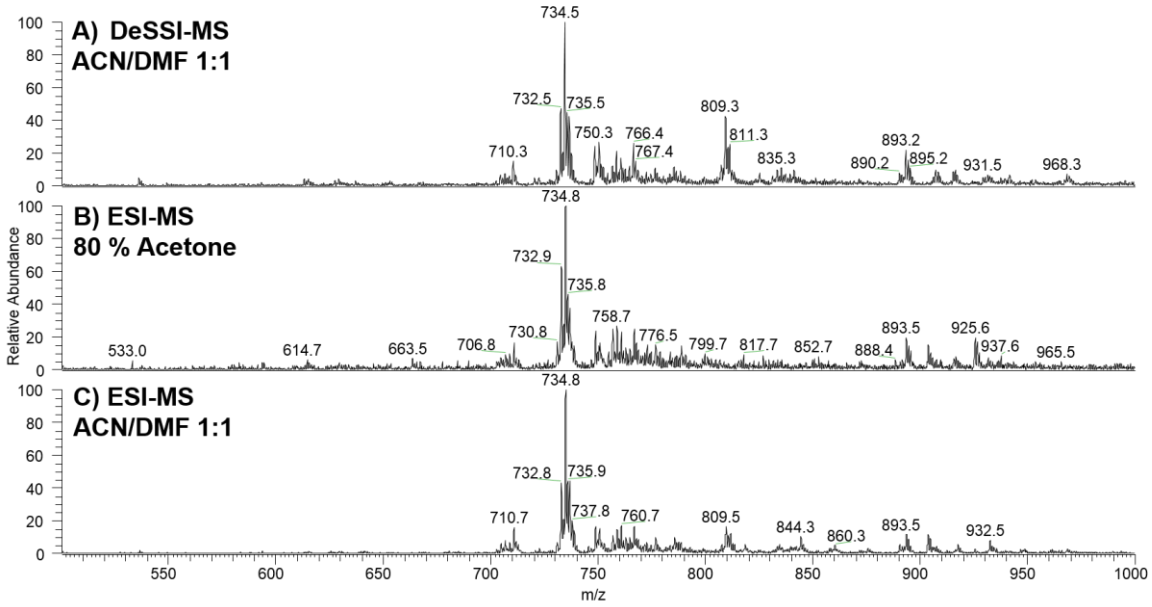

Figure 3.5.3-1. Positive ion mode spectra of *C. reinhardtii* cells obtained by A) DeSSI-MS using ACN/DMF 1:1 as the spraying solvent, B) ESI-MS using 80 % acetone as the extraction solvent and C) ESI-MS using ACN/DMF 1:1 as the extraction solvent.

mode spectra obtained by DeSSI-MS of Synechocystis cells whereas the detected lipids corresponded to Na^+ adducts of neutral MGDG and DGDG lipids.

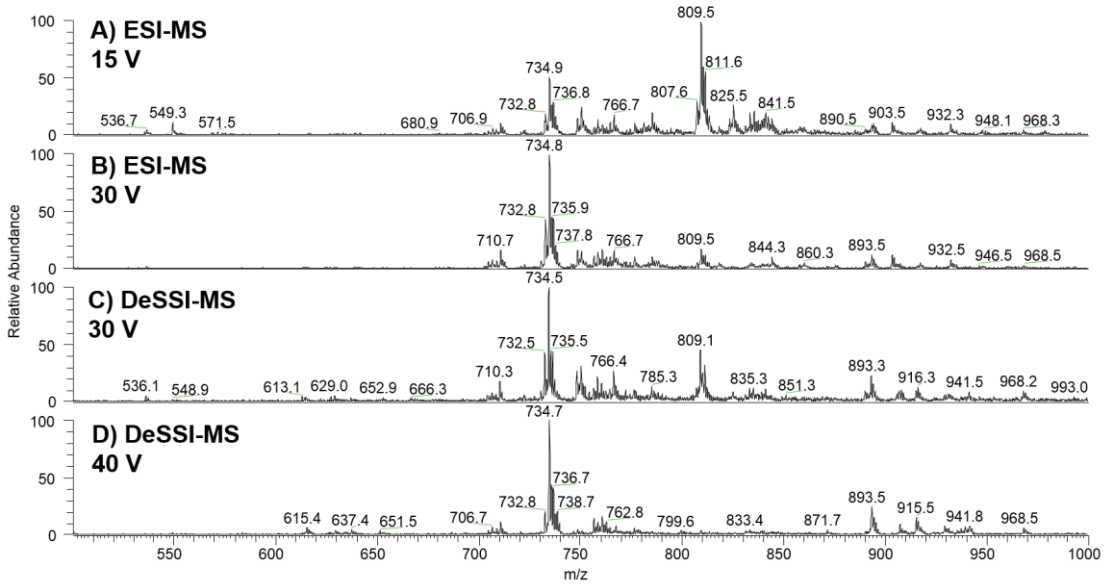

Figure 3.5.3-2. Positive ion mode spectra obtained by A) ESI-MS using ACN/DMF 1:1 as the extraction solvent and 15 V of ion transfer capillary voltage, B) ESI-MS using ACN/DMF 1:1 as the extraction solvent and 30 V of ion transfer capillary voltage, C) DeSSI-MS with ACN/DMF 1:1 as the spraying solvent and 30 V of ion transfer capillary voltage and D) DeSSI-MS with ACN/DMF 1:1 as the spraying solvent and 40 V of ion transfer capillary voltage.

Also, by increasing the ion transfer capillary voltage, these clusters in the m/z region 800-850 were diminished as it can be seen in **Figure 3.5.3-2**.

3.6 DeSSI-MS lipid profiles of *Synechocystis* sp PCC6803 cells

3.6.1 Lipid profiles

In **Figure 3.6.1-1** and **Figure 3.6.1-2** the mass spectra obtained in positive and negative ion mode, respectively, by DeSSI-MS analysis of *Synechocystis* cells are shown. In the positive ion mode mass spectra, intense peaks can be observed in the m/z ranges 700-800 and 850-950. The lipids that were identified to be present included MGDG and DGDG lipids along with Chlrophyll a. Chlorophyll b related peaks were not observed since it is known that cyanobaceteria only contain Chlorophyll a (http://www.ucmp.berkeley.edu/glossary/gloss3/pigments.html).

In the negative ion mode mass spectra, the same classes of lipids as in the case of *C. reinhardtii* cells were identified, which included PG and SQDG.

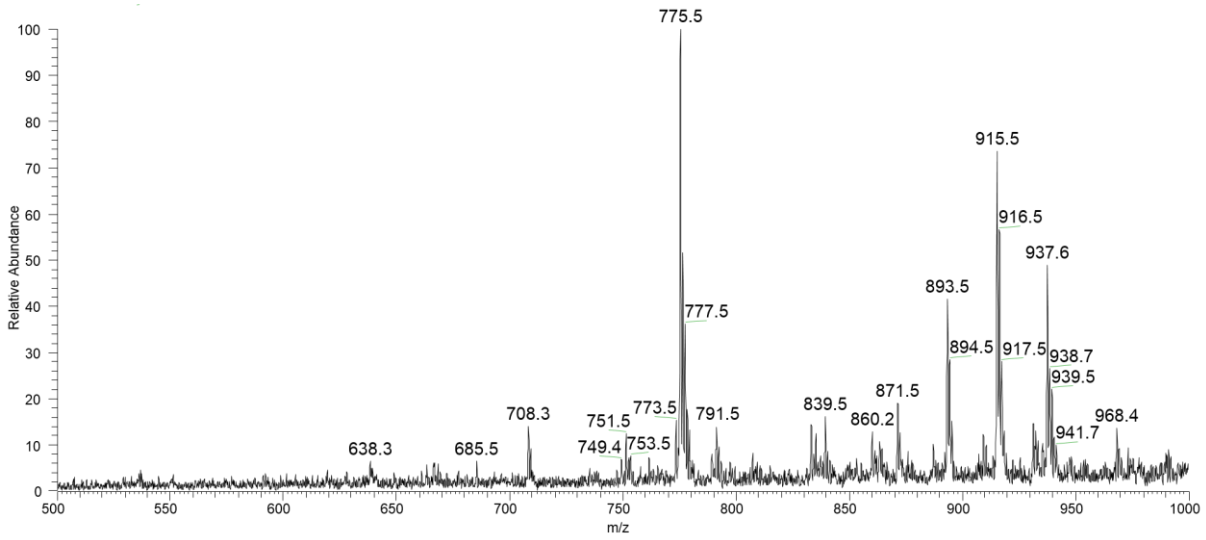

Figure 3.6.1-1. Positive ion mode mass spectrum obtained by DeSSI-MS analysis of *Synechocystis* sp PCC6803 cells.

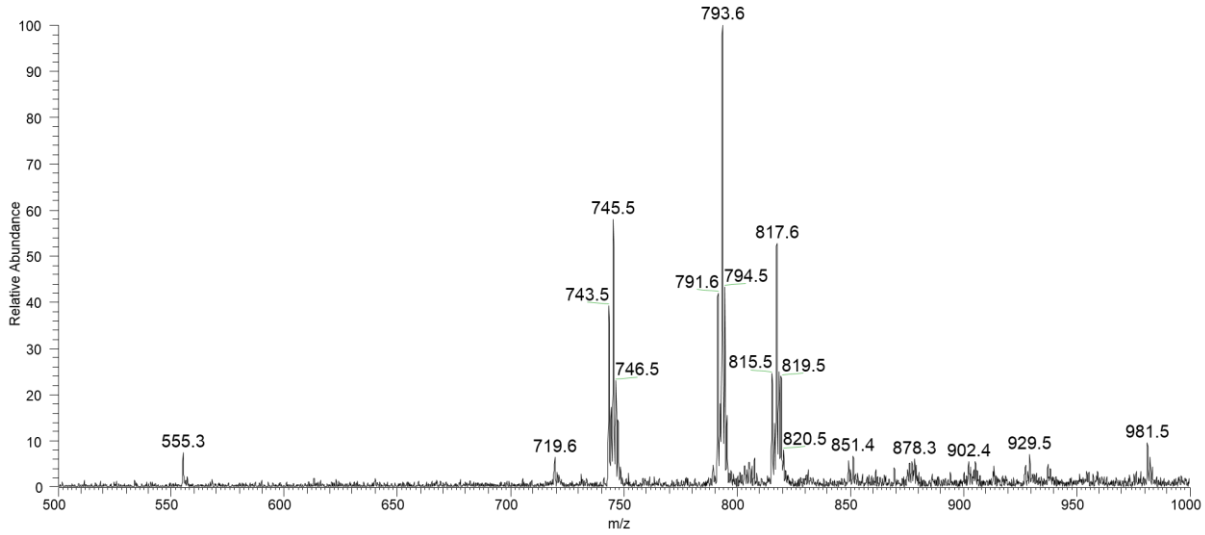

Figure 3.6.1-2. Negative ion mode mass spectrum obtained by DeSSI-MS analysis of *Synechocystis* sp PCC 6803 cells.

3.6.2 Lipids identification

Identification of lipids was also based on literature results [30,38,40–42,44], mass spectral library searches and manual interpretation of the MS/MS spectra acquired.

In **Figure 3.6.2-** the MS/MS spectrum of ion with m/z 775.7 is shown. This ion was putatively identified as the Na^+ adduct of MGDG(18:3/16:0) or MGDG(18:2/16:1) MGDG(18:1/16:2) or MGDG(18:0/16:3). The MS/MS spectrum cannot provide information on the position of the double bonds and the position where each fatty acid is esterified (sn-1 or sn-2)[41], however, the aforementioned isomers can be distinguished based on the fragments. In **Figure 3.6.2-** the MS/MS spectrum of ion 775.7 gave the fragments 497.4 and 519.4 which correspond to the neutral losses of C18:3 fatty acid and C16:0 fatty acid, respectively. Thus, this lipid was identified as MGDG(18:3/16:0).

The ion with m/z 893.5 in the positive ion mode spectrum of *Synechocystis* cells was identified as the $[M+H]^+$ adduct of Chlorophyll a and its MS/MS spectrum yielded the same fragment ions as the ones obtained from *C. reinhardtii* cells. However, in the positive ion mode spectrum of *Synechocystis* a very intense peak with m/z 915.5 was observed which was putatively identified as the $[M+Na]^+$ of Chlorophyll a. In **Figure 3.6.2-** the MS/MS spectrum of ions with m/z 893.5 and 915.5 are shown.

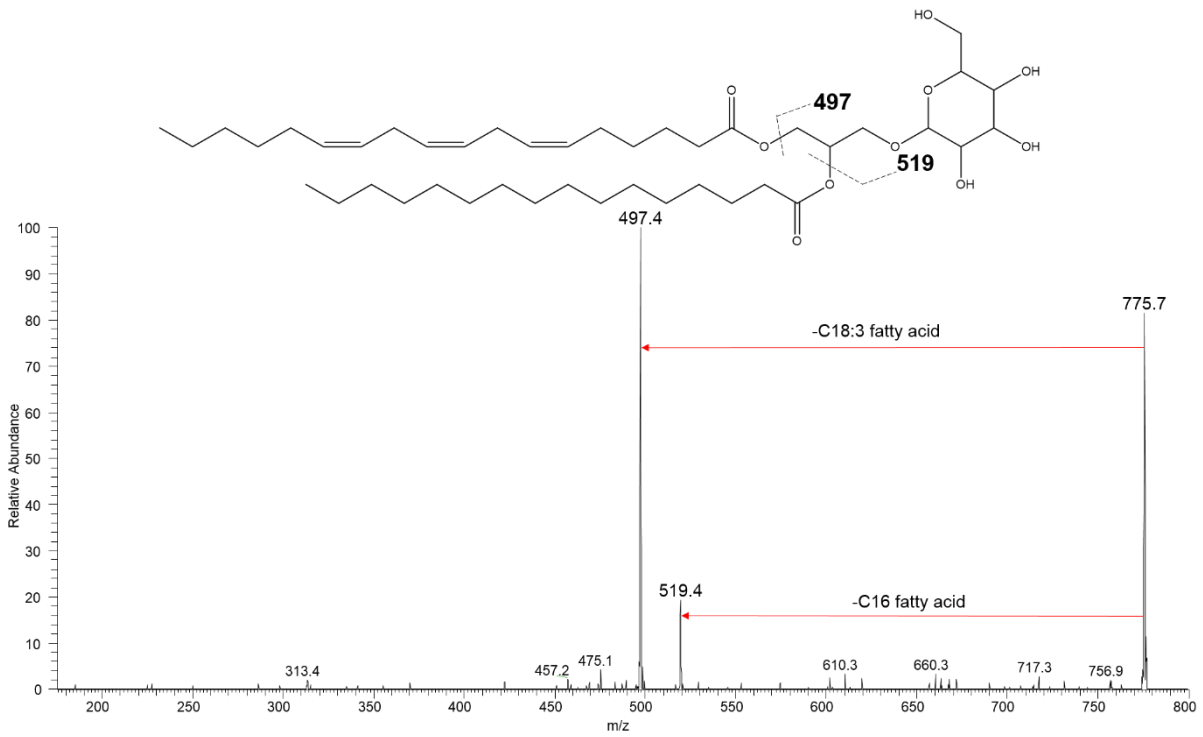

Figure 3.6.2-1. MS/MS spectrum of ion 775.7 identified as the Na^+ adduct of MGDG(18:3/16:0). Inset is shown the structure of MGDG(18:3/16:0).

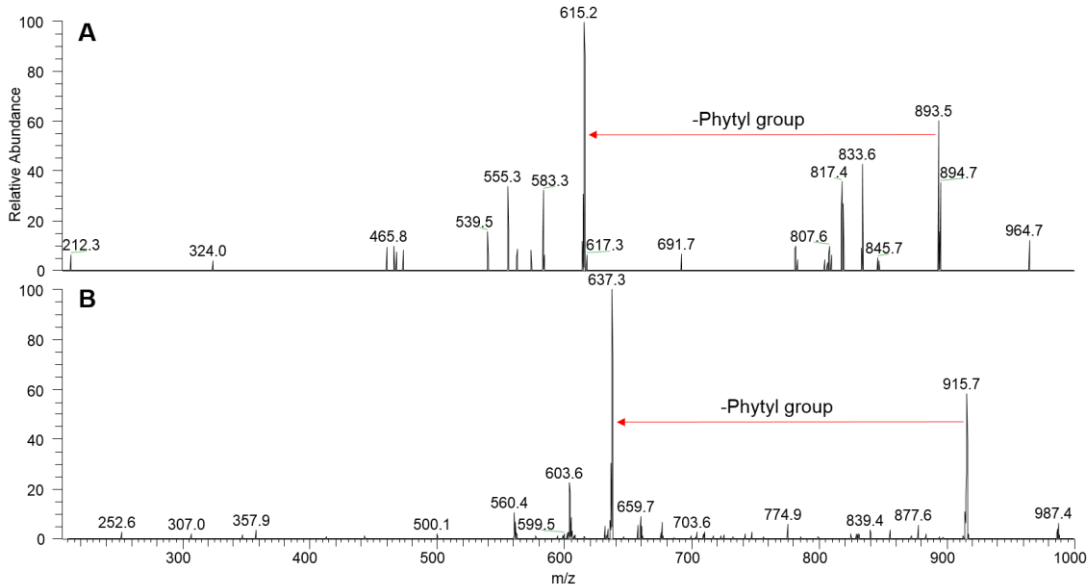

Figure 3.6.2-2. MS/MS spectra of m/z 893.5 (A) and 915.7 (B) identified as $[M+H]^+$ and $[M+Na]^+$ adducts, respectively, of Chlorophyll a.

The main fragment of m/z 893.5 (Chlorophyll a, $[M+H]^+$ adduct) is 615.2 which corresponds to the neutral loss of the phytyl group. The main fragment of m/z 915.7, which is 22 amu higher than m/z 893.5, is 637.3, which is 22 amu higher than the

615.2, thus, the fragment 637.2 corresponds to the neutral loss of phytyl group from the Na^+ adduct of Chlorophyll a.

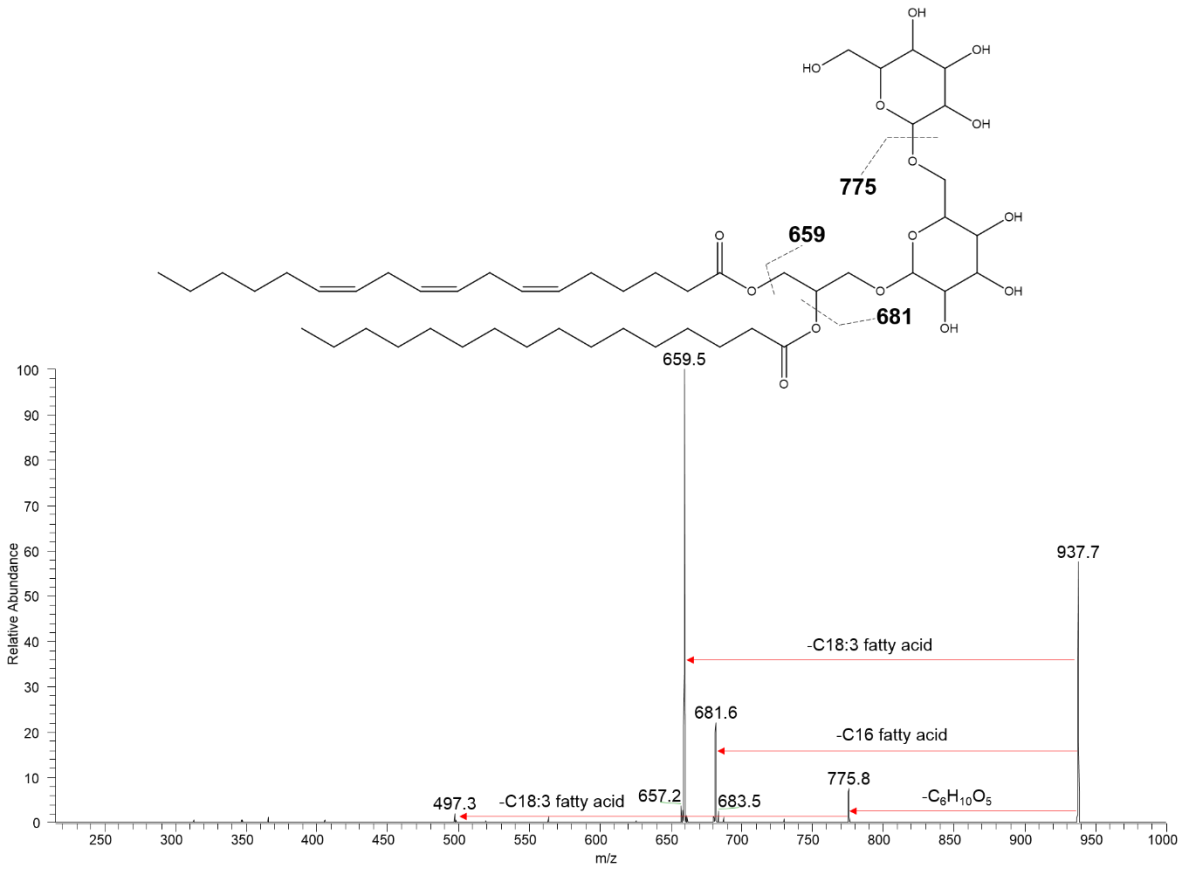

Figure 3.6.2-1. MS/MS spectrum of m/z 937.7 which was identified as $[M+Na]^+$ adduct of MGDG(34:3). Above the spectrum is shown the structure of one isomer of this lipid.

The MS/MS spectrum of ion with m/z 937.7 (**Figure 3.6.2-1**) gave the fragments 775.8, 683.5, 681.6, 659.5, 657.2 and 497.3. The ion 937.7 was putatively identified as the Na^+ adduct of DGDG(18:3/16:0) or DGDG(18:2/16:1) or DGDG(18:1/16:2) or DGDG(18:0/16:3). The fragments 681.6 and 659.5 indicate the neutral loss of C16 and C18:3 fatty acids, respectively. The fragments 683.5 and 657.2 were produced upon neutral loss of C16:1 and C18:2 fatty acids, respectively. The fragment 497.3 corresponds to the neutral loss of C18:3 fatty acid from the ion 775.8 which was produced upon loss of $C_6H_{10}O_5$ from the parent ion. Thus, the ion 937.7 was identified as a mixture of $[M+Na]^+$ adducts of DGDG(18:2/16:1) and DGDG(18:3/16:0).

Lipids in the negative ion mode were the same as those identified in *C. reinhardtii* cells. The MS/MS spectra obtained were the same with those from the aforementioned cells.

In **Table 3.6.2-1** the ions that were identified are summarized.

Table 3.6.2-1. Annotation of species identified in *Synechocystis* sp PCC 6803 cells.

Experimental m/z	Theoretical m/z	Adduct	Identified Species
719.4	719.48	$[M-H]^-$	PG(16:1/16:0)
743.5	743.49	$[M-H]^-$	PG(18:3/16:0)
745.5	745.50	$[M-H]^-$	PG(18:2/16:0)
747.5	747.52	$[M-H]^-$	PG(18:1/16:0)
791.5	791.50	$[M-H]^-$	SQDG(16:0/16:1)
793.5	793.51	$[M-H]^-$	SQDG(16:0/16:0)
803.5	803.50	$[M-H]^-$	SQDG(17:2/16:0)
805.5	805.51	$[M-H]^-$	SQDG(17:1/16:0)
807.5	807.53	$[M-H]^-$	SQDG(17:0/16:0)
815.5	815.50	$[M-H]^-$	SQDG(18:3/16:0)
817.5	817.51	$[M-H]^-$	SQDG(18:2/16:0)
819.5	819.53	$[M-H]^-$	SQDG(18:1/16:0)
751.5	751.53	$[M+Na]^+$	MGDG(16:0/16:1)
773.5	773.52	$[M+Na]^+$	MGDG(18:3/16:1)
775.5	775.53	$[M+Na]^+$	MGDG(18:3/16:0)
777.5	777.55	$[M+Na]^+$	MGDG(18:2/16:0)
779.5	779.56	$[M+Na]^+$	MGDG(18:1/16:0)
871.3	871.57	$[M+H]^+$	Pheophytin a
893.3	893.54	$[M+H]^+$	Chlorophyll a
915.5	915.53	$[M+Na]^+$	Chlorophyll a
937.6	937.59	$[M+Na]^+$	DGDG(34:3)[a]
939.6	939.60	$[M+Na]^+$	DGDG(18:2/16:0)

[a]Mixture of isomers

3.7 Effect of stress conditions on membrane lipids of microorganism cells

Glycerolipids are the major components of photosynthetic membranes that have been conserved in cyanobacteria and green algae during evolution. In **Sections 3.5** and **3.6** the main glycerolipids that consitute the photosynthetic and extraplastidial membranes of *C. reinhardtii* and *Synechocystis* cells were introduced. The chloroplasts of these cells contain low amounts of PG and PI lipids and high amounts of MGDG, DGDG and SQDG lipids. MGDG and DGDG lipids fall in the category of neutral galactoglycerolipids and they are the most abundant lipids in photosynthetic membranes. These lipids possess vital roles in the stabilization of the membrane lipid bilayer.[39] The overall photosynthetic membranes integrity is based on an appropriate proportion of galactoglycerolipids and on a smaller proportion of charged polar lipids such as SQDG and PG.[39] Apart from stabilizing the membrane lipid bilayers, these lipids possess vital roles in biological activities of the cells such as secretion, transportation, signal transduction, photosynthetic light harvesting and electron transfer.[30] The DGTS lipids detected in *C. reinhardtii* cells are components of extraplastidial membranes and substitute for phosphatidylcholine that is normally present in these membranes.[41]

3.7.1 Lipid profile and cells concentration

Absolute quantitative measurements are not straightforward in our case since the analytes detected are extracted during the impact of the solvent plume on the cells. For quantitative measurements, extraction of lipids from a known number of cells and subsequent quantification by using external or internal standards should be followed.

In these experiments we were investigating the relative changes of membrane lipids of the same class that differed by the number of double bonds, e.g. MGDG(34:2)/MGDG(34:3). When analyzing samples with different cell concentrations, the final number of cells that are present on the glass slide for DeSSI-MS analysis is different, thus, the absolute intensity of lipids detected will differ. However, if these cells

in the different samples have been grown under the same conditions, then the lipid profile should stay the same since these cells have the same composition in membrane lipids. Also, the ratio of two lipids should stay the same. This can be seen in **Figure 3.7.1-1** where starting from a cell sample that had known number of cells and performing

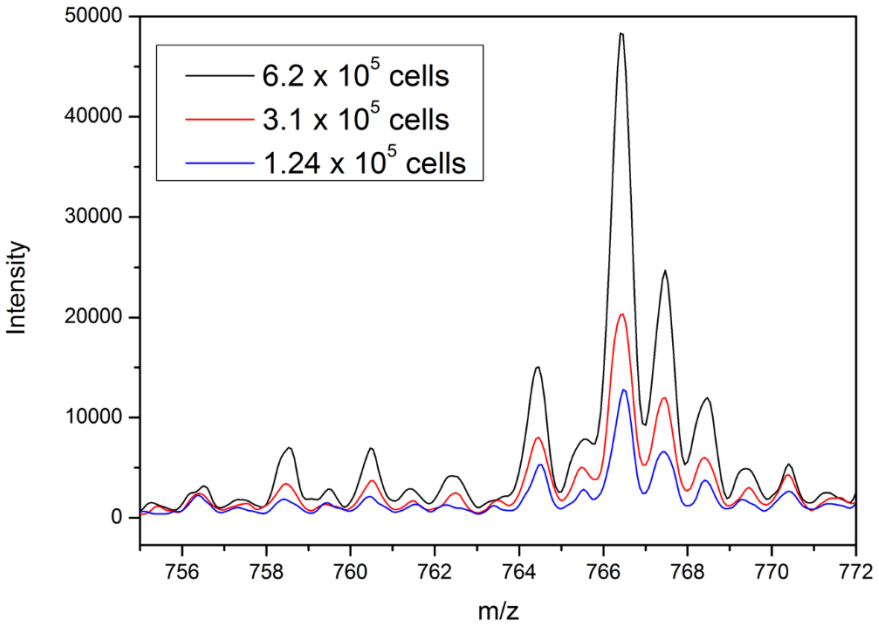

Figure 3.7.1-1. DeSSI-MS spectra obtained after the analysis of *C. reinhardtii* cells spots that varied in the number of cells that were present on the spot.

serial dilutions, we get different number of cells on the spot. It can be clearly observed that the relative ratio of lipids in **Figure 3.7.1-1** is independent from the number of cells that are on the spot that is analyzed. Of course, the absolute intensity of the lipids differs, which is an expected outcome since more lipids will be desorbed from a higher number of cells. Thus, cell counting in each sample analyzed, which is a time-consuming process, was not necessary for monitoring relative changes of membrane lipids.

3.7.2 Effect of toxic metals and metalloids on *C. reinhardtii* cells membrane lipids

The effect of the toxic metals such as Pb and Cd and the metalloid As on the membrane lipid profile of *C. reinhardtii* cells was investigated. These unicellular eukaryotic green

algae cells are used extensively as model organisms for studying physiological processes such as photosynthetic activity and respiration.[45] The cells consist of a single nucleus, chloroplasts where photosynthesis is taking place, contractile vacuoles, two flagella and a thin cell wall which is composed from carbohydrates and glycoproteins[46,47]. The cells were grown in liquid cultures that contained non-lethal concentrations of $Pb(NO_3)_2$, $Cd(NO_3)_2$, $AsHNa_2O_4 \cdot 7H_2O$ and $NaAsO_2$. The addition of these salts resulted in various concentrations of Pb(II), Cd(II), As(V) and As(III). Control experiments were cultivated in three independent cultures (biological replicates) and from each culture two small aliquots were taken. Each aliquot was analyzed in triplicate (technical replicates) by DeSSI-MS, thus, resulting in a total number of 18 analyzed control spots (3 biological replicates x 2 aliquots each x 3 technical replicates each). For the metal and metalloid incubated cells experiments, one culture for each concentration of contaminant was cultivated and two small aliquots from each culture were taken. Subsequently, each aliquot was analyzed in triplicate (technical replicates), thus, resulting in a total number of 6 analyzed spots for each concentration of the contaminant. In the following sections the effect of each metal and metalloid contaminant on the membrane lipids profile will be presented and discussed.

3.7.2.1 Effect of Pb(II) on membrane lipids of *C. reinhardtii* cells

In **Figure 3.7.2.1-1** and **Figure 3.7.2.1-2** the mass spectra in the positive and negative ion mode, respectively, obtained by DeSSI-MS analysis of *C. reinhardtii* cells grown

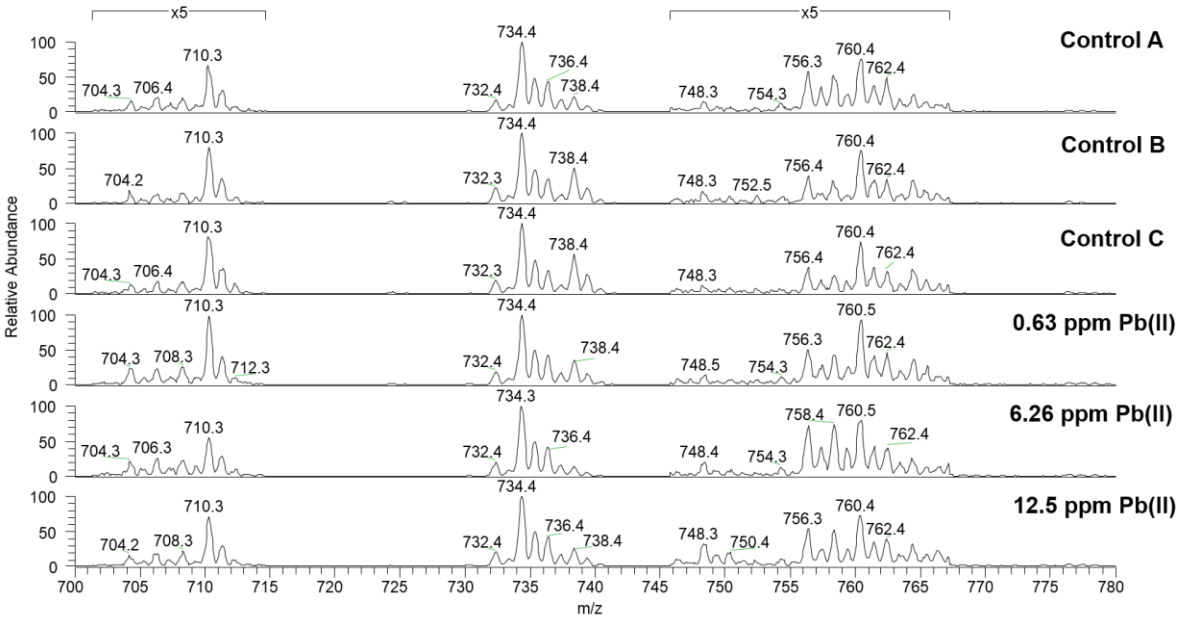

Figure 3.7.2.1-1. Positive ion DeSSI-MS spectra obtained after the analysis of control and lead-incubated cultures.

under normal conditions (Control A, B & C) and in the presence of various concentrations of Pb(II) are shown.

No significant differences were observed for the control and lead-incubated samples in both positive and negative ion modes.

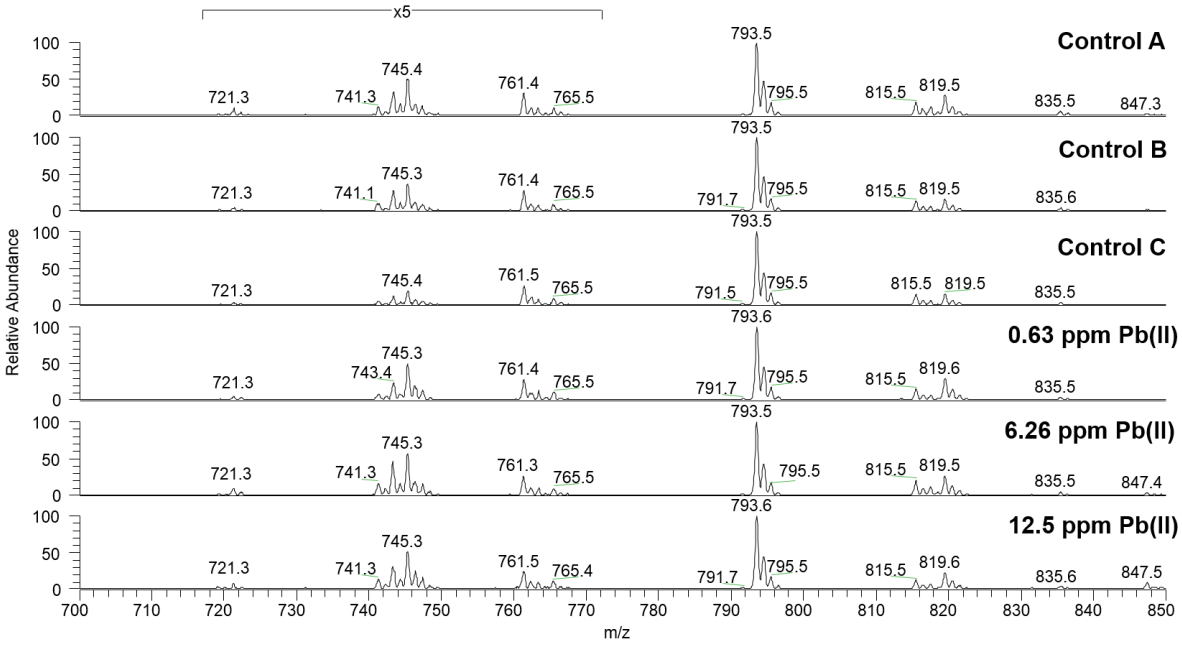

Figure 3.7.2.1-2. Negative ion mode DeSSI-MS spectra obtained after the analysis of control and lead-incubated cultures.

Although lead has been reported to cause reduction of photosynthesis and alteration of thylakoidal, mitochondrial and nuclear structures in concentrations of 1-20 μM [45], in our experiments with Pb(II) concentrations in the range of 3-60 μM the membrane lipid profile did not seem to change. Also, Pb(II) has been reported to cause production of reactive oxygen species which ultimately lead to lipid peroxidation.[48] However, no peroxidized lipids were detected in our experiments.

3.7.2.2 Effect of Cd(II) on membrane lipids of *C. reinhardtii* cells

Cadmium ions can be adsorbed on the cell wall while at higher concentrations some ions can enter the cells and cause damage.[46] The toxicity of cadmium on *Chlamydomonas* strains has been studied and it has been found that inhibition of growth, ultrastructural cellular changes, starch accumulation and decrease of photosynthetic activity.[49] Detoxification mechanisms include the complexation of cadmium with phytochelatins.[50]

The effect of Cd(II) on membrane lipids of *C. reinhardtii* cells was obvious from the positive and negative ion mode DeSSI-MS mass spectra (**Figure 3.7.2.2-2** and **Figure 3.7.2.2-1**). More specifically, in the positive ion mode where the DGTS lipids are prevalent, a sharp increase in the relative intensity of DGTS(34:1) (m/z 738.5) compared to DGTS(34:3) (m/z 734.5) is observed. Also, increases of relative intensities of DGTS(36:4) (m/z 760.5) compared to DGTS(36:6) (m/z 756.5) can be observed. These differences are presented graphically in **Figure 3.7.2.2-3**.

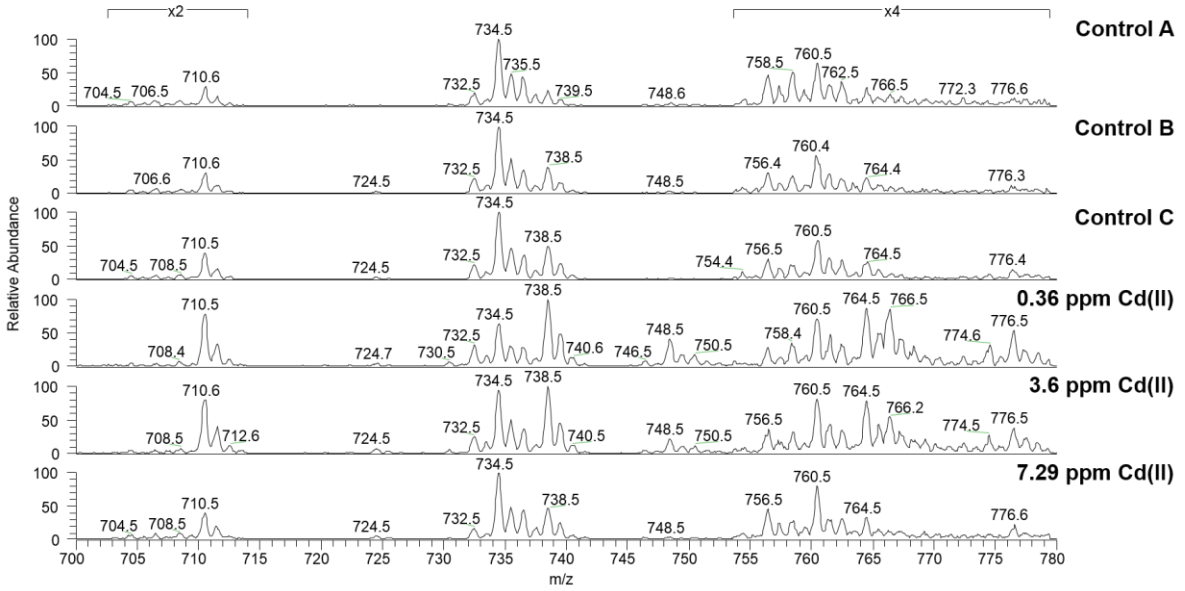

Figure 3.7.2.2-1. Positive ion mode DeSSI-MS spectra obtained after the analysis of control and cadmium-incubated cultures.

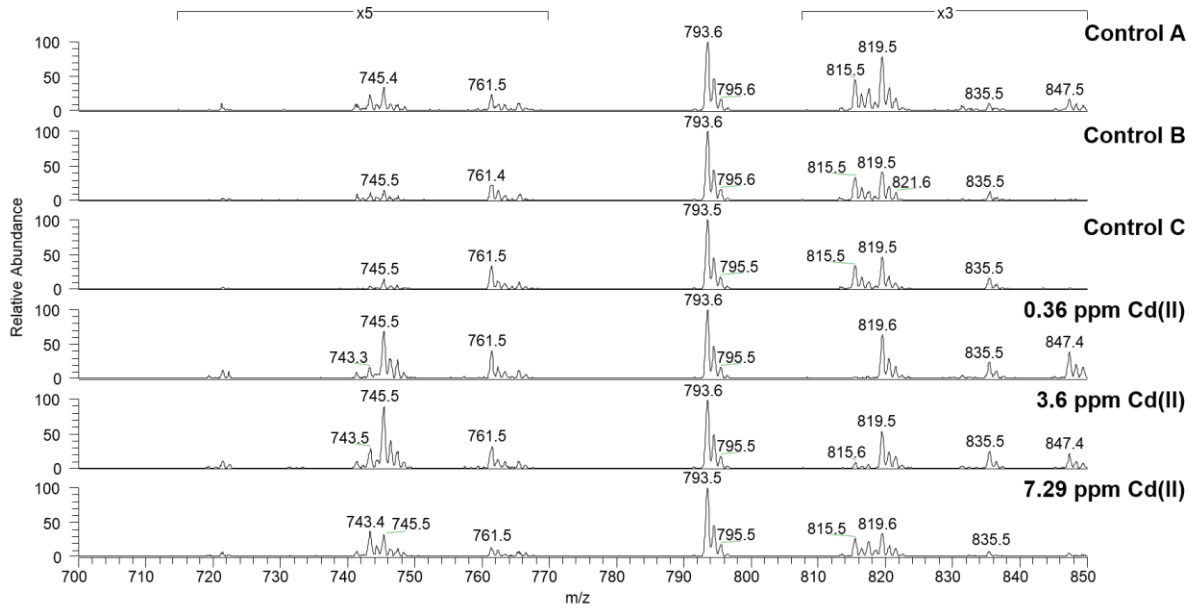

Figure 3.7.2.2-2. Negative ion mode DeSSI-MS spectra obtained after the analysis of control and cadmium-incubated cultures.

In the negative ion mode spectra of control and cadmium-incubated cells, differences in the relative intensities of PG(34:2) (m/z 745.5) compared to PG(34:3) (m/z 743.5) and SQDG(34:1) (m/z 819.5) compared to SQDG(34:3) (m/z 815.5) are observed. In **Figure 3.7.2.2-3**, these differences can be observed graphically.

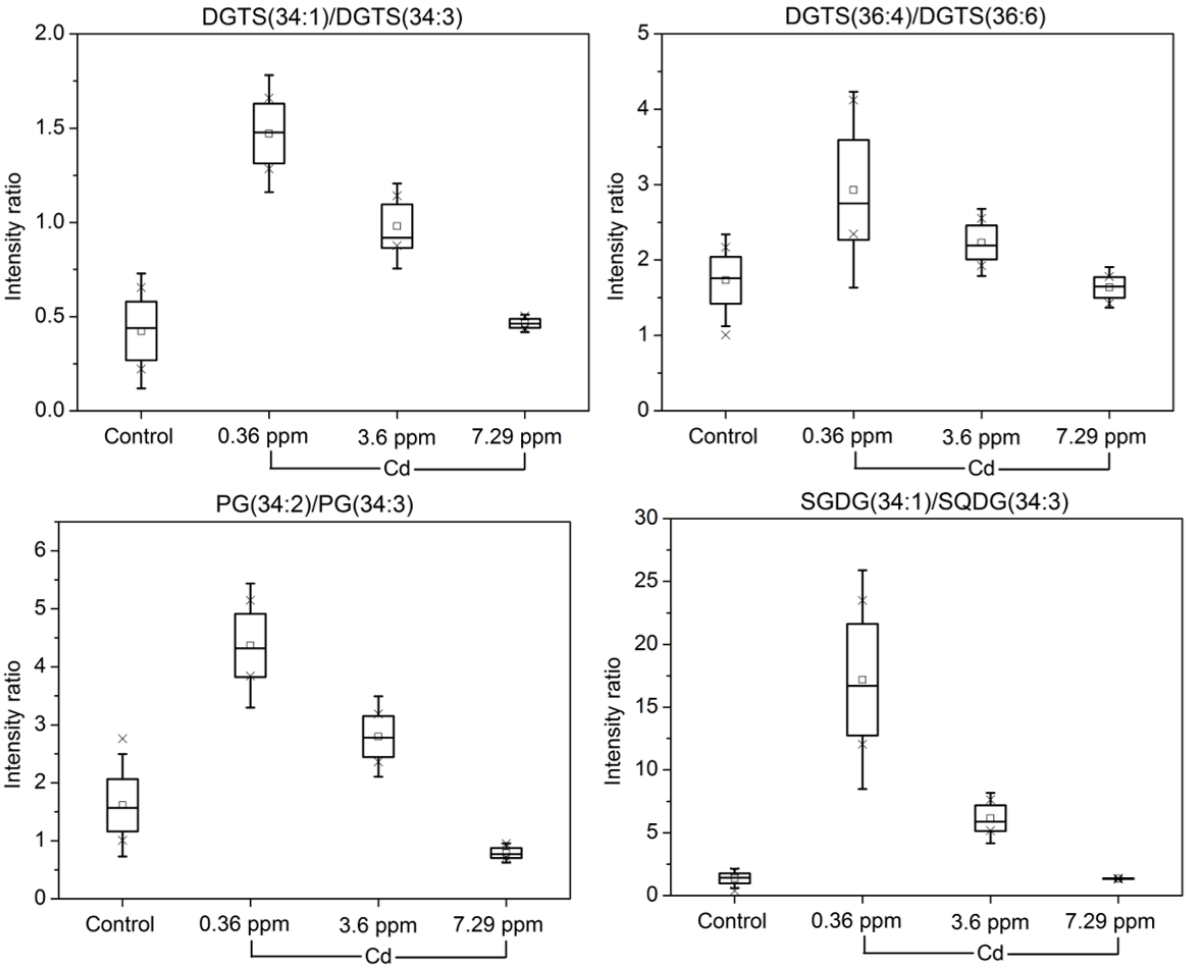

Figure 3.7.2.2-3. Univariate box-whisker plots of DGTS, PG and SQDG lipid species intensity ratio for control and cadmium-incubated C. reinhardtii cell cultures. Arithmetic mean values are represented as small box with ± 1 SD (standard deviation) as larger box and ± 1.96 SD as whiskers. With straight lines inside the larger boxes are represented the median values and with X symbol the minimum and maximum data points.

Noticeably, there is an increase in the intensity ratio of lipid species presented in **Figure 3.7.2.2-3** in cells that were incubated at 0.36 ppm of Cd(II), i.e. the lipids with higher number of double bonds (more unsaturated) were converted into lipids with lower number of double bonds (less unsaturated). It has been reported that cadmium can induce the production of intracellular reactive oxygen species resulting in oxidative damage to cells and lipid peroxidation[48,51], however, lipid peroxidation was not observed in our experiments. It seems that the incubation of cells in cadmium-

containing medium was related to the conversion of more unsaturated membrane lipids into less unsaturated. Interestingly, this phenomenon was not maintained at higher concentrations of cadmium; instead, the intensity ratio returned to the same levels as in the control cells at the highest concentration studied. While the reason to this has not been elucidated, it could possibly indicate toxicity effects at higher concentrations of the toxic metal.

3.7.2.3 Effect of As(III) on membrane lipids of *C. reinhardtii* cells

Inorganic arsenite(iAs(III), referred as As(III) in this text) is a toxic form of arsenic. Arsenite in the form of $As(OH)_3$ at pH < 8.0 can enter the cells through aquaglyceroporins and interact with sulfhydryl groups of enzymes, thus, influencing their function.[52] Besides interactions with proteins, arsenite can reduce photosynthetic activity, respiration and productivity.[53] Also, it can be oxidized into the more toxic form of arsenate (As(V)) intracellularly or on the cell surface.[52] The main mechanism of detoxification includes excretion, methylation to less toxic forms or complexed with phytochelatins and thiol compounds.[54]

In **Figure 3.7.2.3-1**, the positive ion mode DeSSI-MS spectrum of control and arsenite-incubated cells is shown. For arsenite concentrations up to 15 ppm As no significant differences can be observed in the membrane lipids relative intensities. However, at 22.5 ppm As as arsenite, significant differences can be observed.

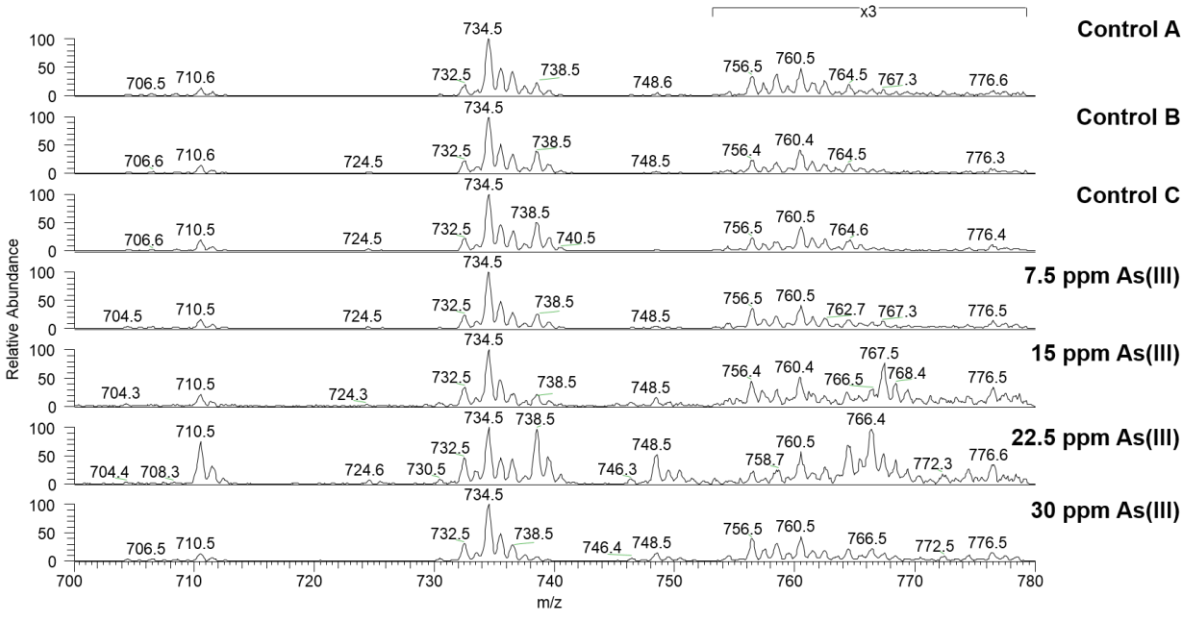

Figure 3.7.2.3-1. Positive ion mode DeSSI-MS spectra obtained after the analysis of control and arsenite-incubated cultures.

The same lipid species as in the case of Cd(II), i.e. DGTS(34:1) & DGTS(34:3) were altered. However, at the highest concentration of arsenite studied, e.g. 30 ppm, the mass spectrum is similar to that of the control samples. The observed differences of relative intensities of specific membrane lipids can be observed graphically in **Figure 3.7.2.3-3**.

The negative ion mode mass spectrum obtained after the DeSSI-MS analysis of control and arsenite-incubated cells is shown in **Figure 3.7.2.3-2**. Since in the positive ion

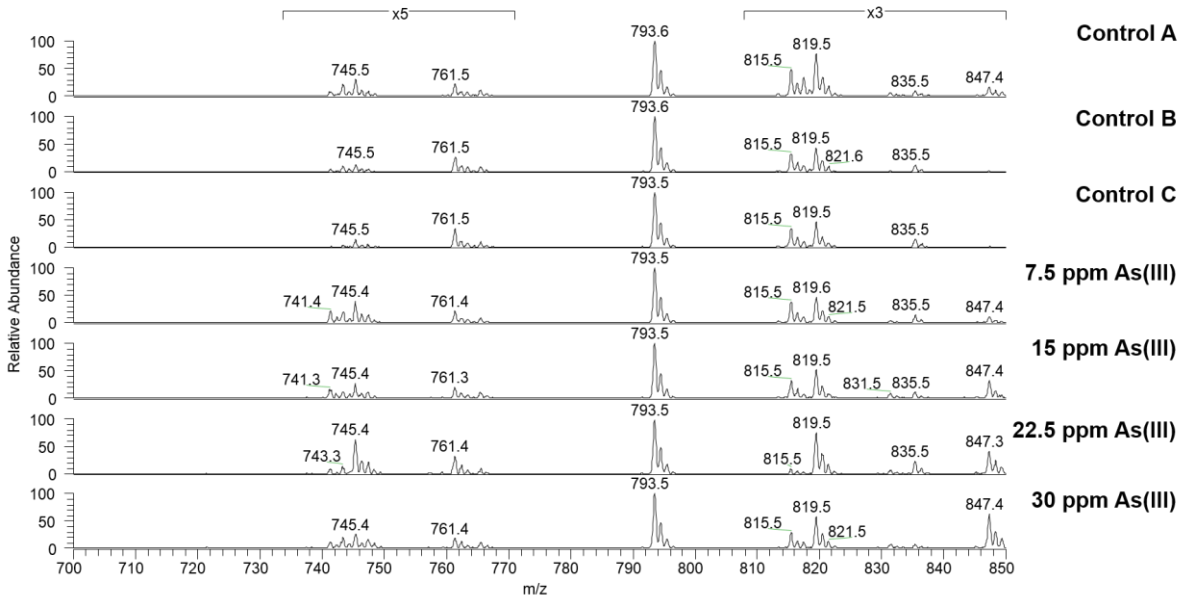

Figure 3.7.2.3-2. Negative ion mode DeSSI-MS spectra obtained after the analysis of control and arsenite-incubated cultures.

mode only the 22.5 ppm As(III) sample had significant differences in the relative intensities of specific membrane lipids, it was expected that the same would occur in the negative ion mode too. Indeed, the relative intensities of PG(34:2) (m/z 745.5) compared to PG(34:3) (m/z 743.5) and SQDG(34:1) (m/z 819.5) compared to SQDG(34:3) (m/z 815.5) in the 22.5 ppm As(III) incubated cells sample were increased (**Figure 3.7.2.3-3**).

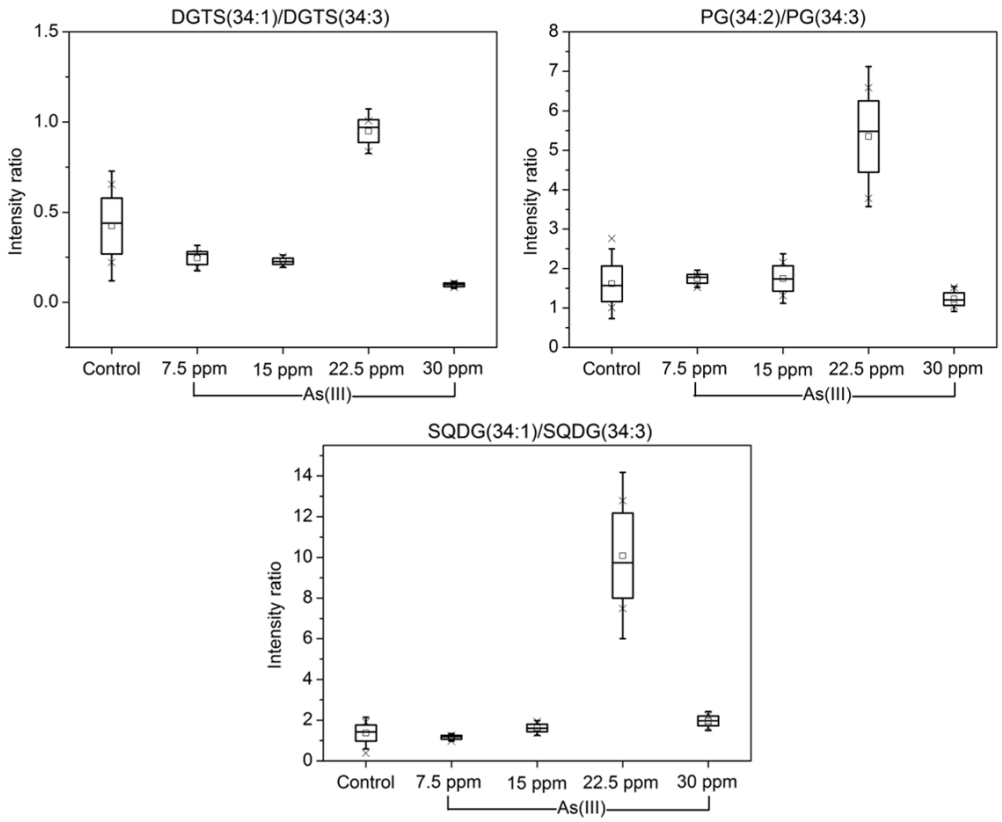

Figure 3.7.2.3-3. Univariate box-whisker plots of DGTS, PG and SQDG lipid species intensity ratio for control and arsenite-incubated C. reinhardtii cell cultures. Arithmetic mean values are represented as small box with ± 1 SD (standard deviation) as larger box and ± 1.96 SD as whiskers. With straight lines inside the larger boxes are represented the median values and with X symbol the minimum and maximum data points.

As it can be seen graphically in **Figure 3.7.2.3-3** the intensity ratio of DGTS(34:1)/DGTS(34:3), PG(34:2)/PG(34:3) and SQDG(34:1)/SQDG(34:3) did not show any increase when cells were incubated with 7.5 and 15 ppm of As(III). One possible explanation to this could be that these concentrations were not able to induce any stress related changes in membrane lipids composition of the cells. However, at 22.5 ppm of As(III), the intensity ratio of the aforementioned lipid species was increased, possibly due to stress induced by the presence of arsenite indicating the conversion of more unsaturated lipids into less unsaturated. Similarly with cadmium-incubated cells, higher concentrations of arsenite, i.e. 30 ppm resulted in intensity ratio that was the same as the control, again, probably due to arsenite-related toxic effects. Arsenite was not found to produce reactive oxygen species according to the work of Szivak *et al.*[48] where much lower concentrations were studied.

3.7.2.4 Effect of As(V) on membrane lipids of *C. reinhardtii* cells

Following As(III), another form of arsenic, As(V), was investigated regarding its potential effect on altering the membrane lipid composition of *C. reinhardtii* cells. Arsenate, being structurally similar to phosphate, can enter the cells through the phosphate transporters and the first step in the detoxification process is the reduction to arsenite.[54–56] Then, arsenite can be excreted, methylated to organic forms or complexed with phytochelatins and thiol compounds, as was mentioned in **Section 3.7.2.3**. Toxic effects of arsenate include growth and photosynthesis inhibition.[57]

In **Figure 3.7.2.4-1** the positive ion mass spectrum of control and arsenate-incubated cells can be seen.

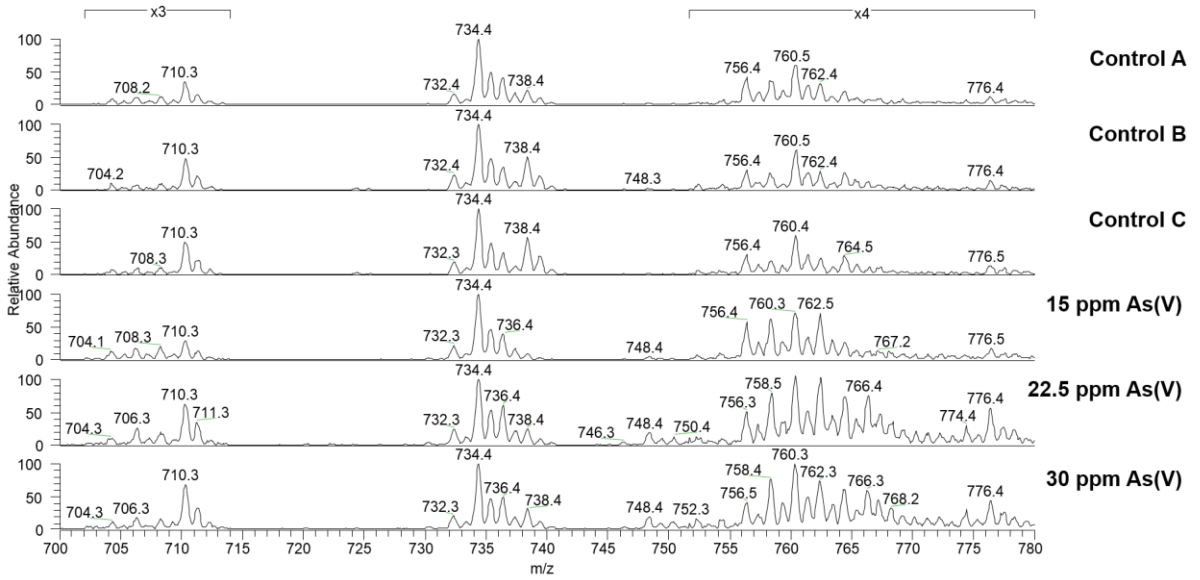

Figure 3.7.2.4-1. Positive ion mode DeSSI-MS spectra obtained after the analysis of control and arsenate-incubated cultures.

The main difference was observed in the m/z region 756-762 in which the lipids DGTS(36:6 – 36:3) can be found (see **Table 3.5.2-1** for lipid species identifications). This difference can also be observed graphically in **Figure 3.7.2.4-3**. In **Figure 3.7.2.4-2** the negative ion mode DeSSI-MS spectrum of control and arsenate-incubated cells can be seen. The most intense differences were observed in the PG region (m/z range 741-747) and in the SQDG region (m/z range 815-821). An intense increase in the relative intensity of PG(34:3) (m/z 743.3) was also observed along with an increase in the relative intensity of PG(34:1) (m/z 747.3) which was very low in the

control samples. Also, in the SQDG(34:3 – 34:0) and SQDG(36:1 – 36:0) regions, significant increases in the relative intensities of SQDG(34:0) (m/z 821.5) and SQDG(36:0) (m/z 849.5) were observed accompanied by a decrease of SQDG(34:3) (m/z 815.5). These differences can be observed graphically in **Figure 3.7.2.4-3**.

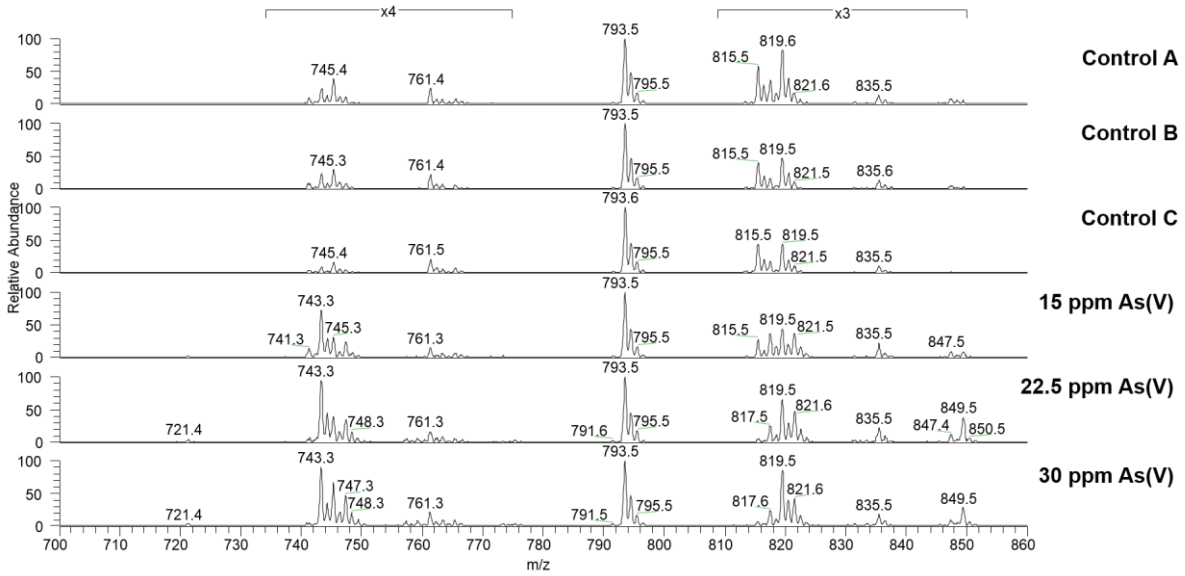

Figure 3.7.2.4-2. Negative ion mode DeSSI-MS spectra obtained after the analysis of control and arsenate-incubated cultures.

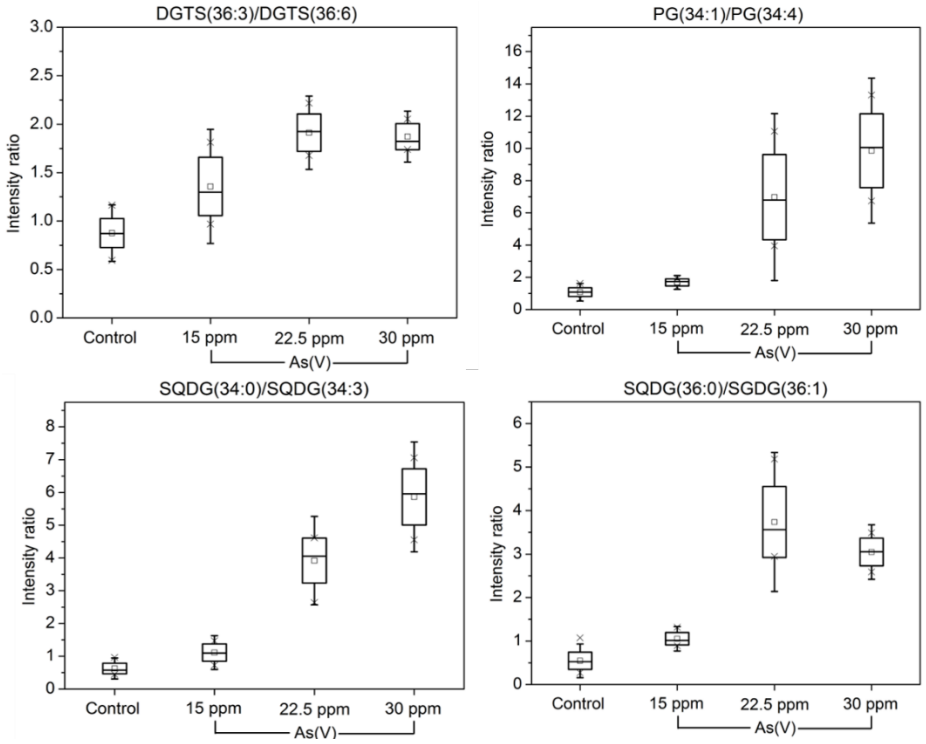

Figure 3.7.2.4-3. Univariate box-whisker plots of DGTS, PG and SQDG lipid species intensity ratio for control and arsenate-incubated C. reinhardtii cell cultures. Arithmetic mean values are represented as small box with ± 1 SD (standard deviation) as larger box and ± 1.96 SD as whiskers. With straight lines inside the larger boxes are represented the median values and with X symbol the minimum and maximum data points.

In contrast with the other metals and metalloids studied, the effect of As(V) on the membrane lipids was more consistent, e.g. with increasing concentration of the metalloid the intensity ratio of the lipids shown in **Figure 3.7.2.4-3** was increasing providing evidence of conversion of the more unsaturated membrane lipids into less unsaturated. These data suggest that the observed differences in membrane lipids composition were related to the incubation with arsenate.

Overall, the data presented suggest that when cells are incubated with toxic contaminants in sub-lethal concentrations, specific membrane lipids are converted into more saturated ones, thus, altering the composition and fluidity of the membranes. To the best of our knowledge, no previous work has investigated the effect of toxic metals and metalloids on the membrane lipids of *C. reinhardtii* cells. Therefore, the validation of the hypothesis generated here requires a more detailed lipidomic approach for absolute quantification of lipid species and enzymatic studies.

3.7.3 Effect of nitrogen deprivation on membrane lipids of *Synechocystis* sp PCC 6803 cells

In these experiments, the effect of nitrogen withdrawal from the culture medium on membrane lipids of Synechocystis cells was studied. The cells (harvested from late exponentional growth phase) were grown for 7 days in normal (control) and nitrogen-deprived (-N) BG-11 medium. Then, the cells from both control and -N cultures were resuspended in fresh N-containing BG-11 medium for 6 days. DeSSI-MS analyses of each sample was carried out in triplicate (three technical replicates per sample). Nitrogen is an essential nutrient for cells and thus, the deprivation of nitrogen from the cultures inhibited cell growth, as can be seen from the growth curve shown in **Figure 3.7.3-1**. These data were kindly provided by Eleftheria Valsami, PhD candidate at the Laboratory of Biochemistry (Prof. Demetrios Ghanotakis).

In **Figure 3.7.3-2** and **Figure 3.7.3-3** the positive and negative ion mode spectra obtained after the DeSSI-MS analysis of *Synechocystis* 6803 cells at different time points are shown. The most distinct difference lies in the relative intensity of m/z 777.5 which was identified as MGDG(34:2) which increased after the cells were grown for 7 days in

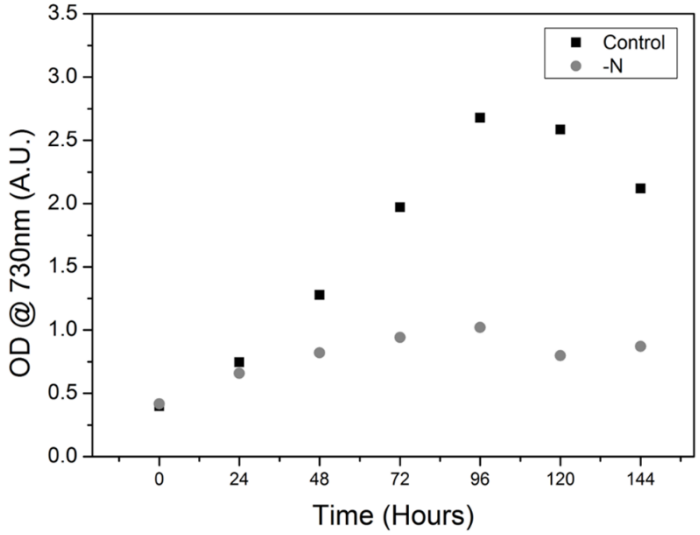

Figure 3.7.3-1. Growth curve of *Synechocystis* 6803 cells grown in normal BG-11 medium (Control) and in nitrogen deprived BG-11 medium (-N).

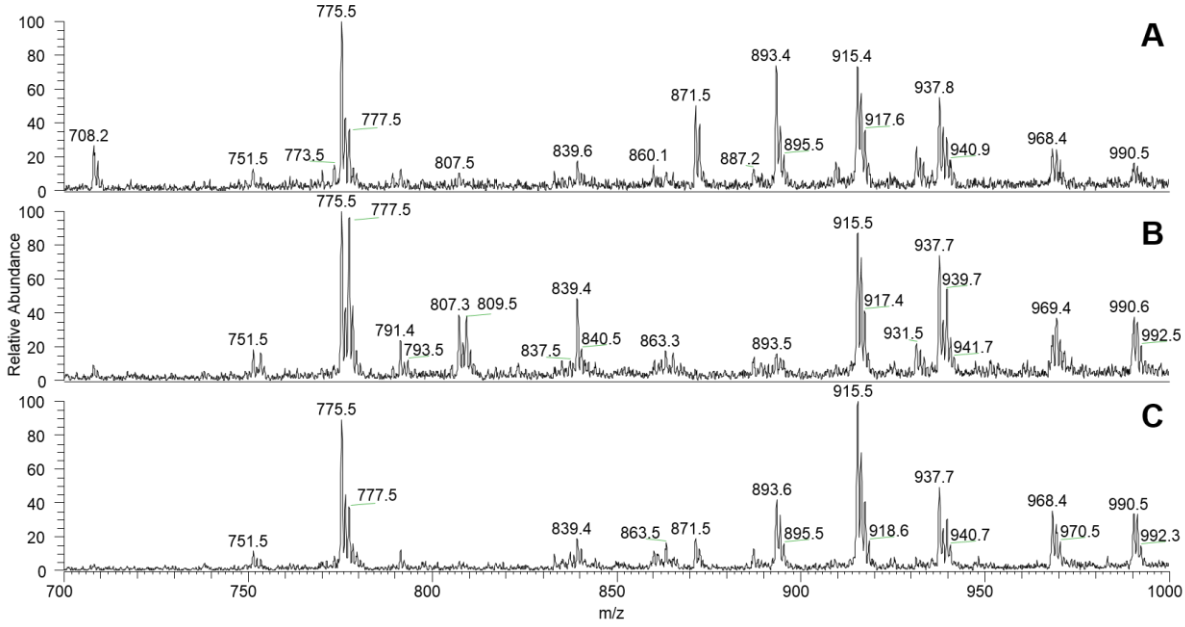

Figure 3.7.3-2. Positive ion mode DeSSI-MS spectra of *Synechocystis* 6803 cells grown in normal BG-11 medium after 1 day (A), 7 days (B) and 1 day after the cells were resuspended in fresh BG-11 medium (C).

normal BG-11 medium (**Figure 3.7.3-2B**). However, when the cells were resuspended in fresh medium, the relative intensity of MGDG(34:2) after 1 day of growth drops to the initial levels (**Figure 3.7.3-2C**). Also, two new peaks at m/z 807.3 and 809.5 appeared in **Figure 3.7.3-2B**, however they were not identified.

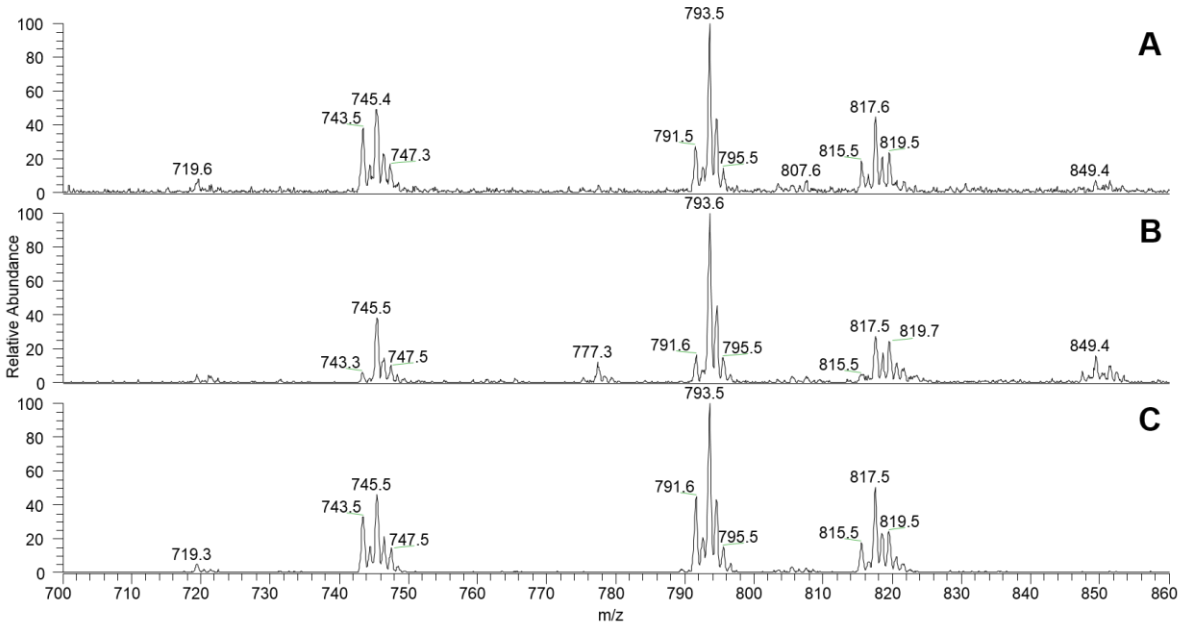

Figure 3.7.3-3. Negative ion mode DeSSI-MS spectra of *Synechocystis* 6803 cells grown in normal BG-11 medium after 1 day (A), 7 days (A) and 1 day after the cells were resuspended in fresh BG-11 medium (C).

In the negative ion mode spectra (**Figure 3.7.3-3**) the main differences observed were the decrease in the relative intensities of ions with m/z 743.5 (PG(34:3)) and 815.5 (SQDG(34:3)).

In **Figure 3.7.3-4** the distribution of C18/C16 PG lipids in cells that were grown under control and under -N conditions can be seen. Also, these distributions are shown for cells that were resuspended in fresh N-containing BG-11 medium. In the control cells (**Figure 3.7.3-4A**) the relative intensity of PG(34:3) lipids decreased as the culture grows older, while the relative intensity of PG(34:1) does not seem to change significantly. Thus, PG(34:3) lipids were converted into the predominant PG(34:2) species. When these cells are resuspended in fresh medium then this cycle starts again (**Figure 3.7.3-4C**). However, in the -N cells this trend was not observed (**Figure 3.7.3-4B**) but when the cells were resuspended in fresh N-containing BG-11 medium, the progeny cells could recover and start this cycle again, i.e. the relative intensity of PG(34:3) has a descending order as the culture grows old. This trend can also be seen in **Figure 3.7.3-6C**, where the intensity ratio of PG(34:2)/PG(34:3) is plotted against the days of cultivation.

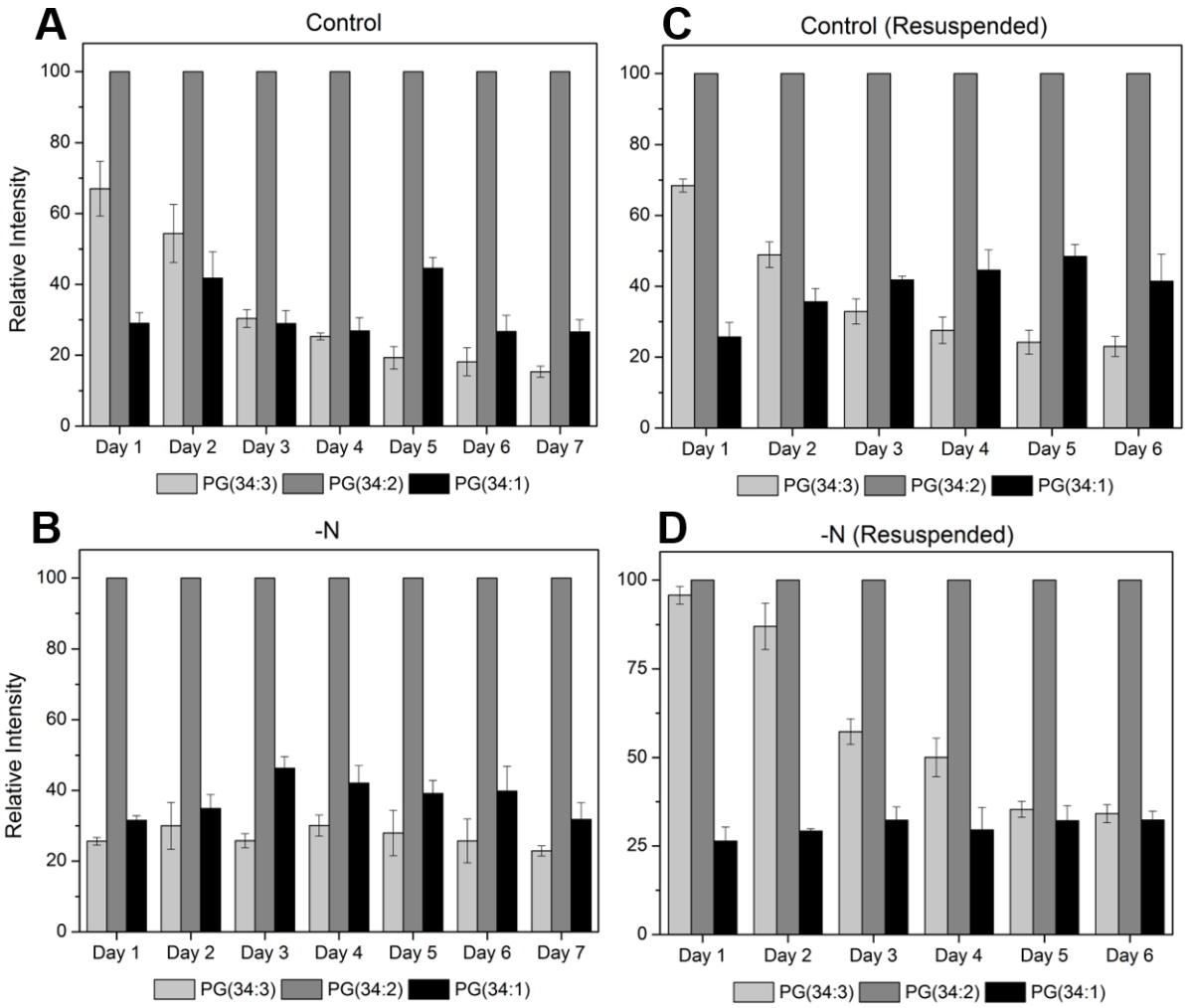

Figure 3.7.3-4. Distributions of PG(C18/C16) lipids in *Synechocystis* cells grown in control (A) and in nitrogen deprived (B) conditions for 7 days. Control and -N cells were resuspended in fresh N-containing BG-11 medium and cultivated for 6 days (C, D).

In **Figure 3.7.3-5** the distribution of C18/C16 SQDG lipids in cells that were grown under normal (control) and nitrogen deprived (-N) conditions along with the distribution upon resuspension of control and -N cells in normal N-containing BG-11 medium can be seen. It is evident that in control cells as the culture grows old the relative intensity of SQDG(34:3) decreases while the relative intensity of SQDG(34:1) increases (**Figure 3.7.3-5A**). This was also the case for control cells that were resuspended in fresh medium (**Figure 3.7.3-5C**). However, the -N cells were not able to convert the SQDG(34:3) lipids into SQDG(34:1) (**Figure 3.7.3-5B**) while after resuspension in normal N-containing medium, the aforementioned conversion was observed again, e.g. the progeny cells were able to recover. This conversion can also be seen in **Figure**

3.7.3-6B where the ratio of SQDG(34:1)/SQDG(34:3) is plotted against the age of culture.

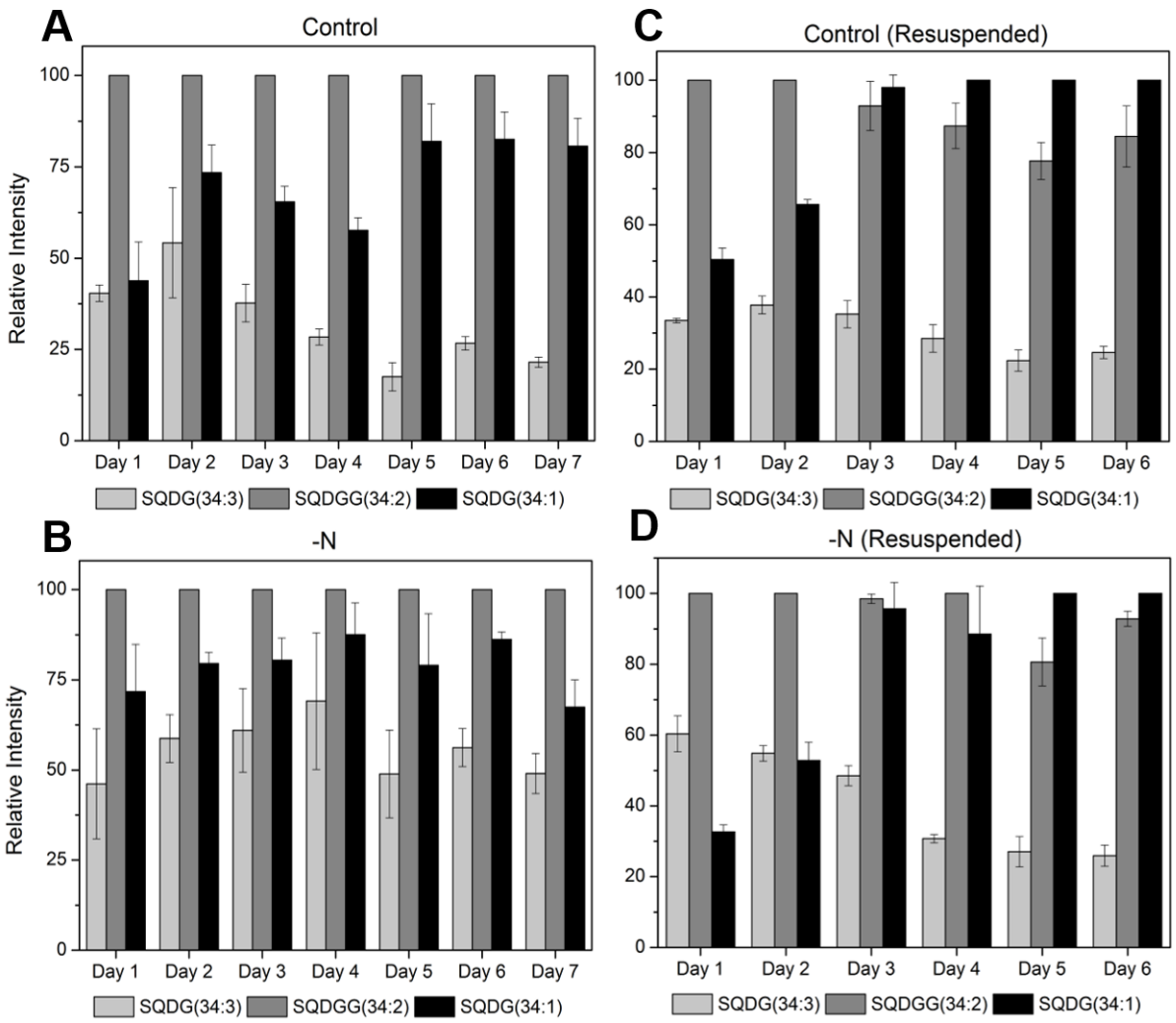

Figure 3.7.3-5. Distributions of SQDG(C16/C18) lipids in *Synechocystis* cells grown in control (A) and in nitrogen deprived (B) conditions for 7 days. Control and -N cells were resuspended in fresh N-containing BG-11 medium and cultivated for 6 days (C, D).

Also, in **Figure 3.7.3-6A** the intensity ratio of MGDG(34:2)/MGDG(34:3), lipid species detected in the positive ion mode, against the age of culture can be seen.

Overall, the data presented in **Figure 3.7.3-6** suggest that as the culture grows old lipid remodeling occurs in the membranes due to the conversion of more unsaturated lipids into less unsaturated. The fluidity of the membranes is altered and as more saturated acyl chains are present in the membrane lipids, the membranes become less fluid. This phenomenon peaks at 5-7 days of culture age in which the cells have entered a stationary phase as it can be seen from the growth curve of **Figure 3.7.3-1**. This is in

accordance with literature results.[30] In their work, Liu *et al*. described the same trend in distribution of PG and SQDG lipids during the life cycle of cyanobacteria, including the species *Synechocystis* 6803. Additionally, our data also suggest that this remodeling of membrane lipids occurs in MGDG lipids too. However, cells that were grown under nitrogen starved conditions lack the ability of converting the more unsaturated membrane lipids into less unsaturated, thus, nitrogen deprivation inhibits, among others, the physiological process of membrane structure reorganization during the life cycle of the cells.

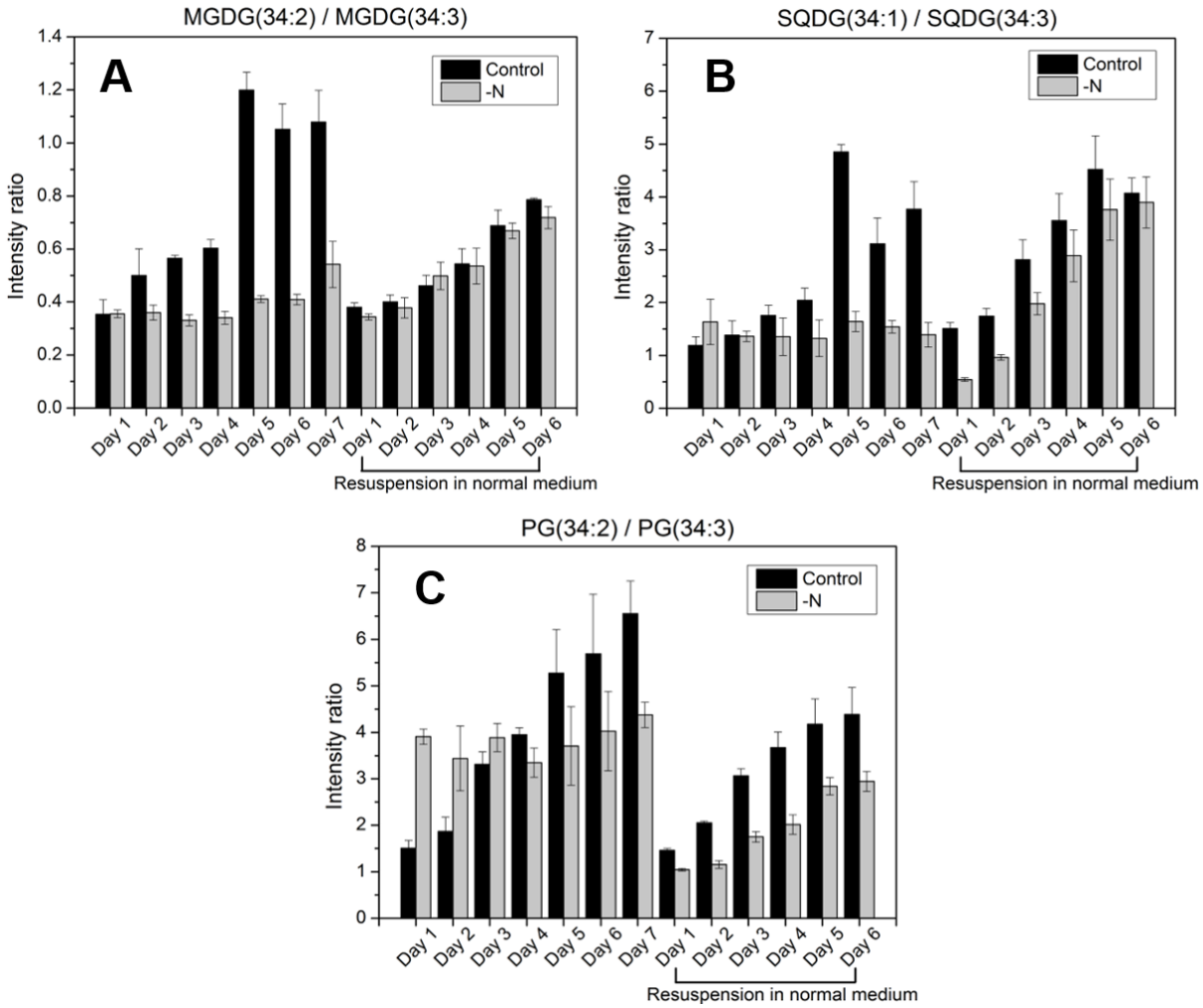

Figure 3.7.3-6. Intensity ratio of MGDG(34:2)/MGDG(34:3) (A), SQDG(34:1)/SQDG(34:3) (B) and PG(34:2/34:3) (C) in *Synechocystis* 6803 cells that were grown under normal (Control) and nitrogen deprived (-N) conditions for 7 days and upon resuspension in fresh N-containing BG-11 medium for 6 days.

After the control and -N cells were resuspended in fresh N-containing medium, the physiological process of membrane lipids conversion was able to occur again.

Cyanobacteria are able to adapt to nitrogen deprivation conditions by adjusting cellular functions but it has been reported that they are able to recover upon addition of nitrogen source in the medium.[58,59] Therefore, the observation of recovering of membrane lipid membranes remodeling upon resuspension in N-containing medium is in supported by evidence of growth recovery in literature. However, so far, the investigation of membrane lipid changes upon nitrogen starvation has not been done and studies that investigated changes in *Synechocystis* cells under nitrogen deprived conditions were focused on changes in expression of genes that are associated with photosynthetic and respiratory activity, carbon and nitrogen uptake and regulation of proliferation.[58,59] One study investigated the lipidome of *Synchocystis* sp PCC 6803 under light-activated heterotrophic conditions and found that there was an increase in the content of membrane lipids with higher degree of saturation of acyl chains[60] under these conditions, similarly to the results presented here. Since the data presented here are novel, for a deeper understanding of the mechanisms that are responsible for this membrane lipid conversion, detailed enzymatic and gene expression studies should be done.

CONCLUSIONS AND PRESPECTIVE

Desorption sonic-spray ionization mass spectrometry was employed for the rapid analysis of membrane lipids from intact cells. The cells did not undergo any extraction procedure prior to analysis; only washing with water to remove the media components was necessary. Thus, the sample preparation procedure was kept to a minimum. By using this approach, we were able to rapidly obtained profiles of membrane lipids. The intactness of cells prior to DeSSI-MS was also investigated and it was found that no cell lysis occurred during the washing and drying on the glass slide procedure. The spraying solvent used was able to efficiently extract membrane lipids such as DGTS, MGDG, DGDG, SQDG, PI and PG along with pigments (Chlorophyll a and b) from the cells. After optimization of certain parameters regarding the DeSSI source, we used this technique for the analysis of the green algae *Chlamydomonas reinhardtii* and the cyanobacteria *Synechocystis* sp PCC 6803 grown under different conditions.

For *C. reinhardtii* cells incubated with various sub-lethal concentrations of toxic metals (Pb(II), Cd(II)) and metalloids (As(III), As(V)) it was observed that the membrane lipids of cells underwent conversion from more unsaturated to less unsaturated, therefore, the fluidity of the photosynthetic and the extraplastidial membranes was altered. The exact mechanisms that are responsible for this conversion are not yet known since this work is the first so far report on the effect of toxic contaminants on membrane lipids of the green algae *C. reinhardtii*. While several publications mention ROS production and lipid peroxidation as the main response to the treatment with toxic contaminants, peroxidised lipids were not detected.

In the cyanobacteria *Synechocystis* 6803, nitrogen deprivation was found to impact the physiological process of membrane lipids conversion from more unsaturated to less unsaturated. MGDG(C18/C16), SQDG(C18/C16) and PG(C18/C16) lipids of the thylakoid membranes in *Synechostis* 6803 were physiologically converted from more unsaturated into less unsaturated as the culture was growing old and the peak of this conversion appeared at 5 days of cultivation, in which the cells were entering a stationary phase. Nitrogen deprived cells were not able exhibit this physiological conversion, however upon resuspension into fresh N-containing medium, the cells were able to recover and membrane lipid remodeling occurred again. The observation

of membrane lipids remodeling during the normal life cycle of *Synechocystis* 6803 was in accordance with literature results, however, the effect of nitrogen deprivation on membrane lipids was not explored.

This aim of this research was to apply an ambient ionization mass spectrometry technique, namely desorption sonic-spray ionization mass spectrometry for the rapid analysis of cells under different stress conditions.

The effect of toxic contaminants on membrane lipids of green algae cells has not been investigated yet, thus, the hypothesis of lipid remodeling during stress conditions generated here needs to be further validated by detailed enzymatic studies that will shed light on the exact mechanisms that lead to the membrane remodeling. This will provide deeper insights into the mechanisms by which the cells are dealing with stress factors such as toxic metals and metalloids.

While the effect of nitrogen starvation on *Synechocystis* cells is a well-studied topic, there is no single report of the effect on membrane lipids. It was known (and confirmed here) that during the normal life cycle, the cyanobacteria remodel their lipid membranes. Under nitrogen deprivation conditions we found that this remodeling was disrupted. However, the mechanisms that lead to that disruption are not known and could be subject of future studies. Further insights on the mechanisms that physiologically lead to membrane remodeling along with how nitrogen deprivation ‘’blocks’’ these mechanisms could provide better understanding of this effect.

Finally, detailed lipidomic studies could be done and provide quantitative information on the distribution of lipid species inside the cells.

REFERENCES

[1] J. B. Fenn, M. Mann, C. K. A. I. Meng, S. F. Wong, C. M. Whitehouse. Electrospray Ionization for Mass Spectrometry of Large Biomolecules. *Science (80-.).* **1989**, *246*, 64.

[2] Z. Takáts, J. M. Wiseman, B. Gologan, R. G. Cooks. Mass Spectrometry Sampling Under Ambient Conditions with Desorption Electrospray Ionization. *Science (80-.).* **2004**, *306*, 471.

[3] R. B. Cody, J. A. Laramee, H. D. Durst. Versatile New Ion Source for the Analysis of Materials in Open Air under Ambient Conditions. *Anal. Chem.* **2005**, *77*, 2297.

[4] R. G. Cooks, Z. Ouyang, Z. Takats, J. M. Wiseman. Ambient mass spectrometry. *Science (80-.).* **2006**, *311*, 1566.

[5] R. M. Alberici, R. C. Simas, G. B. Sanvido, W. Romão, P. M. Lalli, M. Benassi, I. B. S. Cunha, M. N. Eberlin. Ambient mass spectrometry: Bringing MS into the “real world.” *Anal. Bioanal. Chem.* **2010**, *398*, 265.

[6] Z. Ouyang, X. Zhang. Ambient mass spectrometry. *Analyst* **2010**, 659.

[7] F. M. Fernandez, J. F. Garcia-Reyes. Ambient mass spectrometry. *Anal. Methods* **2017**, *9*, 4894.

[8] R. Javanshad, A. R. Venter. Ambient ionization mass spectrometry: real-time, proximal sample processing and ionization. *Anal. Methods* **2017**, *9*, 4896.

[9] C. Hsu, P. C. Dorrestein. Visualizing life with ambient mass spectrometry. *Curr. Opin. Biotechnol.* **2005**, *31*, 24.

[10] Z. Takats, N. Strittmatter, J. S. McKenzie. *Ambient Mass Spectrometry in Cancer Research*. Advances In Cancer Research, Chapter 9, Elsevier Inc., **2017**.

[11] D. N. Correa, J. M. Santos, L. S. Eberlin, M. N. Eberlin, S. F. Teunissen. Forensic Chemistry and Ambient Mass Spectrometry: A Perfect Couple Destined for a Happy Marriage? *Anal. Chem.* **2016**, *88*, 2515.

[12] C. Black, O. P. Chevallier, C. T. Elliott. The current and potential applications of Ambient Mass Spectrometry in detecting food fraud. *TrAC - Trends Anal. Chem.* **2016**, *82*, 268.

[13] C. S. Clendinen, M. E. Monge, F. M. Fernández. Ambient Mass Spectrometry in Metabolomics. *Analyst* **2017**, *142*, 3101.

[14] M. D. Kellogg. *Measurement of Biological Materials*. Clinical And Translational Science, Chapter 8, Elsevier Inc., **2017**.

[15] F. Hillenkamp, R. C. Beavis, T. Brian. Matrix-Assisted Laser Desorption / Ionization Mass Spectrometry of Biopolymers. **1991**, *63*, 1193.

[16] R. Haddad, R. Sparrapan, M. Eberlin. Desorption sonic spray ionization for (high) voltage-free ambient mass spectrometry. *Rapid Commun. Mass Spectrom.* **2006**, *20*, 2901.

[17] P. M. Peacock, W. Zhang, S. Trimpin. Advances in Ionization for Mass Spectrometry. *Anal. Chem.* **2017**, *89*, 372.

[18] A. Hirabayashi, M. Sakairi, H. Koizumi. Sonic spray ionization method for atmospheric pressure ionization mass spectrometry. *Anal. Chem.* **1994**, *66*, 4557.

[19] D. Touboul, M. C. Jecklin, R. Zenobi. Ion internal energy distributions validate the charge residue model for small molecule ion formation by spray methods. *Rapid Commun. Mass Spectrom.* **2008**, *22*, 1062.

[20] L. W. Zilch, J. T. Maze, J. W. Smith, G. E. Ewing, M. F. Jarrold. Charge Separation in the Aerodynamic Breakup of Micrometer-Sized Water Droplets. *J. Phys. Chem. A* **2008**, *112*, 13352.

[21] Z. Takats, C. S. Nanita, G. R. Cooks, G. Schlosser, K. Vekey. Amino acid clusters formed by sonic spray ionization. *Anal. Chem.* **2003**, *75*, 1514.

[22] M. M. Antonakis, A. Tsirigotaki, K. Kanaki, C. J. Milios, S. A. Pergantis. Bipolar mass spectrometry of labile coordination complexes, redox active inorganic compounds, and proteins using a glass nebulizer for sonic-spray ionization. *J. Am. Soc. Mass Spectrom.* **2013**, *24*, 1250.

[23] J. S. Gardner, R. G. Harrison, J. D. Lamb, D. V. Dearden. Sonic spray ionization mass spectrometry: a powerful tool used to characterize fragile metal-assembled cages. *New J. Chem.* **2006**, *30*, 1276.

[24] L. Mavroudakis, E. Mavrakis, A. Kouvarakis, S. A. Pergantis. Determination of Chlorate, Perchlorate and Bromate Anions in Water Samples by Microbore Reversed-Phase Liquid Chromatography Coupled to Sonic-Spray Ionization Mass Spectrometry. *Rapid Commun. Mass Spectrom.* **2017**, *31*, 911.

[25] S. F. Teunissen, A. M. A. P. Fernandes, M. N. Eberlin, R. M. Alberici. Celebrating 10 years of easy ambient sonic-spray ionization. *TrAC Trends Anal. Chem.* **2017**, *90*, 135.

[26] A. Venter, P. E. Sojka, R. G. Cooks. Droplet dynamics and ionization mechanisms in desorption electrospray ionization mass spectrometry. *Anal. Chem.* **2006**, *78*, 8549.

[27] A. B. Costa, R. Graham Cooks. Simulated splashes: Elucidating the mechanism of desorption electrospray ionization mass spectrometry. *Chem. Phys. Lett.* **2008**, *464*, 1.

[28] H. Mirzaei, M. Carrasco. *Modern Proteomics – Sample Preparation , Analysis and Practical Applications*. Advances In Experimental Medicine And Biology, Chapter 7, Springer, **2016**.

[29] T. Finnigan. *LCQ Advantage Hardware Manual*. Technical Publications, Thermo Finnigan, **2001**.

[30] Y. Liu, J. Zhang, H. Nie, C. Dong, Z. Li, Z. Zheng, Y. Bai, H. Liu, J. Zhao. Study on variation of lipids during different growth phases of living cyanobacteria using easy ambient sonic-spray ionization mass spectrometry. *Anal. Chem.* **2014**, *86*, 7096.

[31] A. O. M. and M. N. E. Priscila M. Lalli, Gustavo B. Sanvido, Jerusa S. Garcia, Renato Haddad, Ricardo G. Cosso, Denison R. J. Maia, Jorge J. Zacca. Fingerprinting and aging of ink by easy ambient sonic-spray ionization mass spectrometry. *Analyst* **2010**, *135*, 745.

[32] R. M. Alberici, P. H. Vendramini, M. N. Eberlin. Easy ambient sonic-spray ionization mass spectrometry for tissue imaging. *Anal. Methods* **2017**, *9*, 5029.

[33] M. Moini, B. L. Jones, R. M. Rogers, L. Jiang. Sodium Trifluoroacetate as a Tune/Calibration Compound for Positive- and Negative-Ion Electrospray Ionization Mass Spectrometry in the Mass Range of 100 – 4000 Da. *J. Am. Soc. Mass Spectrom.* **1998**, *9*, 977.

[34] L. S. Eberlin, C. R. Ferreira, A. L. Dill, D. R. Ifa, L. Cheng, R. G. Cooks. Nondestructive, histologically compatible tissue imaging by desorption electrospray ionization mass spectrometry. *ChemBioChem* **2011**, *12*, 2129.

[35] A. M. Meetani, Y.-S. Shin, S. Zhang, R. Mayer, F. Basile. Desorption electrospray ionization mass spectrometry of intact bacteria. *J. Mass Spectrom.* **2007**, *42*, 1186.

[36] Y. Song, N. Talaty, W. A. Tao, Z. Pan, R. G. Cooks. Rapid ambient mass spectrometric profiling of intact, untreated bacteria using desorption electrospray ionization. *Chem. Commun.* **2007**, *0*, 61.

[37] J. I. Zhang, N. Talaty, A. B. Costa, Y. Xia, W. A. Tao, R. Bell, J. H. Callahan, R. G. Cooks. Rapid direct lipid profiling of bacteria using desorption electrospray ionization mass spectrometry. *Int. J. Mass Spectrom.* **2011**, *301*, 37.

[38] I. Lanekoff, O. Geydebrekht, G. E. Pinchuk, A. E. Konopka, J. Laskin. Spatially resolved analysis of glycolipids and metabolites in living Synechococcus sp. PCC 7002 using nanospray desorption electrospray ionization. *Analyst* **2013**, *138*, 1971.

[39] L. Boudière, M. Michaud, D. Petroutsos, F. Rébeillé, D. Falconet, O. Bastien, S. Roy, G. Finazzi, N. Rolland, J. Jouhet, M. A. Block, E. Maréchal. Glycerolipids in photosynthesis: Composition, synthesis and trafficking. *Biochim. Biophys. Acta - Bioenerg.* **2014**, *1837*, 470.

[40] A. Vieler, C. Wilhelm, R. Goss, R. Süß, J. Schiller. The lipid composition of the unicellular green alga Chlamydomonas reinhardtii and the diatom Cyclotella meneghiniana investigated by MALDI-TOF MS and TLC. *Chem. Phys. Lipids* **2007**, *150*, 143.

[41] D. Yang, D. Song, T. Kind, Y. Ma, J. Hoefkens, O. Fiehn. Lipidomic analysis of chlamydomonas reinhardtii under nitrogen and sulfur deprivation. *PLoS One* **2015**, *10*, 1.

[42] C. Giroud, A. Gerber, W. Eichenberger. Lipids of Chlamydomonas reinhardtii. Analysis of Molecular Species and Intracellular Site(s) of Biosynthesis. *Plant Cell Physiol.* **1988**, *29*, 587.

[43] T. Kind, K. H. Liu, D. Y. Lee, B. Defelice, J. K. Meissen, O. Fiehn. LipidBlast in silico tandem mass spectrometry database for lipid identification. *Nat. Methods* **2013**, *10*, 755.

[44] Y. H. Kim, J.-S. Choi, J. S. Yoo, Y.-M. Park, M. S. Kim. Structural identification of glycerolipid molecular species isolated from cyanobacterium Synechocystis sp. PCC 6803 using fast atom bombardment tandem mass spectrometry. *Anal. Biochem.* **1999**, *267*, 260.

[45] M. Hanikenne. Chlamydomonas reinhardtii as a eukaryotic photosynthetic model for studies of heavy metal homeostasis and tolerance. *New Phytol.* **2003**, *159*, 331.

[46] A. Jamers, R. Blust, W. De Coen, J. L. Griffin, O. A. H. Jones. An omics based assessment of cadmium toxicity in the green alga Chlamydomonas reinhardtii. *Aquat. Toxicol.* **2013**, *126*, 355.

[47] S. H. Imam, M. J. Buchanan, H. C. Shin, W. J. Snell. The Chlamydomonas cell wall: Characterization of the wall framework. *J. Cell Biol.* **1985**, *101*, 1599.

[48] I. Szivák, R. Behra, L. Sigg. Metal-induced reactive oxygen species production in chlamydomonas reinhardtii (chlorophyceae). *J. Phycol.* **2009**, *45*, 427.

[49] M. Samadani, F. Perreault, A. Oukarroum, D. Dewez. Effect of cadmium accumulation on green algae Chlamydomonas reinhardtii and acid-tolerant Chlamydomonas CPCC 121. *Chemosphere* **2018**, *191*, 174.

[50] A. Bräutigam, D. Schaumlöffel, H. Preud'Homme, I. Thondorf, D. Wesenberg. Physiological characterization of cadmium-exposed Chlamydomonas reinhardtii. *Plant, Cell Environ.* **2011**, *34*, 2071.

[51] Z. Yu, R. Hao, L. Zhang, Y. Zhu. Effects of TiO2, SiO2, Ag and CdTe/CdS quantum dots nanoparticles on toxicity of cadmium towards Chlamydomonas reinhardtii. *Ecotoxicol. Environ. Saf.* **2018**, *156*, 75.

[52] N. X. Wang, B. Huang, S. Xu, Z. B. Wei, A. J. Miao, R. Ji, L. Y. Yang. Effects of nitrogen and phosphorus on arsenite accumulation, oxidation, and toxicity in Chlamydomonas reinhardtii. *Aquat. Toxicol.* **2014**, *157*, 167.

[53] J. M. Vega, I. Garbayo, M. J. Domínguez, J. Vigara. Effect of abiotic stress on photosynthesis and respiration in Chlamydomonas reinhardtii Induction of oxidative stress. *Enzyme Microb. Technol.* **2006**, *40*, 163.

[54] X. Yin, L. Wang, G. Duan, G. Sun. Characterization of arsenate transformation and identification of arsenate reductase in a green alga Chlamydomonas reinhardtii. *J. Environ. Sci.* **2011**, *23*, 1186.

[55] N. X. Wang, Y. Li, X. H. Deng, A. J. Miao, R. Ji, L. Y. Yang. Toxicity and bioaccumulation kinetics of arsenate in two freshwater green algae under different phosphate regimes. *Water Res.* **2013**, *47*, 2497.

[56] C. Murota, H. Matsumoto, S. Fujiwara, Y. Hiruta, S. Miyashita, M. Shimoya, I. Kobayashi, M. O. Hudock, R. K. Togasaki, N. Sato, M. Tsuzuki. Arsenic tolerance in a Chlamydomonas photosynthetic mutant is due to reduced arsenic uptake even in light conditions. *Planta* **2012**, *236*, 1395.

[57] I. Kobayashi, S. Fujiwara, H. Saegusa, M. Inouhe, H. Matsumoto, M. Tsuzuki. Relief of arsenate toxicity by Cd-stimulated phytochelatin synthesis in the green alga Chlamydomonas reinhardtii. *Mar. Biotechnol.* **2006**, *8*, 94.

[58] V. Krasikov, E. Aguirre von Wobeser, H. L. Dekker, J. Huisman, H. C. P. Matthijs. Time-series resolution of gradual nitrogen starvation and its impact on photosynthesis in the cyanobacterium Synechocystis PCC 6803. *Physiol. Plant.* **2012**, *145*, 426.

[59] L. G. W. Oa, E. A. Von Wobeser, B. W. Ibelings, J. Bok, V. Krasikov, J. Huisman, H. C. P. Matthijs. Concerted Changes in Gene Expression and Cell Physiology of the Cyanobacterium Synechocystis sp . Strain PCC 6803 during Transitions between Nitrogen. **2011**, *155*, 1445.

[60] N. Plohnke, T. Seidel, U. Kahmann, M. Rögner, D. Schneider, S. Rexroth. The Proteome and Lipidome of *Synechocystis* sp. PCC 6803 Cells Grown under Light-Activated Heterotrophic Conditions. *Mol. Cell. Proteomics* **2015**, *14*, 572.

[61] C. Wu, D. R. Ifa, N. E. Manicke, R. G. Cooks. Rapid, direct analysis of cholesterol by charge labeling in reactive desorption electrospray ionization. *Anal. Chem.* **2009**, *81*, 7618.

APPENDIX

A.1. Analysis of pharmaceutical ointments

These samples were kindly provided by fellow colleagues and a small aliquot of the sample was kept in Eppendorf tube. Also, the full list of ingredients was recorded.

Fucidin®

Ingredients: fusidic acid (2 % w/w), butylhydroxyanisole (E320), cetyl alcohol, glycerol, liquid paraffin, potassium sorbate, polysorbate 60, purified water, all-rac-α-tocopherol, hydrochloric acid and white soft paraffin.

Fubecot®

Ingredients: fusidic acid (2 % w/w), betamethasone (0.1 % w/w), white soft paraffin, cetostearyl alcohol, liquid paraffin, cetomacrogol 1000, sodium dihydrogen phosphate, chlorocresol, sodium hydroxide, purified water.

Flenazole®

Ingredients: miconazole nitrate (2 % w/w), fluprednidene acetate (0.1 % w/w), dimethicone, medium chain triglycerides, white soft paraffin, glyceryl monostearate 40-50 %, glyceryl monostearate – macrogol stearate 5000 (1:1), stearyl alcohol, propylene glycol, purified water.

Fungoral®

Ingredients: ketoconazole (2 % w/w), propylene glycol, stearyl alcohol, cetyl alcohol, sorbitan stearate, polysorbate, isopropyl myristate, sodium sulphite anhydrous, purified water.

Ygiele®

Ingredients: clindamycin phosphate (2 % w/w), liquid paraffin, propylene glycol, polysorbate 60, cetostearyl alcohol, polysorbate 60, cetyl palmitate, stearic acid, sorbitan monostearate, benzyl alcohol, purified water.

In **Figure A.1-1**, the mass spectrum of Fucidin® cream obtained by DeSSI-MS in the negative ion mode is shown and intense signals of the deprotonated fucidic acid ([M – H]$^-$) with m/z 515.4 can be seen. Also, the ion with m/z 551.3 can be observed, which corresponds to the chloride adduct of fusidic acid ([M + Cl]$^-$) that is present due to the hydrochloric acid contained in the cream.

Additionally, the ions with m/z 471.5 (not shown in Figure A1), 473.5 and 455.5 can be observed. These ions possibly correspond to either fragments created inside the mass spectrometer due to ion transfer capillary temperature or degradation products of the fusidic acid. The possible structures of these ions are shown in **Figure A.1-2**.

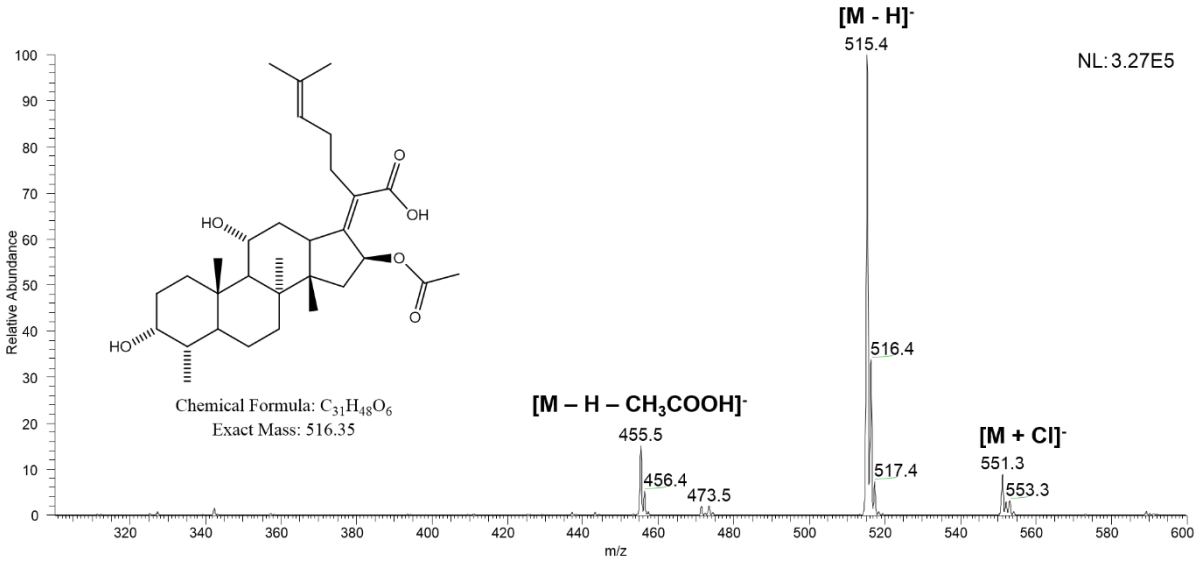

Figure A.1-1. Full mass spectrum of Fucidin® cream obtained by DeSSI-MS analysis. Inset is shown the structure of the active ingredient, fucidic acid.

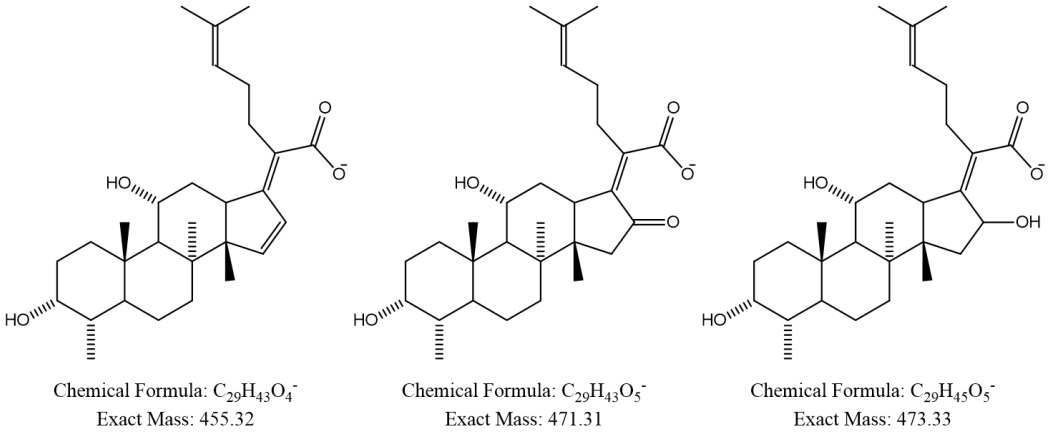

Figure A.1-2. Possible structures of ions with m/z 455.5, 471.5 and 473.5 observed in the mass spectrum of Fucidin cream.

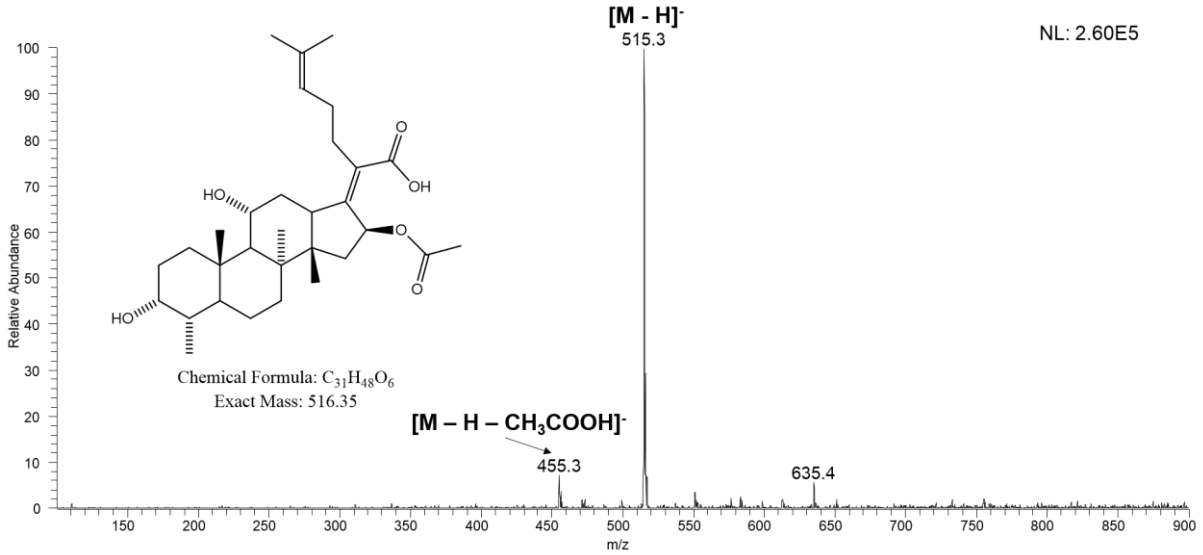

Figure A.1-3. Mass spectrum in the negative ion mode obtained by DeSSI-MS analysis of Fubecot® cream. Ion with m/z 635.4 was not identified.

In **Figure A.1-3** the mass spectrum in the negative ion mode obtained from the DeSSI-MS analysis of the Fubecot® cream can be seen. The active ingredients of this ointment are fucidic acid, which can be seen as deprotonated ion with m/z 515.3 along with other characteristic ions such as 455.3, and betamethasone, which was not detected either in the positive or the negative ion mode. This could be attributed to the low concentration (0.1 % w/w) in the cream and in the low ionization efficiency of steroidal compounds.

For the improvement of the analytical performance for steroidal compounds it has been proposed that using betaine aldehyde compounds in the spraying solvent can react rapidly with the alcohol groups of the steroidal analyte and the product is charged due to the presence of betaine group[61].

Micogen® cream active ingredients include miconazole nitrate and fluprednidene acetate. In **Figure A.1-5** the mass spectrum in the positive ion mode obtained by DeSSI-MS can be seen. The set of peaks with m/z 415.2-417.2-419.2-421.2 correspond to the miconazole ion and exhibit this isotopic pattern due to the presence of 4 chlorine atoms. The peak with m/z 159.1 is an unidentified ion while the set of peaks with m/z 488.3, 516.4 and 544.4 that were identified as medium chain triglycerides. These medium chain triglycerides are present in the ingredients list of the product. In **Figure A.1-4**, an expanded region in the mass spectrum is shown so that the peaks that correspond to medium chain triglycerides can be clearly seen. These peaks were assigned to medium chain triglycerides based on their m/z and the MS/MS

spectra. Medium chain triglycerides contain 6, 8, 10 or 12 carbon atoms in the aliphatic chains. As it can be seen in **Figure A.1-4**, m/z 488.3 was identified as ammonium adduct of TG(24:0), m/z 493.5 as sodium adduct of TG(24:0), m/z 509.3 as potassium adduct of TG(24:0), m/z 516.4 as ammonium adduct of TG(26:0), m/z 521.5 as sodium adduct of TG(26:0), m/z 537.3 as potassium adduct of TG(26:0), m/z 544.4 as ammonium adduct of TG(28:0), m/z 549.2 as sodium adduct of TG(28:0), m/z 565.3 as potassium adduct of TG(28:0), m/z 572.3 as ammonium adduct of TG(30:0) and m/z 577.5 as sodium adduct of TG(30:0). As in the case of Fubecot® cream, the other active ingredient, fluprednidene acetate, was not detected due to its steroidal structure.

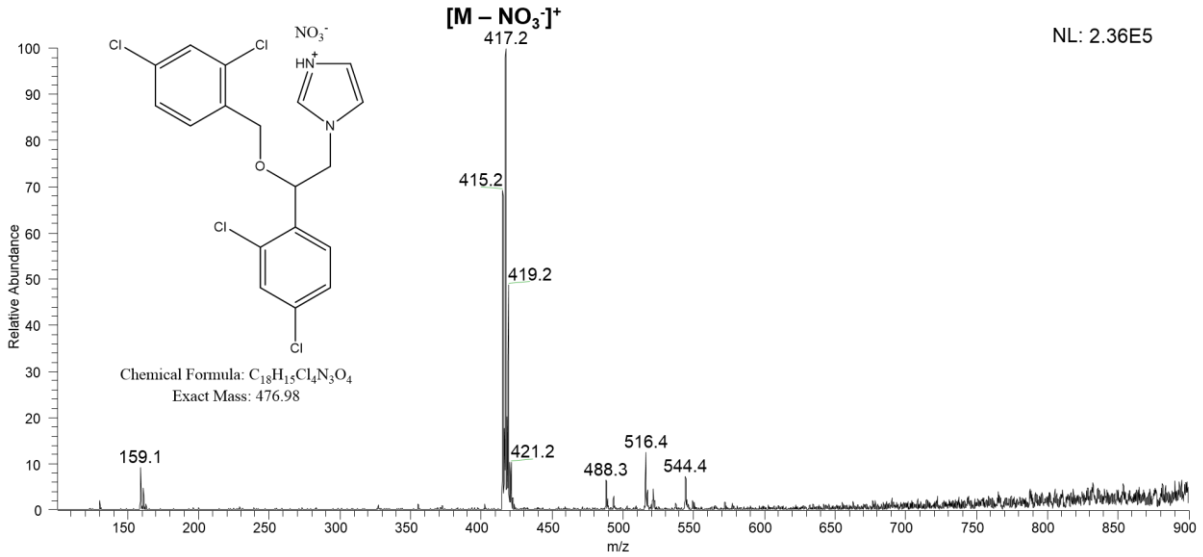

Figure A.1-5. Mass spectrum in the positive ion mode obtained by DeSSI-MS analysis of Flenazole® cream. Inset is shown the structure of miconazole nitrate.

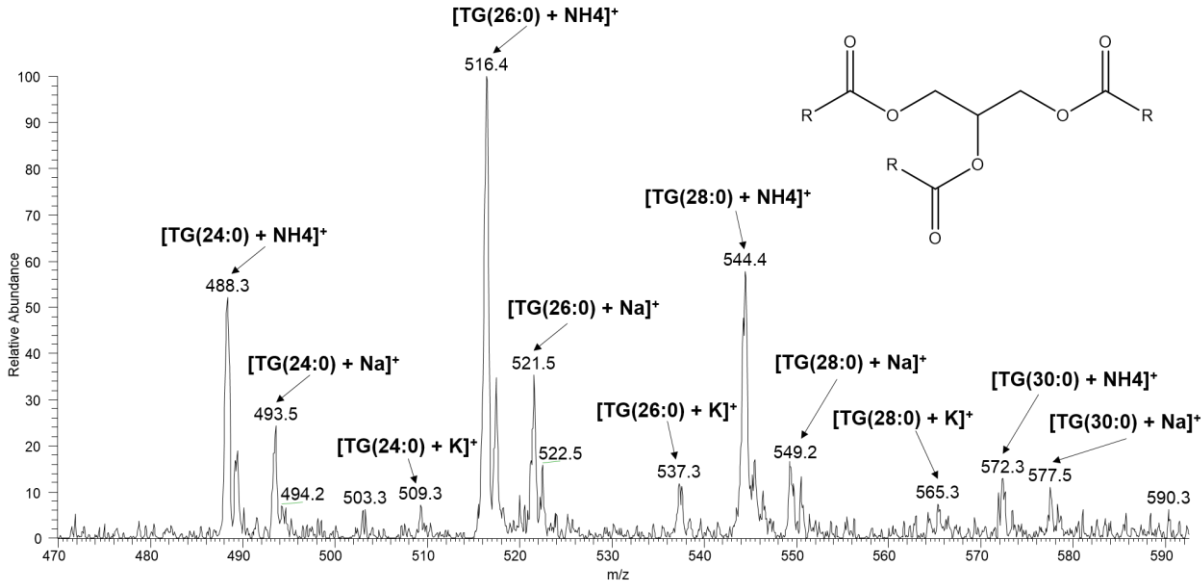

Figure A.1-4. Expanded m/z region of the positive ion mass spectrum obtained by DeSSI-MS analysis of Flenazole® cream showing the medium chain triglycerides. Inset is shown the general structure of a triglyceride.

Fungoral® cream contains as active ingredient the compound ketoconazole. The positive ion mass spectrum obtained by DeSSI-MS is shown in **Figure A.1-6** and a clear signal for the protonated analyte can be observed with m/z 531.4. The characteristic isotopic pattern of two chlorine atoms in the compound was also observed.

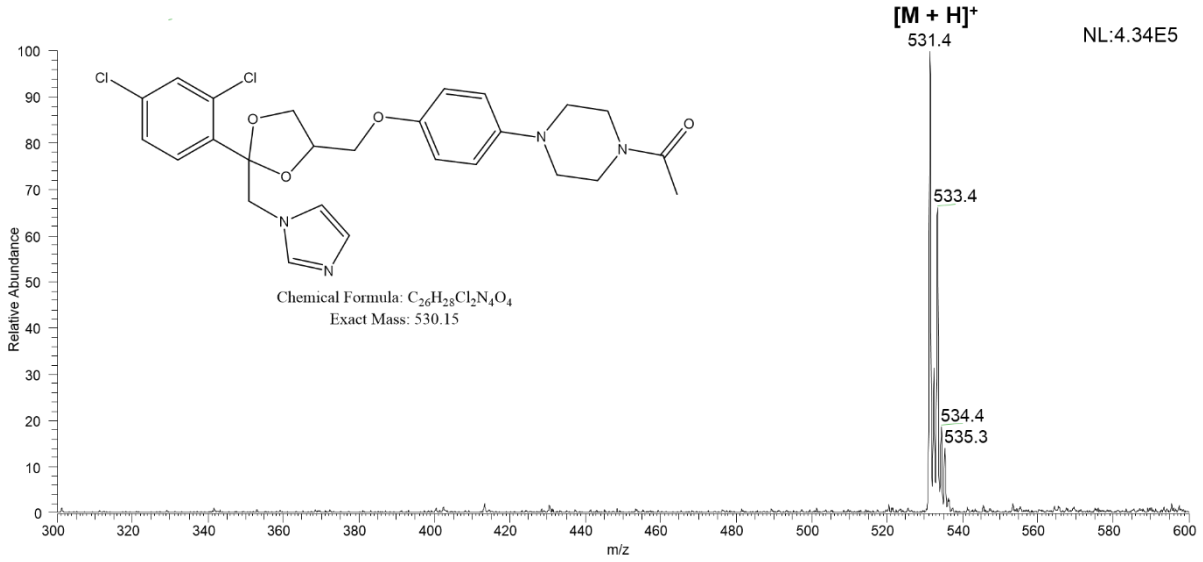

Figure A.1-6. Mass spectrum in the positive ion mode obtained by DeSSI-MS analysis of Fungoral® cream. Inset is shown the structure of ketoconazole.

Clindamycin phosphate is the active ingredient in Ygiele® cream and the mass spectrum in the positive ion mode obtained by DeSSI-MS analysis of this pharmaceutical ointment is shown in **Figure A.1-7**. Two main peaks with m/z 425.3 and 505.3 can be clearly seen and these correspond to clindamycin phosphate after the possible loss of HPO_3 and clindamycin phosphate, respectively. However, in the MS/MS spectrum of m/z 505.3 the ion 425.3 is not the main fragment, indicating that the origin of ion 425.3 in the full mass spectrum is due to either thermal fragmentation inside ion transfer capillary of the mass spectrometer or degradation of the compound in the sample. Also, the ion 126.1 in the full mass spectrum was identified as a fragment that possible occurred as indicated in the inset of **Figure A.1-7**.

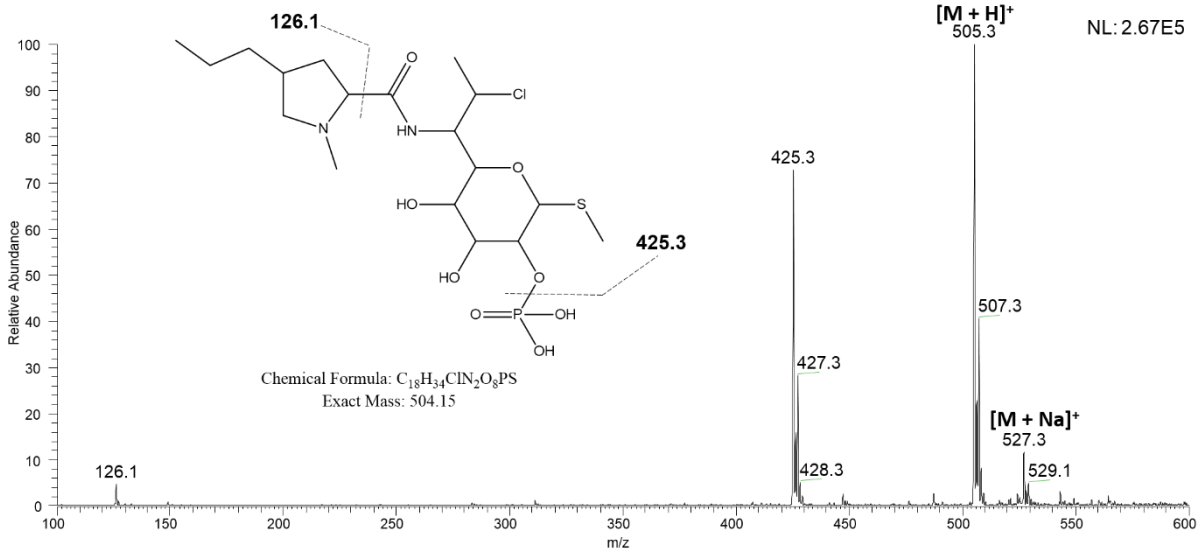

Figure A.1-7. Mass spectrum in positive ion mode obtained by DeSSI-MS analysis of Ygiele® cream. Inset is shown the structure of clindamycin phosphate along with the possible fragmentations that produce the ions with m/z 126.1 and 425.3.

A.2. Analysis of pharmaceutical tablets

These samples were kindly provided by fellow colleagues and analyzed with no sample preparation at all.

Aerius®

Ingredients: desloratadine (5 mg per tablet), calcium hydrogen phosphate dihydrate, microcrystalline cellulose, corn starch, talc, lactose monohydrate, hypromellose, titanium dioxide, polyethylene glycol 400, indigo carmine E312, carnauba wax, white wax.

Loxitan®

Ingredients: meloxicam (15 mg per tablet), lactose mononhydrate, anhydrous colloidal silica, sodium citrate, magnesium stearate, microcrystalline cellulose, povidone, crospovidone.

Norgesic®

Ingredients: orphenadrine citrate (35 mg), paracetamol (450 mg), magnesium stearate, colloidal anhydrous silica, microcrystalline cellulose, starch 1500.

Panadol Cold & Flu®

Ingredients: paracetamol (500 mg), pseudoephedrine hydrochloride (30 mg), cellulose microcrystalline, colloidal anhydrous silica, stearic acid, magnesium stearate, starch pregelatinized, povidone, crospovidone, croscarmellose sodium, hypromellose, macrogol, carnuba wax, indigo carmine E312.

In **Figure A.2-1** the mass spectrum in the positive ion mode obtained by DeSSI-MS analysis of Aerius® tablet is shown. The active ingredient of this tablet is desloratadine and it can be detected as a protonated ion with m/z 311.3 and the characteristic isotopic pattern due to the presence of chorine atom is also observed. In the mass spectrum several other peaks are observed in the region 327 – 652 which correspond to polyethylene glycol (PEG) that is contained in the tablet. PEG has the general chemical formula $C_{2n}H_{4n+2}O_{n+1}$ and being a polymeric compound, the observed ions would have a constant m/z difference of 44 amu. The ion with m/z 283.3 was identified as the protonated PEG polymer with n=6 and by looking at the mass spectrum it is clear that there are several other peaks with difference of 44 amu from this peak, i.e. m/z 327.3 which is the protonated PEG polymer with n=7, m/z 371.2 which corresponds to n=8 and so on. In this spectrum peaks of protonated PEG molecules are observed for n values ranging from 6 to 14. Additionally, mass differences of 17, 22 and 38 amu correspond to H^+ adduct exchange with NH_4^+, Na^+ and K^+, respectively. For example, the set of peaks with m/z 327.3, 344.2, 349.4 and 365.3 were identified as H^+ adduct of PEG with n=7, NH_4^+ adduct of PEG with n=7, Na^+ adduct of PEG with n=7 and K^+ adduct of PEG with n=7, respectively. Finally, lactose monohydrate contained in the tablet formulation could be observed as the Na^+ adduct of lactose with m/z 365.3, however, due to isobaric interferences with PEG ions and the unit resolution of the mass spectrometer, these two peaks cannot be separated. No ions were detected for the indigo carmine dye contained in the tablet.

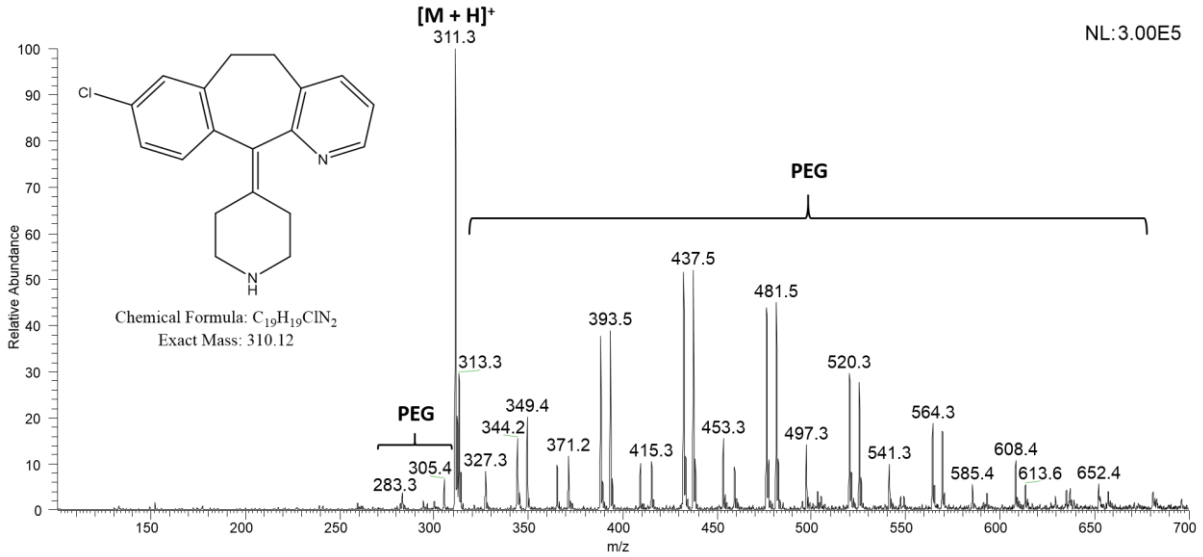

Figure A.2-1. Mass spectrum in the positive ion mode obtained by DeSSI-MS analysis of Aerius® tablet. Inset is shown the structure of the active ingredient, desloratadine.

In **Figure A.2-2** the mass spectrum in the positive ion mode obtained by DeSSI-MS analysis of Loxitan® tablet is shown and it clearly observed that the active ingredient, meloxicam, is detected as a protonated ion with m/z 352.1 and as Na^+ adduct with m/z 374.0. The peak with m/z 365.3 corresponds to protonated lactose. Meloxicam was also detected as deprotonated molecule in the negative ion mode (spectrum not shown).

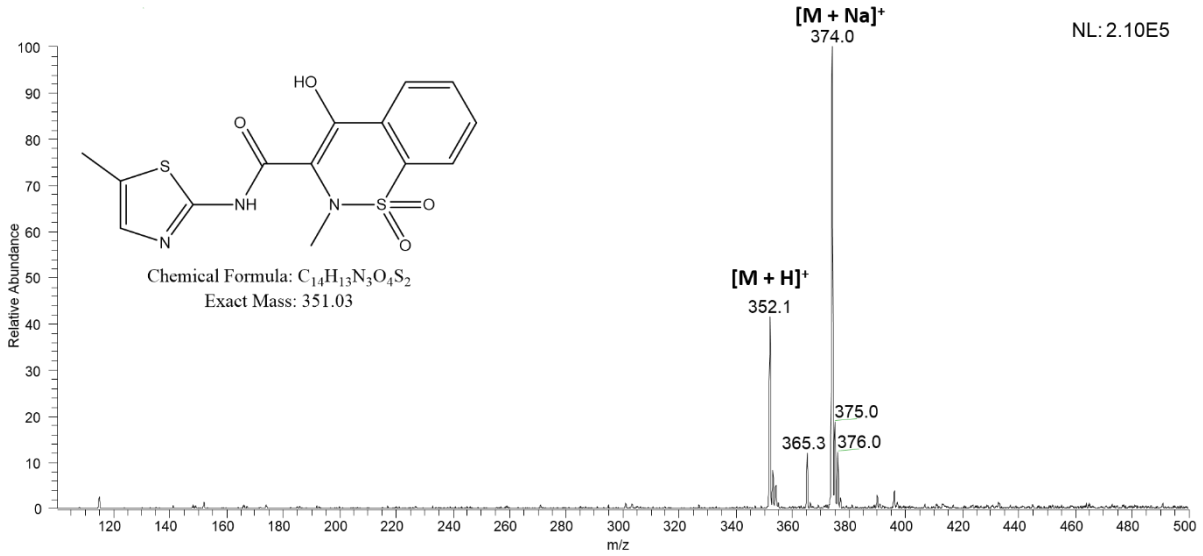

Figure A.2-2. Mass spectrum in the positive ion mode obtained by DeSSI-MS analysis of Loxitan® tablet. Inset is shown the structure of the active ingredient, meloxicame.

Norgesic® tablets contain the active ingredients paracetamol and orphenadrine citrate which can be easily detected in the positive ion mode mass spectrum by DeSSI-MS analysis (**Figure A.2-3**). Both molecules are detected as protonated ions and also their corresponding Na^+ adducts are detected. In the mass spectrum of Norgesic® tablet it can be seen that there is a very intense peak with m/z 181.1 which was identified as a fragment of orphenadrine. Since DeSSI is a very soft ionization source, this fragment is possibly created either inside the ion transfer capillary of the mass spectrometer due to the heating or from the degradation of the active compound in the tablet. Peaks with m/z 246.5 and 286.1 were not identified.

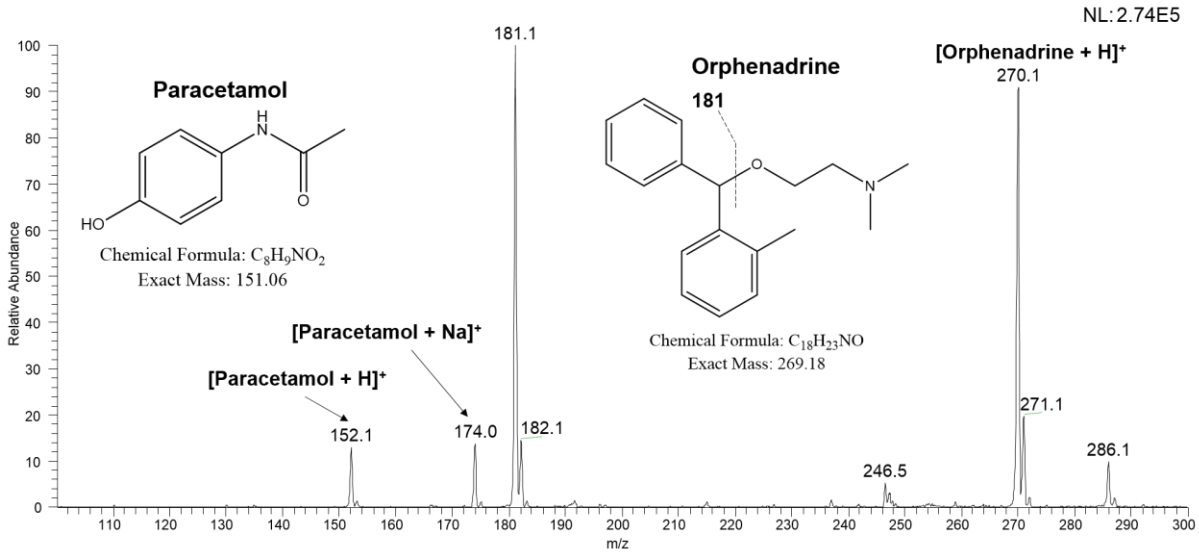

Figure A.2-3. Mass spectrum in the positive ion mode obtained by DeSSI-MS analysis of Norgesic® tablet. Inset are shown the structures of the active ingredients, paracetamol and orphenadrine.

Panadol Cold & Flu® tablets contain as active ingredients the compounds paracetamol and pseudoephedrine hydrochloride. Both of the active compounds were detected as protonated ions in the positive ion mass spectrum obtained by DeSSI-MS (**Figure A.2-4**). Paracetamol was detected as protonated and Na^+ adduct ion with m/z 152.1 and 173.9, respectively, while pseudoephedrine was detected as protonated ion with m/z 166.0. The dehydration product (m/z 148.1) of pseudoephedrine was also observed in the mass spectrum along with a protonated dimer with m/z 330.9. Peaks with m/z 324.9 and 366.9 were not identified.

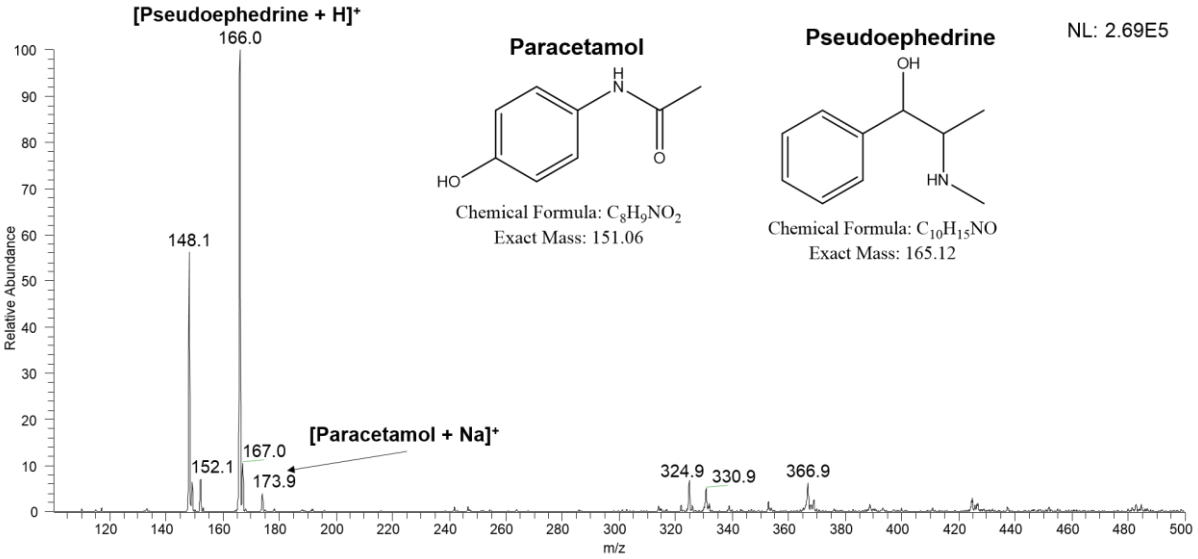

Figure A.2-4. Mass spectrum in the positive ion mode obtained by DeSSI-MS analysis of Panadol Cold & Flu® tablet. Inset are shown the structures of the active ingredients, paracetamol and pseudoephedrine.

A.3. Analysis of pharmaceutical solution

The potential of DeSSI-MS to analyze pharmaceutical solutions with absolutely no sample preparation or pre-separation was examined by analyzing a pharmaceutical solution (Hairway®) containing minoxidil (50 mg ml^{-1}) as the active ingredient. Other constituents include ethanol, propylene glycol and purified water. One µl of the sample was placed on Teflon-coated glass slide, left to dry under ambient conditions and subsequently analyzed by DeSSI-MS using acetonitrile as the spraying solvent at a flow rate of 30 µl min^{-1} and nitrogen backpressure of 6 bar. In **Figure A.3-1.** Mass spectrum obtained in the positive ion mode by DeSSI-MS analysis of Hairway® pharmaceutical solution. Inset is shown the structure of the active ingredient, minoxidil.

, the positive ion mass spectrum obtained is shown. Clear signals for the protonated minoxidil ion (m/z 210.1) and the protonated dimer (m/z 419.1) were observed. Also, the Na^+ adducts of the dimer and trimer were also detected with m/z 441.0 and 649.8, respectively.

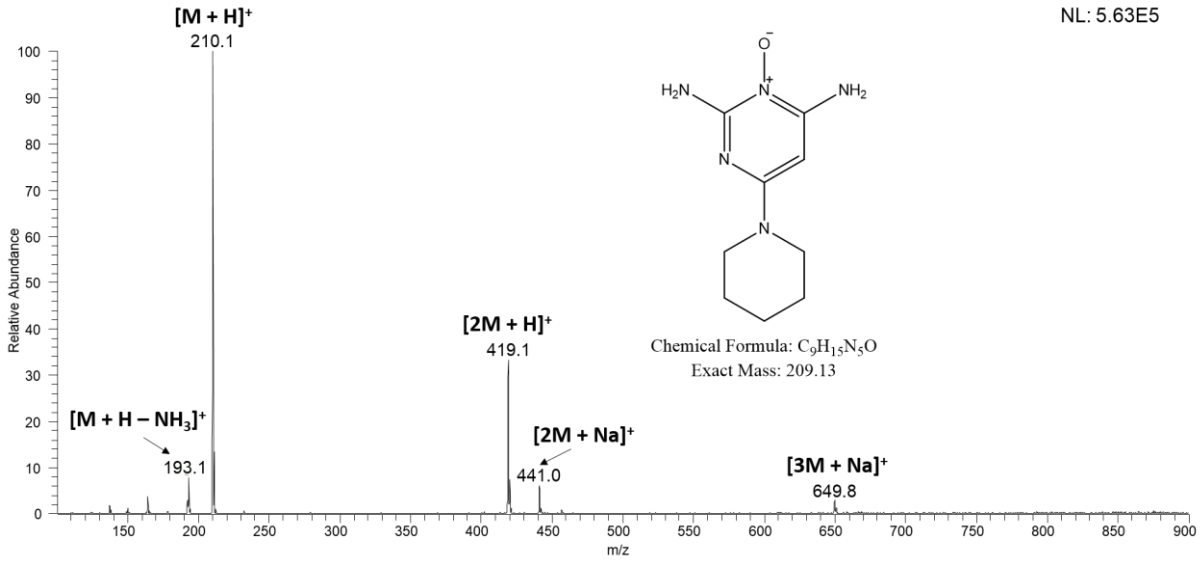

Figure A.3-1. Mass spectrum obtained in the positive ion mode by DeSSI-MS analysis of Hairway® pharmaceutical solution. Inset is shown the structure of the active ingredient, minoxidil.

A.4. Mass spectra of C. reinhardtii cells using different spraying solvents

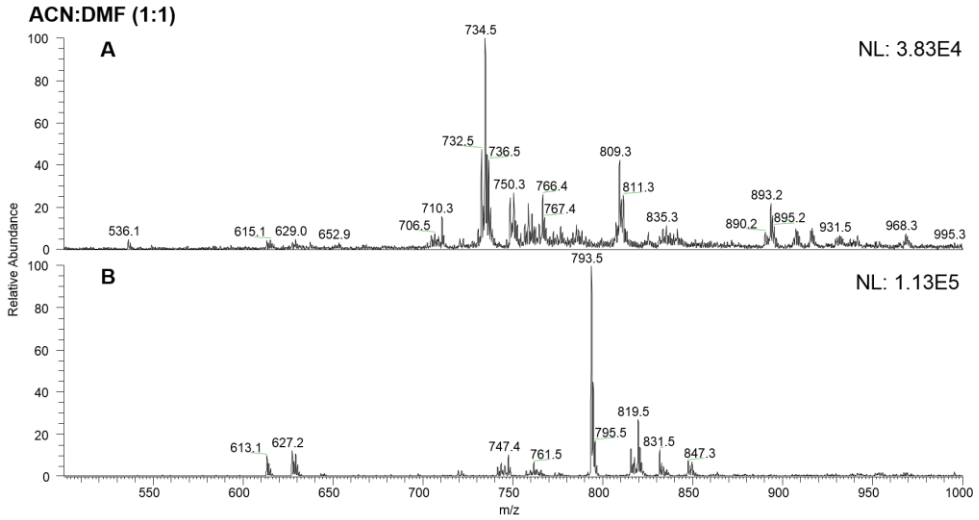

Figure A.4-1. DeSSI-MS spectrum in the positive (A) and negative (B) ion mode obtained when spraying *C. reinhardtii* cells with ACN:DMF 1:1 v/v.

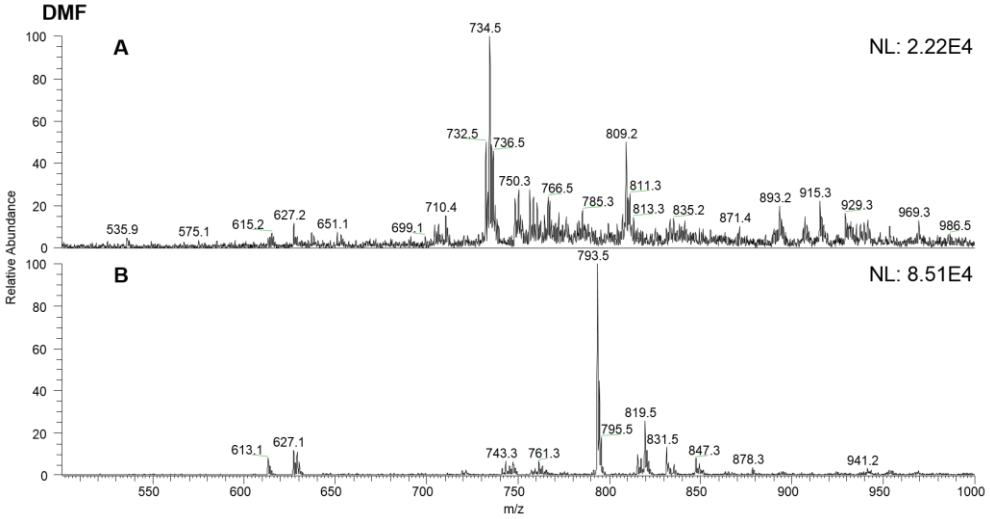

Figure A.4-2. DeSSI-MS spectrum in the positive (A) and negative (B) ion mode obtained when spraying *C. reinhardtii* cells with DMF.

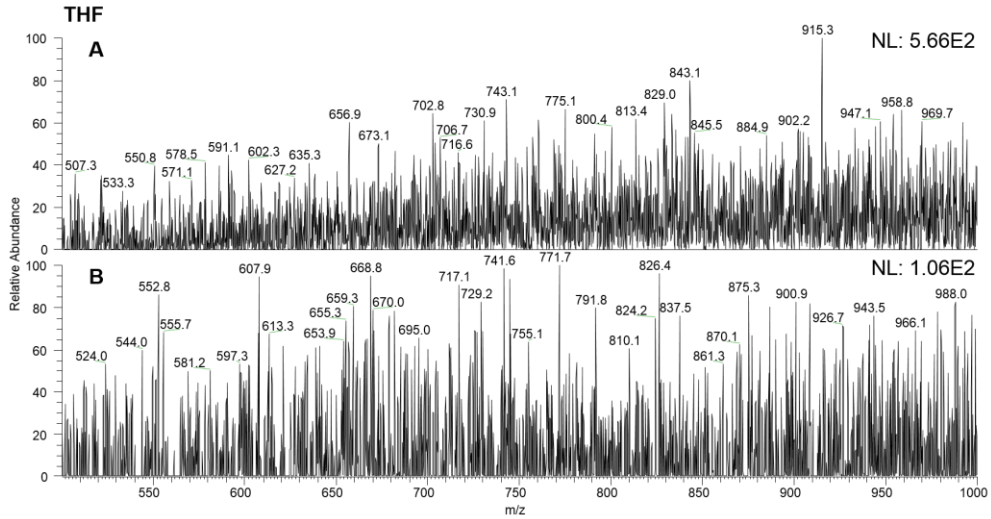

Figure A.4-3. DeSSI-MS spectrum in the positive (A) and negative (B) ion mode obtained when spraying *C. reinhardtii* cells with THF.

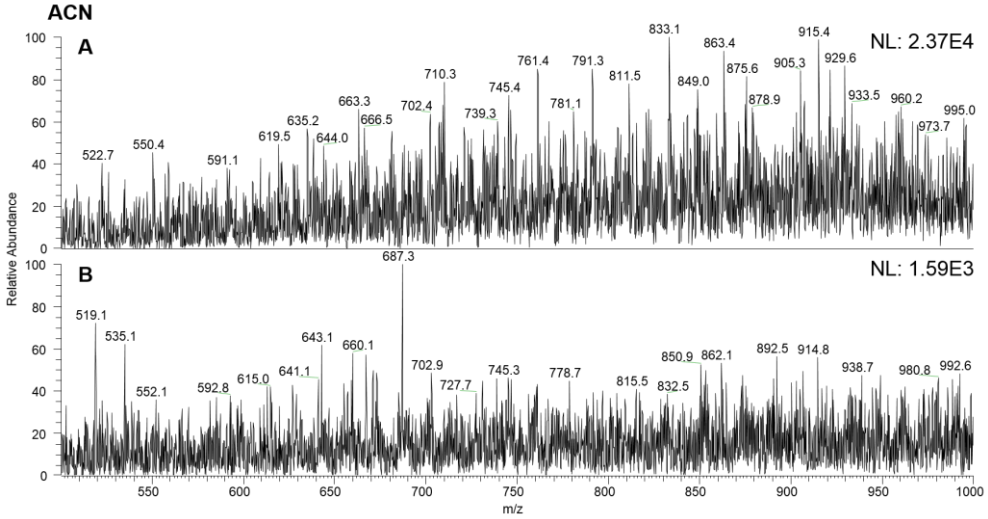

Figure A.4-4. DeSSI-MS spectrum in the positive (A) and negative (B) ion mode obtained when spraying *C. reinhardtii* cells with ACN.

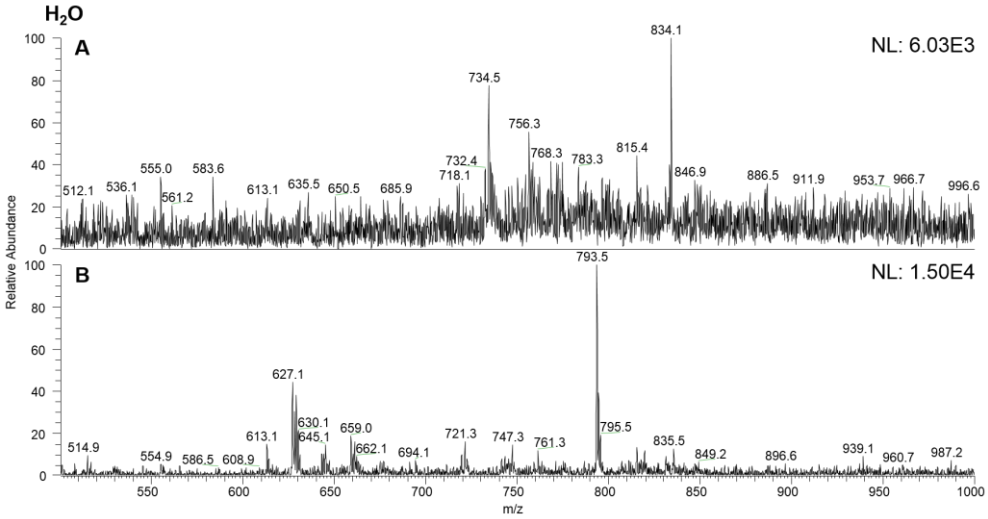

Figure A.4-5. DeSSI-MS spectrum in the positive (A) and negative (B) ion mode obtained when spraying *C. reinhardtii* cells with H_2O.

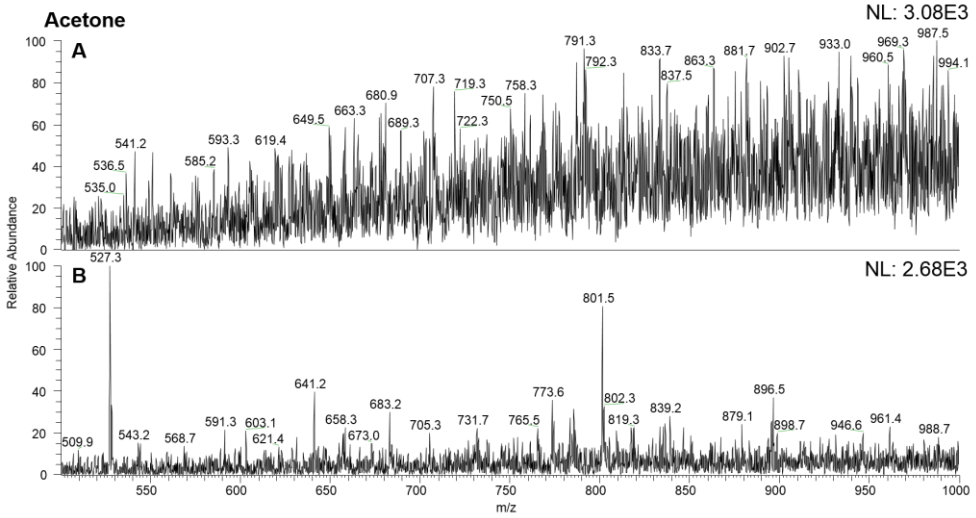

Figure A.4-6. DeSSI-MS spectrum in the positive (A) and negative (B) ion mode obtained when spraying *C. reinhardtii* cells with Acetone.

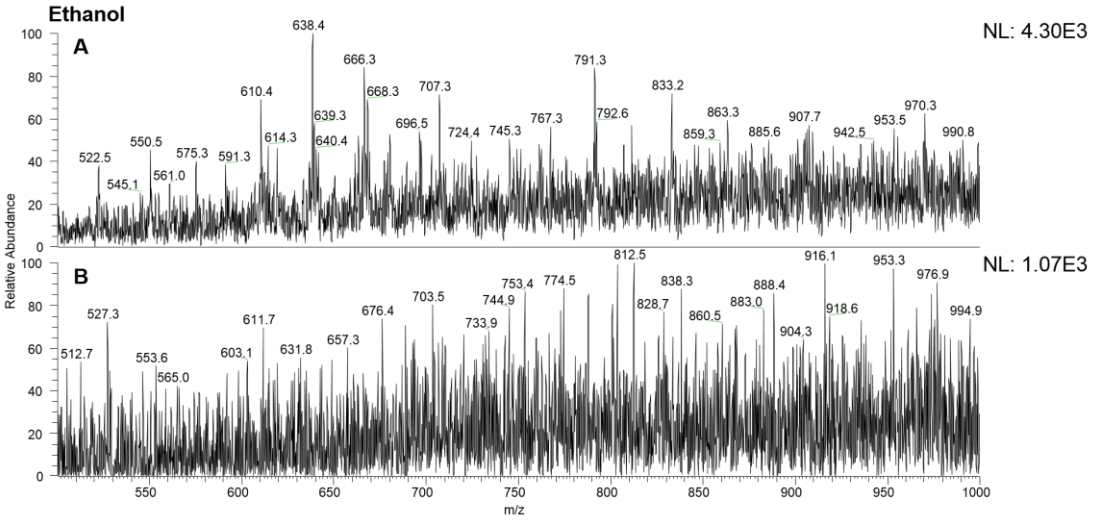

Figure A.4-7. DeSSI-MS spectrum in the positive (A) and negative (B) ion mode obtained when spraying *C. reinhardtii* cells with Ethanol.

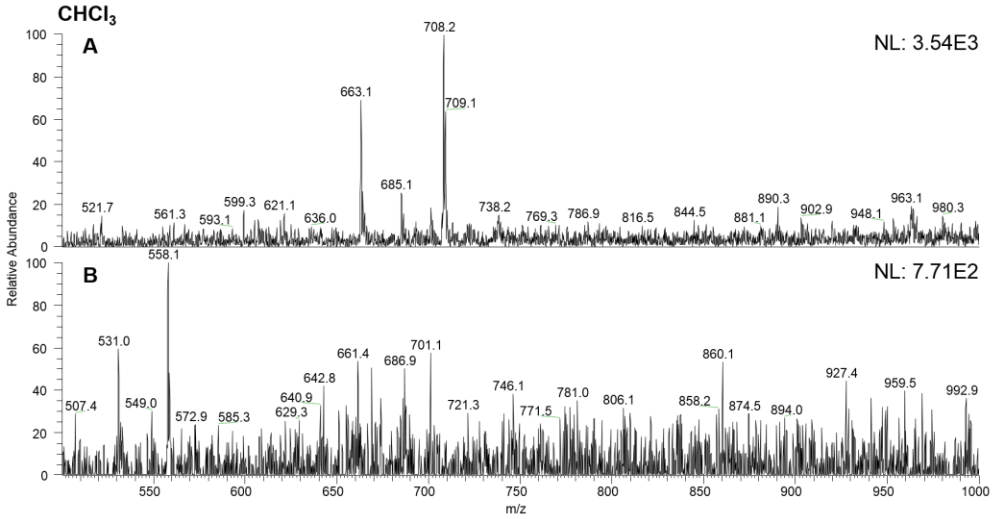

Figure A.4-8. DeSSI-MS spectrum in the positive (A) and negative (B) ion mode obtained when spraying *C. reinhardtii* cells with $CHCl_3$.

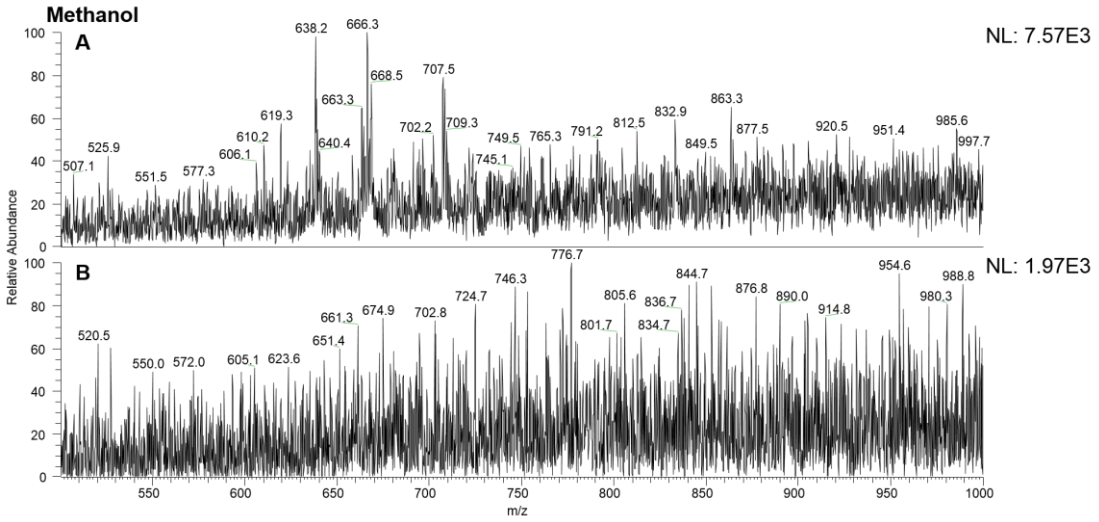

Figure A.4-9. DeSSI-MS spectrum in the positive (A) and negative (B) ion mode obtained when spraying *C. reinhardtii* cells with Methanol.

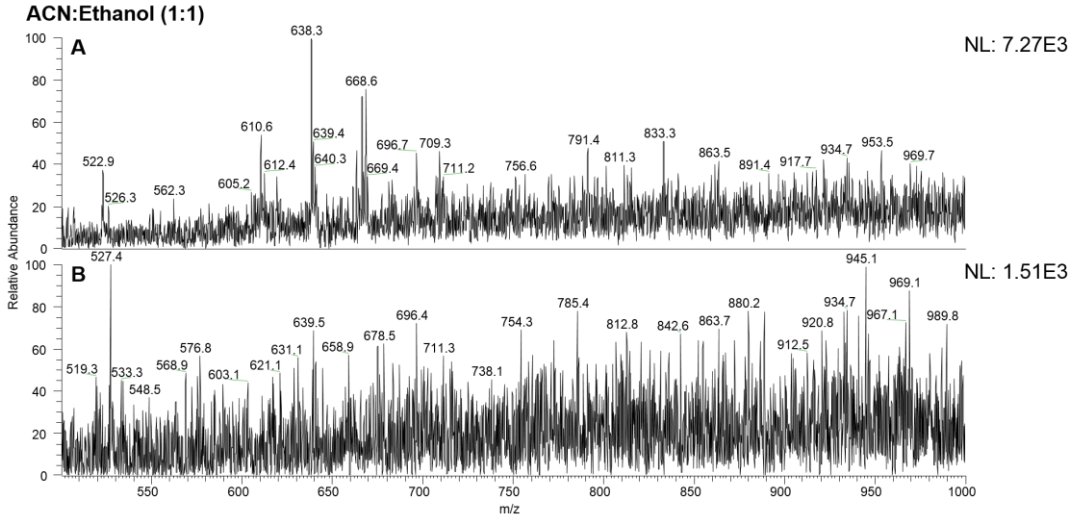

Figure A.4-10. DeSSI-MS spectrum in the positive (A) and negative (B) ion mode obtained when spraying *C. reinhardtii* cells with ACN:Ethanol 1:1 v/v.

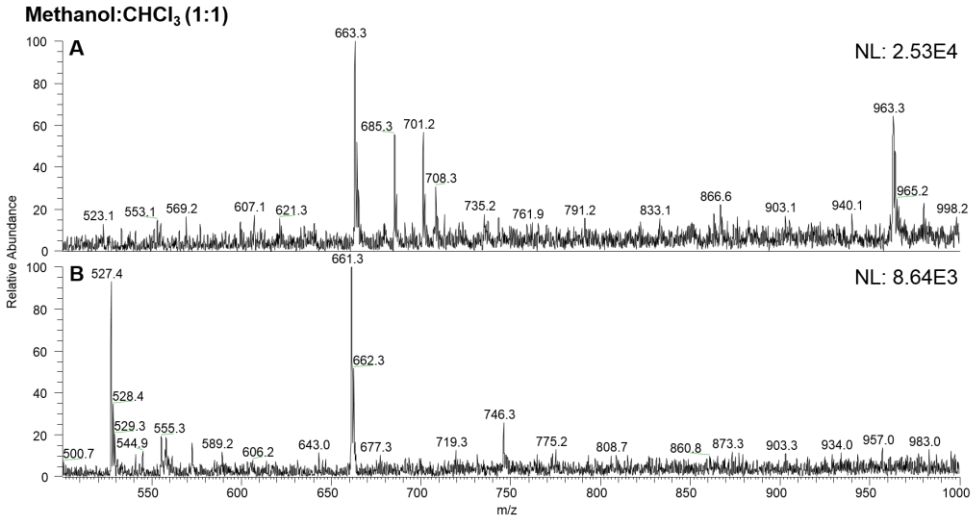

Figure A.4-11. DeSSI-MS spectrum in the positive (A) and negative (B) ion mode obtained when spraying *C. reinhardtii* cells with Methanol:$CHCl_3$ 1:1 v/v.

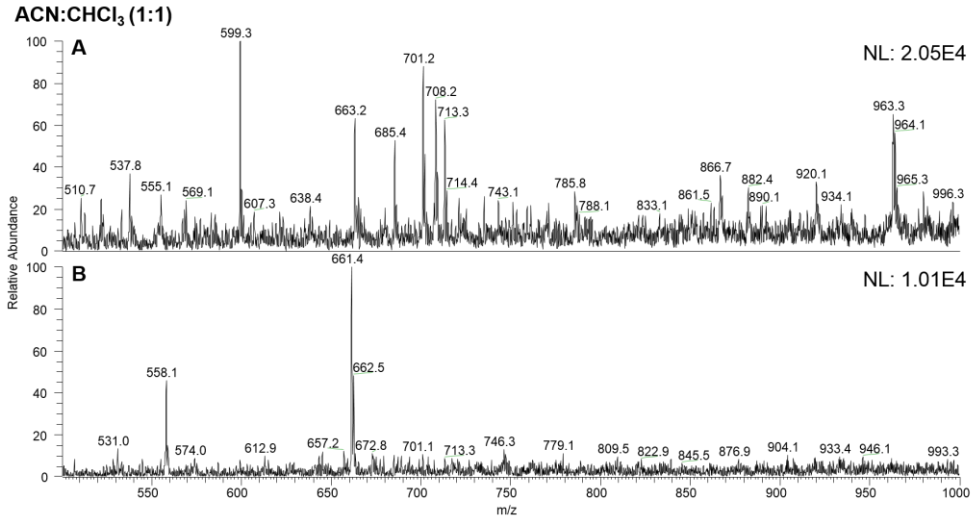

Figure A.4-12. DeSSI-MS spectrum in the positive (A) and negative (B) ion mode obtained when spraying *C. reinhardtii* cells with ACN:$CHCl_3$ 1:1 v/v.

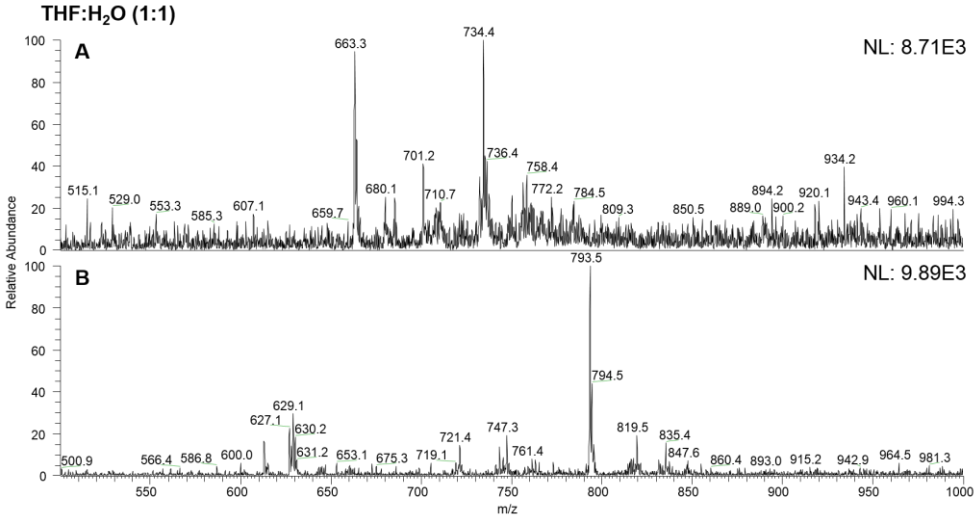

Figure A.4-13. DeSSI-MS spectrum in the positive (A) and negative (B) ion mode obtained when spraying *C. reinhardtii* cells with THF:H_2O 1:1 v/v.

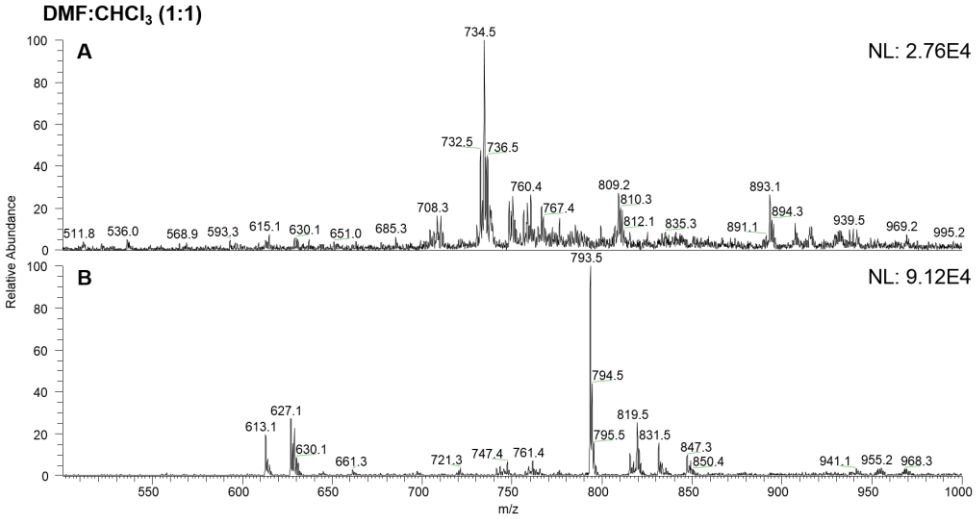

Figure A.4-14. DeSSI-MS spectrum in the positive (A) and negative (B) ion mode obtained when spraying *C. reinhardtii* cells with DMF:$CHCl_3$ 1:1 v/v.

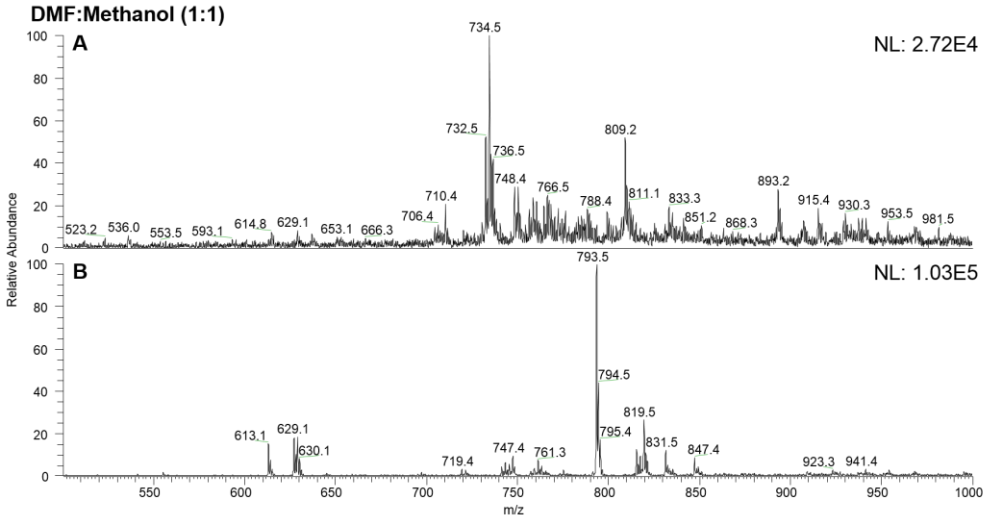

Figure A.4-15. DeSSI-MS spectrum in the positive (A) and negative (B) ion mode obtained when spraying *C. reinhardtii* cells with DMF:Methanol 1:1 v/v.

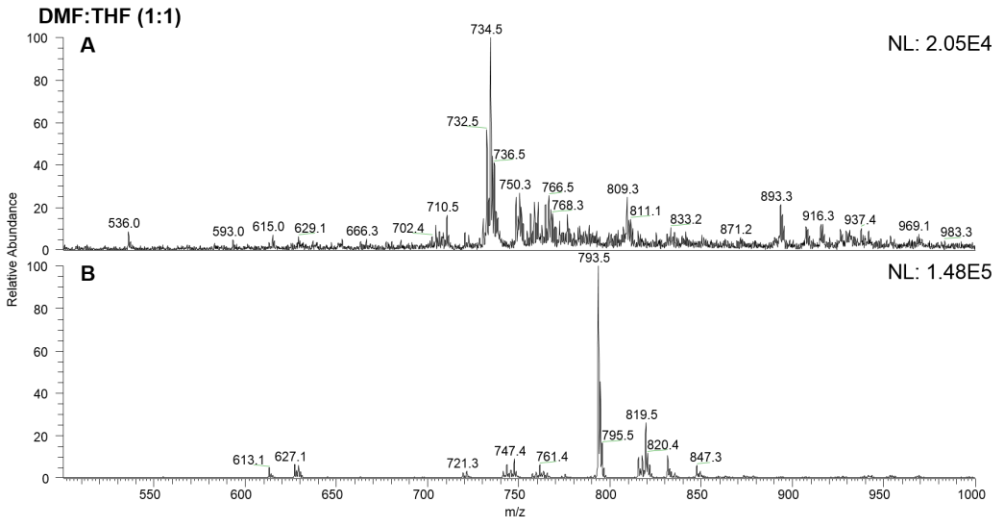

Figure A.4-16. DeSSI-MS spectrum in the positive (A) and negative (B) ion mode obtained when spraying *C. reinhardtii* cells with DMF:THF 1:1 v/v.

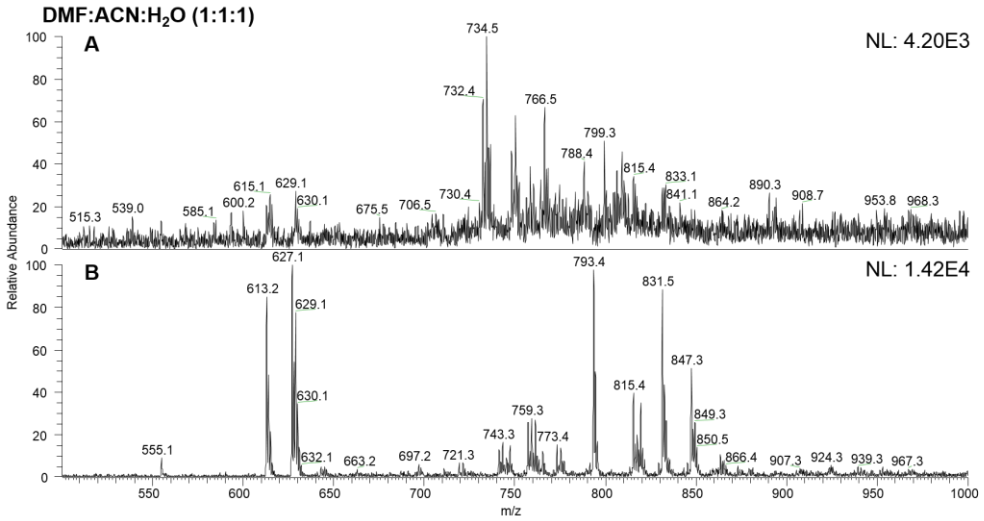

Figure A.4-17. DeSSI-MS spectrum in the positive (A) and negative (B) ion mode obtained when spraying *C. reinhardtii* cells with DMF:ACN:H_2O 1:1:1 v/v.

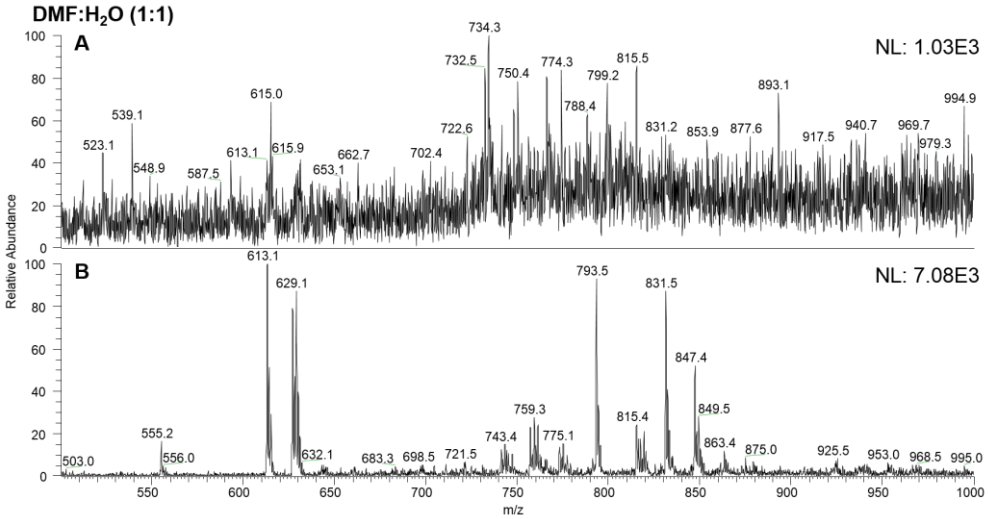

Figure A.4-18. DeSSI-MS spectrum in the positive (A) and negative (B) ion mode obtained when spraying *C. reinhardtii* cells with DMF:H_2O 1:1 v/v.

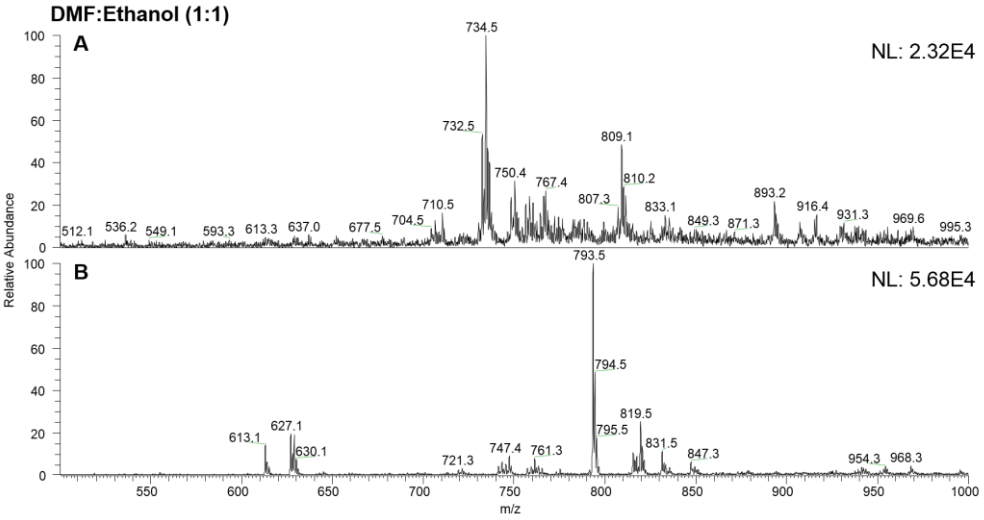

Figure A.4-19. DeSSI-MS spectrum in the positive (A) and negative (B) ion mode obtained when spraying *C. reinhardtii* cells with DMF:Ethanol 1:1 v/v.

A.5. DeSSI-MS and ESI-MS comparison of spectra obtained from *C. reinhardtii* cells

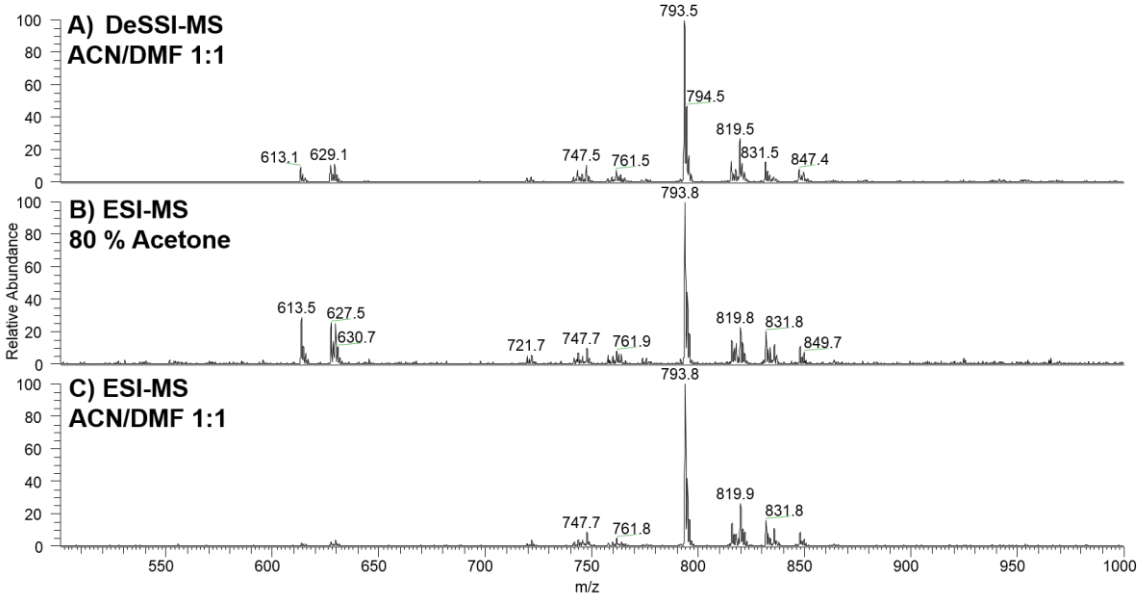

Figure A.5-1. Negative ion mode spectra of *C. reinhardtii* cells obtained by A) DeSSI-MS using ACN/DMF 1:1 as the spraying solvent, B) ESI-MS using 80 % acetone as the extraction solvent and C) ESI-MS using ACN/DMF 1:1 as the extraction solvent Ions with m/z 613-630 were also present in the ESI-MS spectrum with ACN/DMF 1:1 but in lower abundance, thus, they are not labeled in the figure.